MULTIDISCIPLINARY DESIGN OF AN UNMANNED AERIAL VEHICLE WING

A THESIS SUBMITTED TO
THE GRADUATE SCHOOL OF NATURAL AND APPLIED SCIENCES
OF
MIDDLE EAST TECHNICAL UNIVERSITY

BY

ARZU SAKARYA

IN PARTIAL FULFILLMENT OF THE REQUIREMENTS
FOR
THE DEGREE OF MASTER OF SCIENCE
IN
AEROSPACE ENGINEERING

SEPTEMBER 2011

Approval of the thesis:

MULTIDISCIPLINARY DESIGN OF AN UNMANNED AERIAL VEHICLE WING

submitted by **ARZU SAKARYA** in partial fulfillment of the requirements for the degree of **Master of Science in Aerospace Engineering Department, Middle East Technical University** by,

Prof. Dr. Canan Özgen _____
Dean, Graduate School of **Natural and Applied Sciences**

Prof. Dr. Ozan Tekinalp _____
Head of Department, **Aerospace Engineering**

Prof. Dr. Yavuz Yaman _____
Supervisor, **Aerospace Engineering Dept., METU**

Examining Committee Members:

Prof. Dr. Serkan Özgen _____
Aerospace Engineering Dept., METU

Prof. Dr. Yavuz Yaman _____
Aerospace Engineering Dept., METU

Assist. Prof. Dr. Melin Şahin _____
Aerospace Engineering Dept., METU

Assist.Prof. Dr. Ercan Gürses _____
Aerospace Engineering Dept., METU

Dr. Gürsel Erarslanoğlu _____
Structural Engineering Management, TUSAŞ

Date: 09.09.2011

I hereby declare that all information in this document has been obtained and presented in accordance with academic rules and ethical conduct. I also declare that, as required by these rules and conduct, I have fully cited and referenced all material and results that are not original to this work.

Name, Last name : Arzu Sakarya

Signature :

ABSTRACT

MULTIDISCIPLINARY DESIGN OF AN UNMANNED AERIAL VEHICLE WING

Sakarya, Arzu

M.Sc., Department of Aerospace Engineering

Supervisor: Prof. Dr. Yavuz Yaman

September 2011, 153 pages

In this thesis, the structural design, structural analysis and producibility analysis of an unmanned aerial vehicle wing were performed. Three different wing models, made of different materials, were designed. The wings were aluminum wing model and composite wing models; made of prepreg and wet lay-up. All wings have the same aerodynamic geometry and structural configuration under the same flight conditions. The structural designs of three wings were done by using Unigraphics NX. The finite element modeling of the wings were built by using MSC Patran package program. After the application of the loads on models, structural analyses were performed by MSC Nastran. Finally, the producibility analysis of prepreg wing model was conducted by using FiberSIM package program. The prepreg wing model was selected as optimum design with studies conducted in the study considering weight, producibility, cruise and gust stress and displacement conditions.

Keywords: Aircraft Structural Design, Finite Element Analysis, Producibility Analysis, Composite Materials, UAV

ÖZ

BİR İNSANSIZ HAVA ARACI KANADININ ÇOK YÖNLÜ TASARIMI

Sakarya, Arzu

Yüksek Lisans, Havacılık ve Uzay Mühendisliği Bölümü

Tez Yöneticisi: Prof. Dr. Yavuz Yaman

Eylül 2011, 153 sayfa

Bu tezde, bir insansız hava aracı kanadının yapısal tasarımı, yapısal analizi ve üretilebilirlik analizi yapılmıştır. Farklı malzemelerden yapılmış üç tane kanat tasarlanmıştır. Alüminyum ve kompozit; prepreg ve ıslak serme ile yapılmış, olan kanat modelleri aynı uçuş koşulları altında aynı aerodinamik geometriye ve yapısal configurasyona sahiptirler. Üç kanadın yapısal tasarımı Unigraphics NX ile yapıldı. Sonlu eleman modeli MSC Patran paket programı kullanılarak yapıldı. Modellere yükler uygulandıktan sonra MSC Nastran ile yapısal analizi yapıldı. Son olarak FiberSIM paket programı kullanılarak prepreg kanat modelinin üretilebilirlik analizi yapıldı. Prepreg kanat modeli tez kapsamındaki çalışmalar sonucunda ağırlık, üretilebilirlik, seyir ve sağnak gerilim ve yer değiştirme koşulları düşünülerek en uygun tasarım seçildi.

Anahtar Kelimeler: Hava Araçlarının Yapısal Tasarımı, Sonlu Eleman Analizi, Üretilebilirlik Analizi, Kompozit Malzemeler, IHA

To my father and grandmother.

ACKNOWLEDGEMENTS

I would like to express my sincere gratitude to my supervisor Prof. Dr. Yavuz Yaman for his assistance, encouragement, guidance and patience throughout my study. I appreciate for his support in not only my thesis but also in every respect.

I would like to thank you my thesis committee member and my manager in the company Dr. Gürsel Erarslanoğlu, Structural Engineering Manager of Integrated Aircraft Group, TUSAŞ, my chief Hakan Taşkaya, Structural Design Chief of Integrated Aircraft Group, TUSAŞ, and my leader Gülgün Bahtiyar, ANKA Wing and Tail Structural Design Leader, for their support and guidance.

I am also grateful to my friend and colleague Tolga Insuyu for his support.

Finally, I specially thank to my parents for their love and support, to my father for his encouragement, to my grandmother for always being proud of me and my beloved husband Evren Sakarya for his endless support, guidance, assistance and his patience throughout my life.

TABLE OF CONTENTS

LIST OF TABLES

TABLES

LIST OF FIGURES

FIGURES

CHAPTER 1

INTRODUCTION

1.1 Background to the Study

The design of aircraft structures is a critical issue, because the structure has to provide enough strength while keeping the weight minimum. In order to achieve a successful design, the aircraft structures must meet all design requirements satisfying optimal weight criteria. Mission of the aircraft and flight conditions determine the loads on the aircraft. Materials selection affects the structural design, weight and strength. The material also has a direct impact on production technique and the overall cost.

1.2 Scope of the Study

In this thesis, the structural design of the three different wings, which have the same aerodynamic geometry and structural configuration under the same flight conditions, were conducted. Three different candidate materials were considered in the structural design of the wing and their structural characteristics were compared and presented. The main aim was to determine a suitable material for the UAV wing to be designed.

1.3 Limitations of the Study

In the thesis, structural design and analyses of a UAV wing with torque box and two control surfaces; flap and aileron; were conducted and presented. Main geometry was fixed throughout the study. Material selection was limited to aluminum and composites and manufacturing constraints affects the structural

design. The control surfaces were assumed as locked during the analyses. In structural sizing, analyses were conducted only for stress and maximum displacement criteria; buckling, fatigue and aeroelastic analysis were not currently taken into consideration.

CHAPTER 2

LITERATURE REVIEW

2.1 Materials

There are different materials used in aviation industry. They can be collected in two main groups as metals and composites.

The metals generally usually used in aircraft structures are aluminum, steel, titanium and magnesium.

The materials which are composed of at least two distinct materials without any chemical reaction are called as composites. There are two main components in the composite materials; matrix and reinforcements. The matrix holds the reinforcements in their desired position, protects them from abrasion, transfers loads between fibers and provides the interlaminar shear strength [5]. The reinforcement, which provides strength and stiffness, is the load carrying member and responsible for tensile, compressive, flexural strength and stiffness. The reinforcements are three types; fibers, whisker and particles. The fibers are circular long elements and are very strong in length direction. They carry tensile load but they are weak under compressive and shear load.

Fiber materials can be carbon, glass, aramid (Kevlar) and baron. There are different forms of fiber. The mostly used ones in aerospace structures are UD (Uni-Directional), Woven, Non Crimp Fabric (NFC) and Chopped Strand [5].

UDs are in the form of a tape where all the fibers are in the same direction. The material strength of the UDs is large in the fiber direction, however in transverse direction their strength is lower.

In woven fabric, the fibers are oriented in 0º and 90º in order to form a fabric and can be used in 45º layups. Material strength is lower than UD, but the drapeability quality is higher than UDs over curved surfaces [5]. Figure 2.1 shows different woven fabrics.

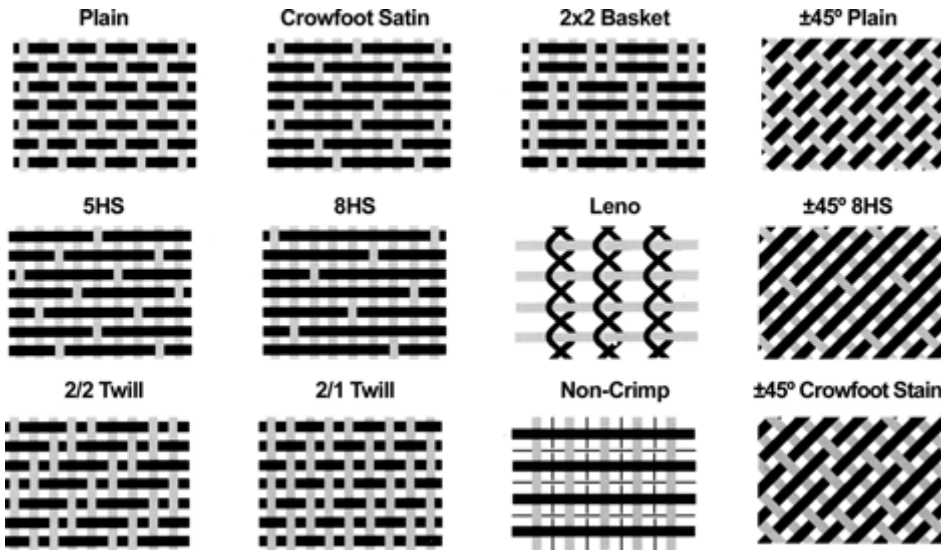

Figure 2.1 Different Kinds of Woven Fabric [5]

There are two principal material axes; fill direction and warp direction shown in Figure 2.2 for UD and woven fabrics [7].

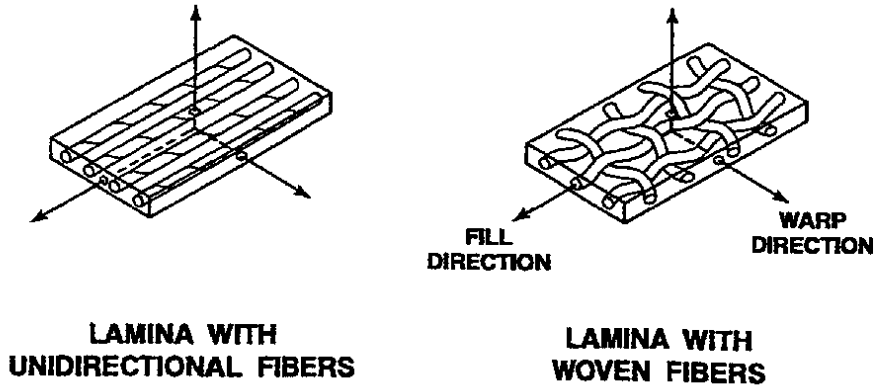

Figure 2.2 Principal Material Axes of the UD and Woven Fabric [7]

Non crimp fabrics are composed of 3 or 4 UD fabrics in different directions knitted together to form a fabric. Material strength and stiffness are higher than UDs. However fibers are destroyed while knitting. Figure 2.3 shows an example NCF.

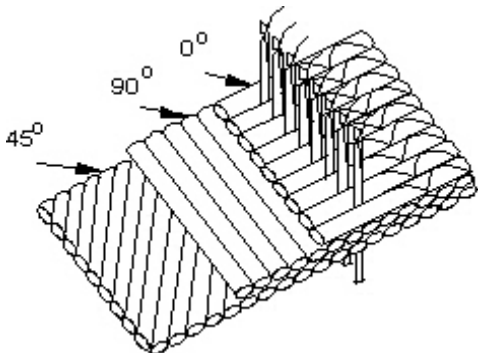

Figure 2.3 Typical NCF [5]

When the glass fibers are chopped and bonded with a binder, a sheet called chopped strand, is obtained as shown in Figure 2.4.

Figure 2.4 Typical Chopped Strand [5]

There are two kinds of matrix materials; thermosets and thermoplastics. Once thermosets are cured, they cannot be remelted. On the other hand, thermoplastics can be remelted after curing. Epoxies are the most preferred matrix materials because of their adequate strength, high temperature properties and low viscosity.

The structures which have a combination of two thin parallel sheets and light weighted cores are called sandwich structures. The cores increase inertia in the panel and prevent the buckling of the panels. Also, the highest stiffness-to-weight ratio and strength-to-weight ratio are provided. Figure 2.5 shows a typical cross section of the sandwich structures. As it can be seen from the figure that the laminate under the core, core and laminate over the core are bonded by a strong adhesive, which is called film adhesive.

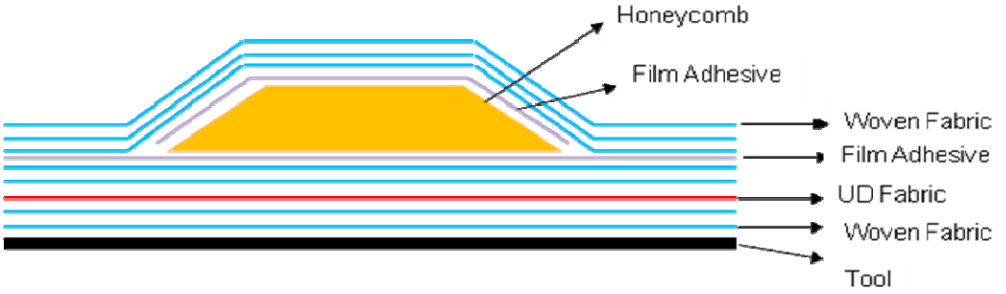

Figure 2.5 Cross-section of Sandwich Laminate

Widely used core materials are honeycomb, foam cores and balsa wood. The honeycombs can be aluminum, nomex and thermoplastic. Aluminum and nomex cores have generally hexagonal shapes, whereas thermoplastic cores have circular shape as shown Figure 2.6.

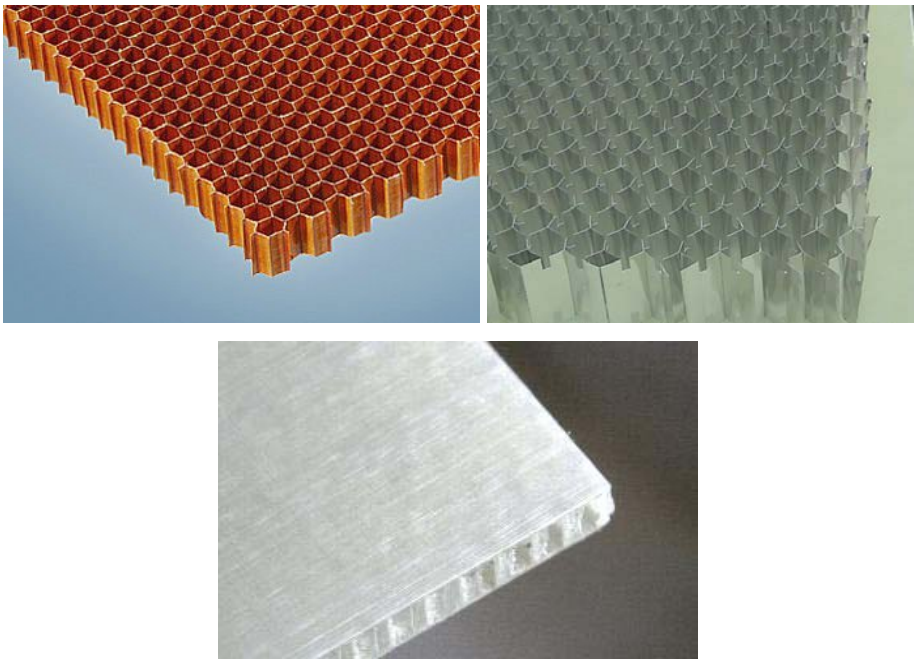

Figure 2.6 Core Types [5]

There are two principal axes in core materials; ribbon direction and transverse direction, shown in Figure 2.7. The material strength in ribbon direction is much higher than the material strenght in transverse direction. In a sandwich laminate, the ribbon direction and the fiber direction of UDs are parallel.

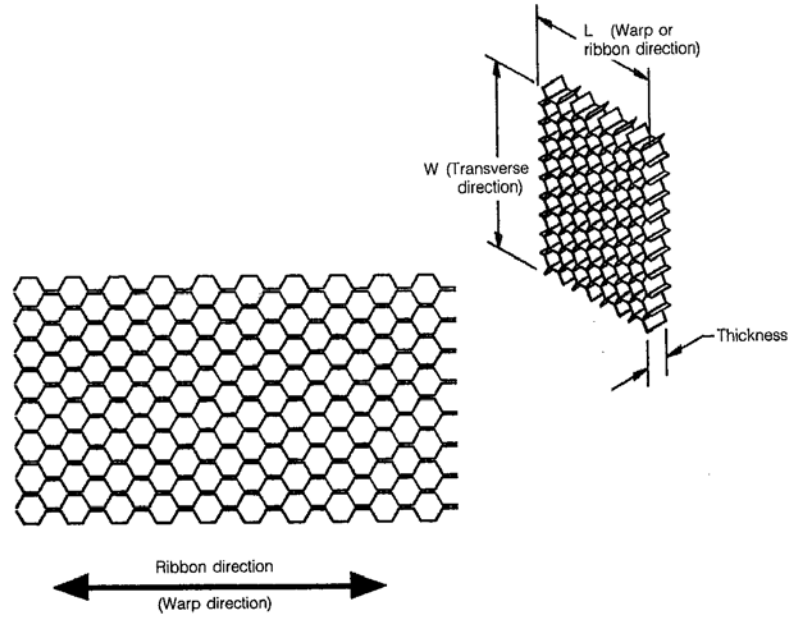

Figure 2.7 Principal Axes of Honeycomb Core [4]

In the composite manufacturing, three types of tooling are used [4].

1. *Male Tool:* Male tool, shown in Figure 2.8, is generally used for composite parts, which has non aerodynamic surfaces.

Figure 2.8 Example for Male Tool [4]

Lay-up cost and manufacturing cost are lowest. Composite parts, which have small radius less than 1.3 mm, can be manufactured.

2. *Female tool:* Female tool, shown in Figure 2.9, is used when the surface of composite part, like skin, spar, etc. is considerable from aerodynamic aspect.

Figure 2.9 Example for Female Tool [4]

Lap-up cost is highest. Composite parts, which have radius greater than 6.35 mm, can be manufactured.

3. *Matched Die tool:* Match die tool is used in order to control the laminate thickness. Figure 2.10 shows an example.

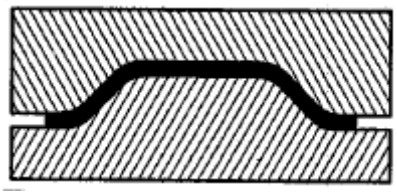

Figure 2.10 Example for Matched Die Tool [4]

Manufacturing cost is highest. Both sides of composite parts can be manufactured smooth.

2.2 The Manufacturing Processes for Metals

The metals are generally processed by machining such as milling, drilling, shaping, grinding and swaging or extrusion or various sheet metal processes like cutting, bending forming. Different joining processes like welding and fastening can be conducted. If required metals can also be cast.

2.3 The Manufacturing Processes for Composites

1. *Prepreg Hand Lay-up Method*: The process of prepreg hand lay-up is similar to wet hand lay-up process. The difference is that the fibers are impregnated by predetermined amounts of uniformly distributed resin before. The tool is prepared by release agent. The fibers are laid up by hand on the tool. Then, vacuum bagging is done. After vacuum bagging, the material is leaved for curing to become hard in autoclave, which applies temperature and pressure at the same time. The figure shows the vacuum bagging method for prepreg method.

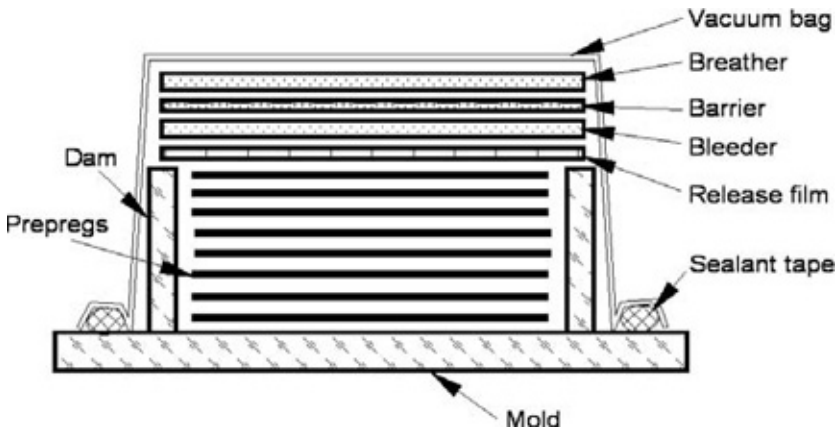

Figure 2.11 Vacuum Bagging Method for Prepreg Hand Lay-up Method [5]

2. *Wet Hand Lay-up Method*: The fibers are laid up by hand on the tool (mold). The release agent is applied on the tool in order to separate the part easily from the tool before lay-up. The fibers are impregnated in resin by brush after lay-up. Then, the vacuum bagging is done. In the vacuum bagging, the air is sucked out in order to obtain a distributed compression over the surface. The bobbles and wrinkles; voids; are minimized between the layers. After vacuum bagging, the material is leaved to become hard in room temperature for a while, which is called curing.

3. *Resin Transfer Molding (RTM)*: In this process, the products which have complex shapes with smooth surface finish can be obtained by injecting resin into a closed mold. The dry reinforcement and the resin are combined in the mold to form the composite product. The fiber reinforcement, which may be preshaped, is laid up on tool, which is then closed. Then, resin and reinforcement cure in pressure and temperature.
4. *Filament Winding*: The process of wrapping the fibers around a rotating mandrel in order to produce a closed form hollow parts is called filament winding. The filament winding can be done with resin, called as wet winding and without resign, called as dry winding.
5. *Pultrusion*: The pultrusion process for composite materials is similar the extrusion for metal materials. In this process desired constant cross section is obtained by mixture of resin and fibers. The mixture is pulled through a heated steel die by a pulling device.
6. *Structural Reaction Injection Molding (SRIM) Process*: There is a compatibility between SRIM process and RTM process. The resin and mixture of the resin is different from the resin in RTM process. There are two resins which are mixed in the mixing chamber at high velocity. After obtaining the mixture, the resin is injected in to a closed mold. The mold is heated for curing process. Complex shapes in large dimensions can be easily manufactured by this process.

7. *Sheet Molding Compound*: The chopped fibers and polyester resin are combined in the form of sheet. After obtaining the sheet, the sheet in desired dimension is laid on heated mold. The press pressure is applied on sheet in order to be taken the shape of the mold. At the same time the sheet cures under the heat of the mold and the press pressure.

2.4 Composite Structural Design Guidelines

There are many rules for designing composite structures. These rules were either drawn from past experience or theoretical studies [4].

Some of those design rules used extensively used in this thesis:

1. All laminates except sandwich laminates were designed as symmetric with respect to the midplane. For sandwich laminates, upper and lower parts are symmetric in themselves, even though the sandwich laminate may not be symmetric.

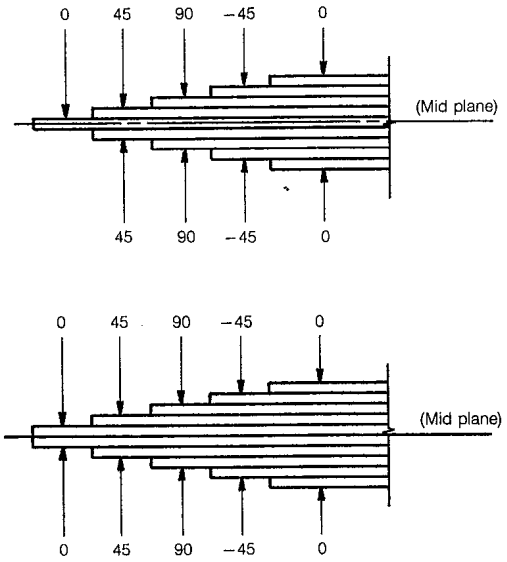

Figure 2.12 Examples for a Symmetrical Laminate [4]

2. The change of thickness in the laminate is called as add-on or drop-off plies. There are some considerations to perform a drop-off in the design. [4, 12].

    a. The symmetric laminate should be maintained in all areas, which has constant thickness.
    b. The distance between the add-on plies or drop-off plies should be determined by load direction.
       The ratio of d/t, shown in Figure 2.13, should be maintained greater than 20 in primary load direction and greater than 10 in secondary load direction.

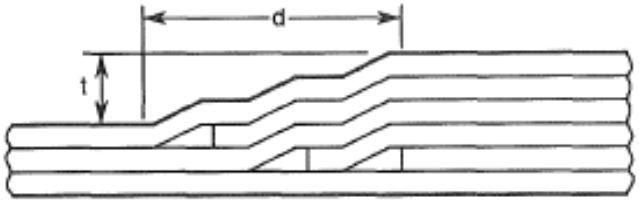

Figure 2.13 A Typical Cross Section of a Drop-off [12]

    c. The add-on plies or drop-off plies should be on outer surface due to peeling risk.
    d. The outer plies should be continuous or full ply in order to prevent edge delamination and to obtain smooth load flow.
    e. The outer plies should be +45°/-45° ply combination when UD fabric is used or 45° ply when woven fabric is used.
    f. The inner plies should be dropped off first. The cross section of the drop-off should be made as diamond if possible.
    g. The angle of the incline, shown in Figure 2.14, should not exceed 10°.

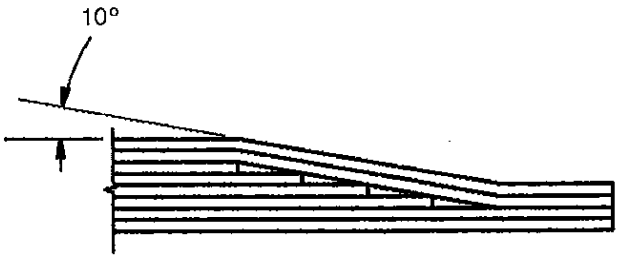

Figure 2.14 Drop-off Rule [4]

3. The honeycomb edges should be cut as tapered at maximum 30º, shown in Figure 2.15.

Figure 2.15 Taper Rule for Honeycomb [4]

4. The distance between the center of fastener and edge is called the edge distance. In the load direction, the edge distance is 3d and in transverse direction edge distance is 2.5d, where d is the fastener diameter. This case, called as the mechaning fastening rule is highlighted in Figure 2.16.

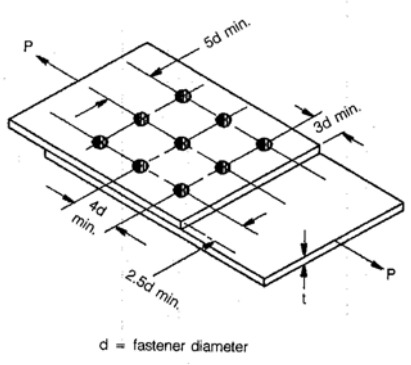

Figure 2.16 Mechanical Fastening Rules [4]

2.5 Other Studies

Klomp-de Boer studied a composite wing box, whose aerodynamic geometry belongs to the aluminum benchmark torque box of a small canard business aircraft Piaggio P180 Avanti, called as CESAR (Cost Effective Small Aircraft) [13]. The torque box was manufactured by using prepreg composite material. The result of the study shows that both weight and cost decreased by using composite material rather than using aluminum material. The aileron geometry of Piaggio P180 Avanti was studied by Romano et. al. where the composite aileron was manufactured by RTM process [14]. In their study they developed a methodology, which consists of preliminary sizing, finite element modeling and load application, to find an optimum design in order to reduce cost, weight and design time.

Guillermin made a tight integration of MSC Patran and FiberSIM in order to use the same model by designer, analysts and manufacturer [15]. It is determined that the final design of a composite part contains details and it is hard to transfer MSC Patran model to manufacturing. There must be a CAD model, which will be used by designer and analysts at the same time to make an interaction.

CHAPTER 3

STRUCTURAL MODELING OF THE WING

3.1 Introduction

In this section, the structural design of the wing using different materials is presented.

3.2 Geometry of the Wing

A wing which was previously studied in a TUBITAK (Turkish Scientific and Technological Research Council) project [1, 2, 3] was chosen as the starting point for overall sizing. The general geometry and configuration of the selected wing is given in Figure 3.1. The wing consists of a torque box, a flap and an aileron. The torque box has 2 spars and 5 ribs. The wing dimensions are given in Table 3.1.

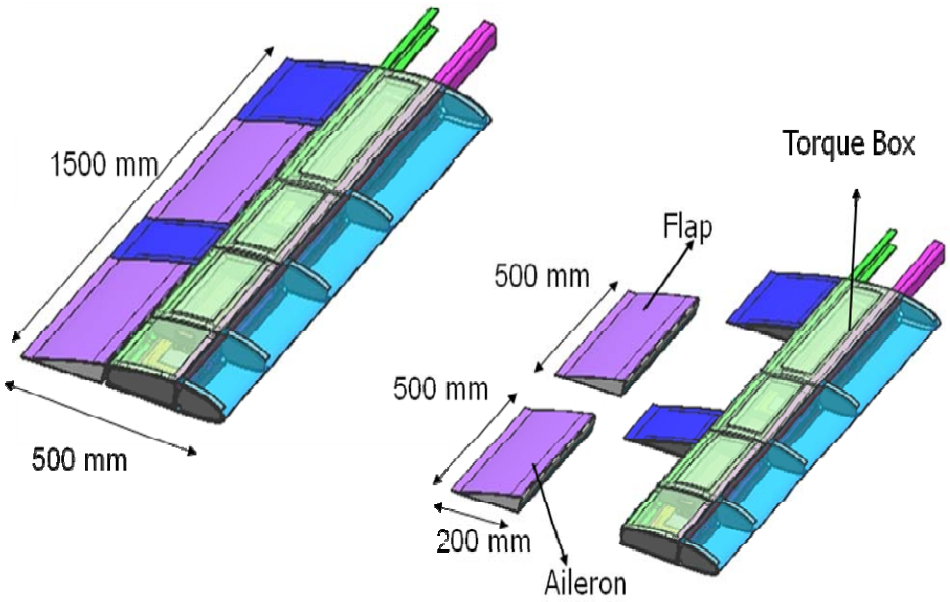

Figure 3.1 General Configuration of the Designed UAV Wing

Table 3.1 The Dimensions of the Designed UAV Wing

Geometry Dimension	**[mm]**
Wing span (b_{wing})	1500
Wing chord (c_{wing})	500
Flap span (b_{flap})	500
Flap chord (c_{flap})	200
Aileron span ($b_{aileron}$)	500
Aileron chord ($c_{aileron}$)	200

3.3 Wing Model Properties

In this section, the design details for all the designed UAV wing models are given.

The motion of each control surface was decided to be controlled by a single servo motor. In order to integrate the servo motor on the ribs of the structure, some cut-outs were provided in the lower skin. The covers were then used in the cutouts. On the covers, there were little slots which were for linkage arms of the servo motors. The covers can be seen in Figure 3.2.

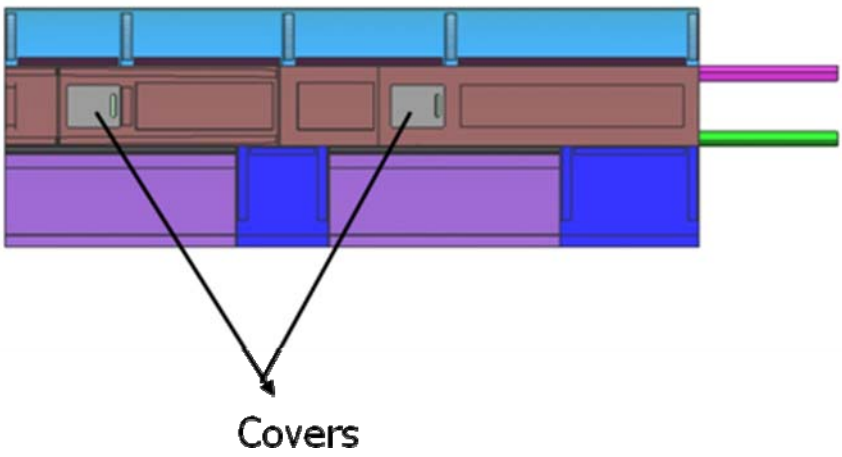

Figure 3.2 Cover Design Concept Used in the Study

Since these cutouts weaken the overall strength of the structure, the lower skin was further strengthened by using doublers. Doublers, which are shown in Figure 3.3, also provided the lapping surface for the removable fasteners; like nutplates, in order to connect the covers.

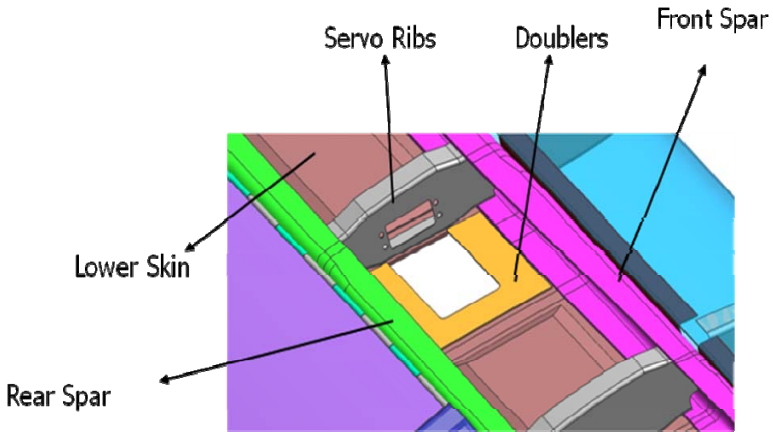

Figure 3.3 Doublers, Servo Ribs Used in the Study

The control surfaces were connected to the rear spar with piano type hinges. Figure 3.4 shows the details of the piano hinge concept.

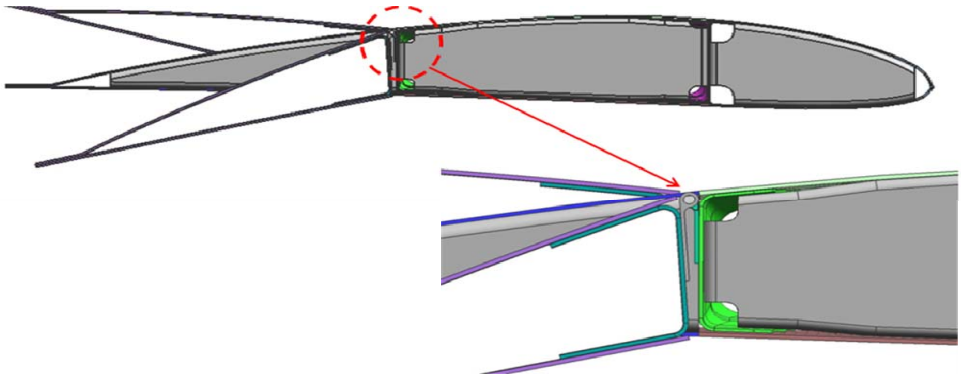

Figure 3.4 Piano Type Hinge Concept Used in the Study

The structural design of the wing was conducted for three different material and related production techniques. The structural design was done with Unigraphics NX. The first model was designed by using prepreg composite materials, while

second model was designed using wet lay-up composite materials in order to see the difference in composite manufacture processes. Another model was designed using aluminum to differentiate between composites and metals. Each structural member was designed according to design constraints of each material used.

3.4 Composite Models

3.4.1 Prepreg Model

In the model only the carbon fiber prepreg materials were used. Two kinds of fibers were used; woven fabric and UD fabric. The core material is honeycomb; nomex.

The general view of the wing is shown in Figure 3.5.

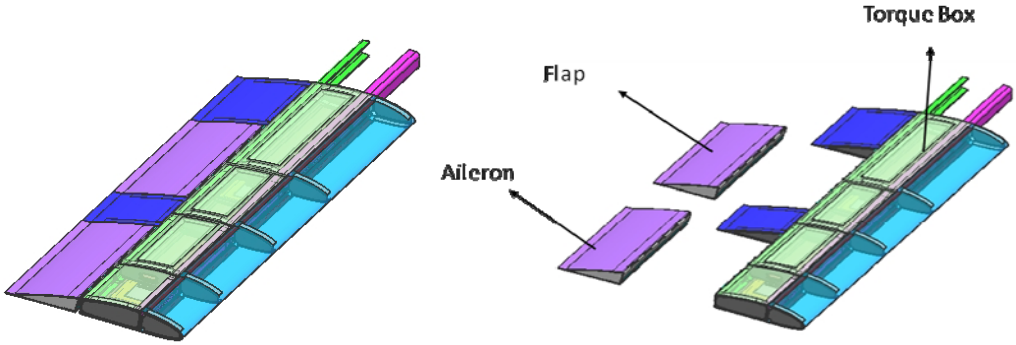

Figure 3.5 General View of Prepreg UAV Wing Model

3.4.1.1 Torque Box of Prepreg Wing Model

The detailed view of the torque box, showing structural components, for the prepreg composite design is given in Figure 3.6.

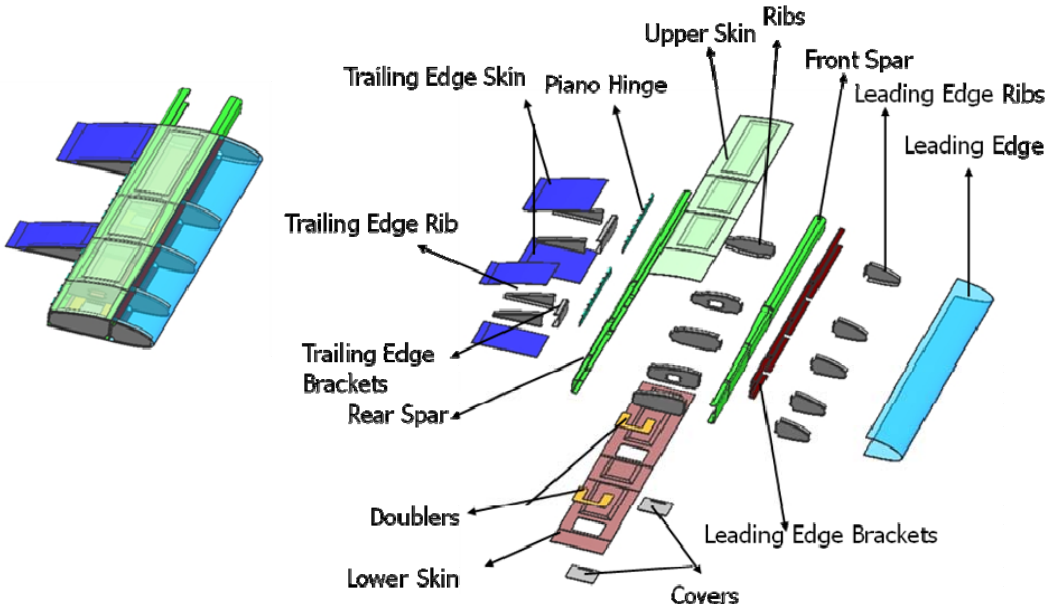

Figure 3.6 Detailed View of the Prepreg UAV Torque Box Model

The following paragraphs detail the structural members utilized in the design of prepreg composite UAV wing.

Lower Skin and Upper Skin:

There were four bays in lower and upper skins, with bays bounded by ribs. Skin thickness changed through the span, which was kept constant in each bay. The upper and lower skins with bay definitions are shown in Figure 3.7 and Figure 3.8.

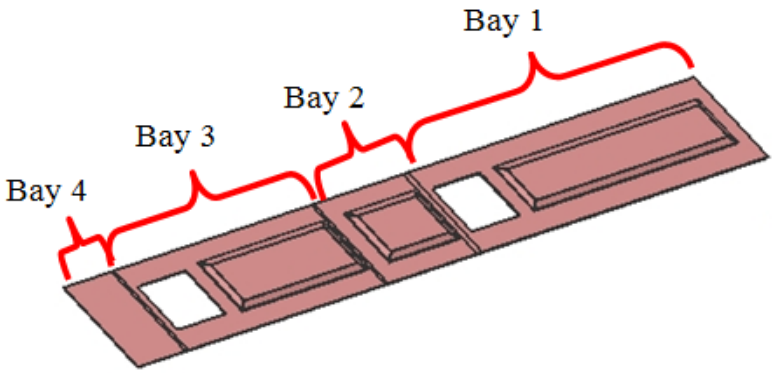

Figure 3.7 Lower Skin

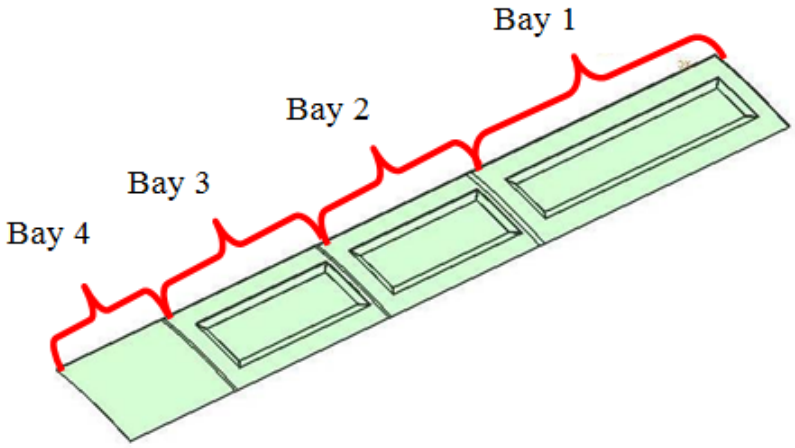

Figure 3.8 Upper Skin

The skins were modeled with manufacturing constraints. In the scenario of manufacturing of a skin, skin is produced in two cycles, because of core material usage. In the first cycle, the plies below honeycomb core are laid in the tool and are cured. In the second cycle, film adhesive is laid up on the cured part. Then the honeycombs are located and core stabilization process is done by smearing a special resin around the cores. After core stabilization, film adhesive is laid on honeycomb and the other plies are laid over honeycomb core. Whole laminate is

then cured. This process is called as co-bonding. In co-bonding, the cured material and uncured materials are bonded. The woven fabric plies are used for outer surfaces because of higher tolerance to damage.

The ply sequences for lower and upper skin laminates are given in Table 3.2. In the table the italic and underlined plies are UD fabric, other plies are woven fabric. Table 3.3 shows the total number of plies and the thicknesses of each bay.

Table 3.2 The Ply Sequence of Lower and Upper Skin

BAY 1	45/*0*/45/45/*0*/45/Core/45/0/0/45
BAY 2	45/*0*/*0*/45/Core/45/0/0/45
BAY 3	45/*0*/45/Core/45/0/45
BAY 4	45/45/Core/45/45

Table 3.3 The Total Number of Ply and The Thickness Information of the Bays

	BAY 1	BAY 2	BAY 3	BAY 4
Woven Number	8	6	5	4
UD Number	2	2	1	0
Thickness [mm]	2.808	2.248	1.784	1.32

Front and Rear Spar:

There were four bays in front and rear spar, with bays bounded by ribs, shown in Figure 3.9. Thickness changed spanwise, kept constant in each bay. The thickness of the cap and the webs for the spar sections were same.

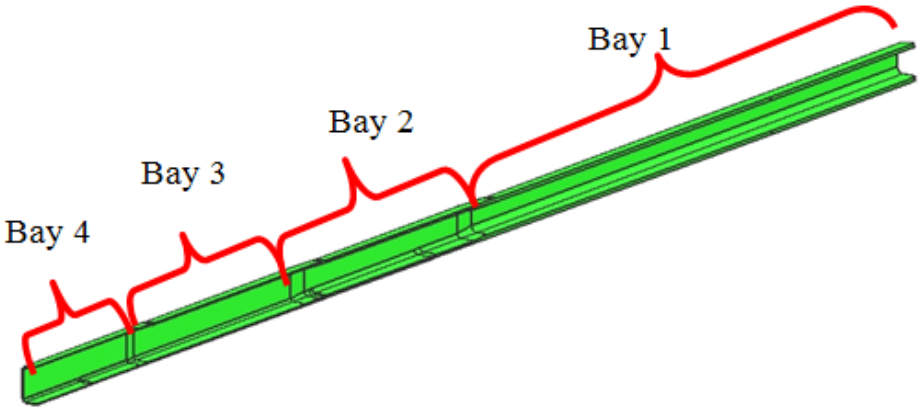

Figure 3.9 Front and Rear Spar

In the scenario of manufacturing of a spar, the plies were laid on the tool and then cured.

The sequences for front and rear spar are given in Table 3.4; where italic and underlined plies are UD fabric, other plies are woven fabric. Table 3.5 shows total number of plies and thickness for each bay.

Table 3.4 The Ply Sequence of Front and Rear Spar

BAY 1	$[45/\underline{0}/45/\underline{0}/0/\underline{0}/45/\underline{0}/45]_S$
BAY 2	$[45/\underline{0}/\underline{0}/0/45/\underline{0}]_S$
BAY 3	$[45/\underline{0}/0/0/\underline{0}/45]$
BAY 4	[45/0/45]

Table 3.5 The Total Number of Ply and the Thickness Information of the Bays

	BAY 1	BAY 2	BAY 3	BAY 4
Woven Number	10	6	4	3
UD Number	8	6	2	0
Thickness [mm]	4.272	2.784	1.12	0.84
Cap Length	20	20-15	15	15

Ribs:

All ribs used in the wing design has the same thickness. The thickness of the cap and the webs for the rib sections were also kept same. The ribs in torque box are shown in Figure 3.10.

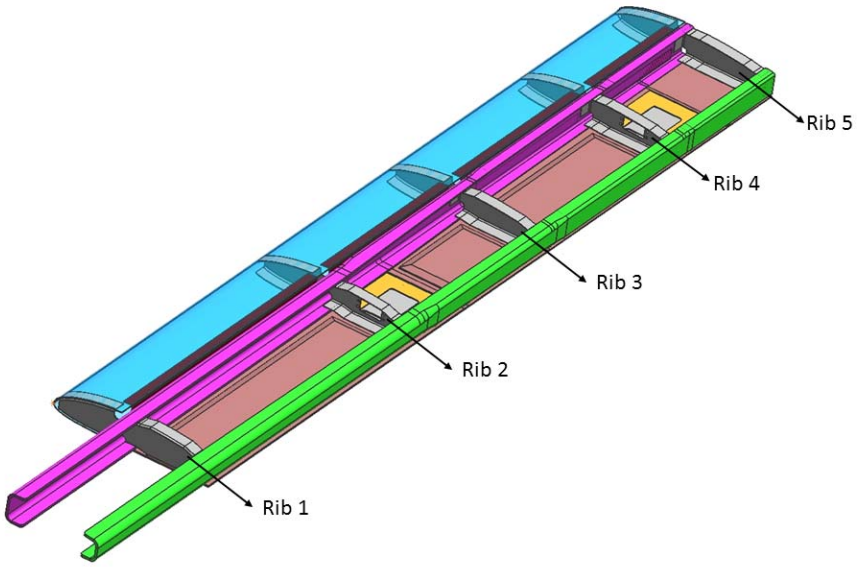

Figure 3.10 Ribs in the Torque Box

Ply sequences for ribs are shown in Table 3.6. Ply numbers, thickness and cap length information is given in Table 3.7.

Table 3.6 The Ply Sequence of the Ribs in the Torque Box

Rib 1	[45/0/45]
Rib 2	[45/0/45]
Rib 3	[45/0/45]
Rib 4	[45/0/45]
Rib 5	[45/0/45]

Table 3.7 The Ply Number, Thickness and Cap Length Information of the Ribs in the Torque Box

	Rib 1	Rib 2	Rib 3	Rib 4	Rib 5
Woven Number	3	3	3	3	3
UD Number	0	0	0	0	0
Thickness [mm]	0.84	0.84	0.84	0.84	0.84
Cap Length [mm]	30	30	30	30	30

Leading Edge:

The leading edge skin has uniform thickness. The leading edge skin connection to torque box was done by leading edge brackets. Leading edge ribs and leading edge brackets were bonded to front spar and the leading edge skin was bonded to leading edge brackets and leading edge ribs by adhesive. Leading edge components are shown in Figure 3.11.

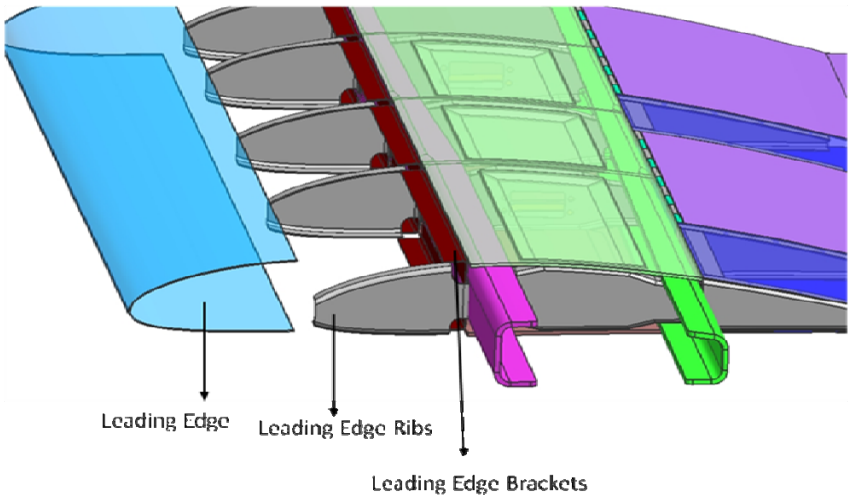

Figure 3.11 Leading Edge Connection Concept

The sequence of the leading edge skin is [45/0/0/45], the sequences of the brackets are [45/0/45] and the sequences of the leading edge ribs are [45/0/0/45].

Table 3.8 The Ply Number and Thickness Information of the Structural Members in the Leading Edge

	Leading Edge Skin	Leading Edge Brackets	Leading Edge Ribs
Woven Number	4	3	4
Thickness [mm]	1.12	0.84	1.12

Trailing Edge:

The trailing edge skin has uniform thickness. The trailing edge skin connection concept was similar to the leading edge concept, which was done by brackets. Trailing edge ribs and trailing edge brackets were bonded to rear spar and the

trailing edge skin was bonded to trailing edge brackets and trailing edge ribs by adhesive. Trailing edge components are shown in Figure 3.12.

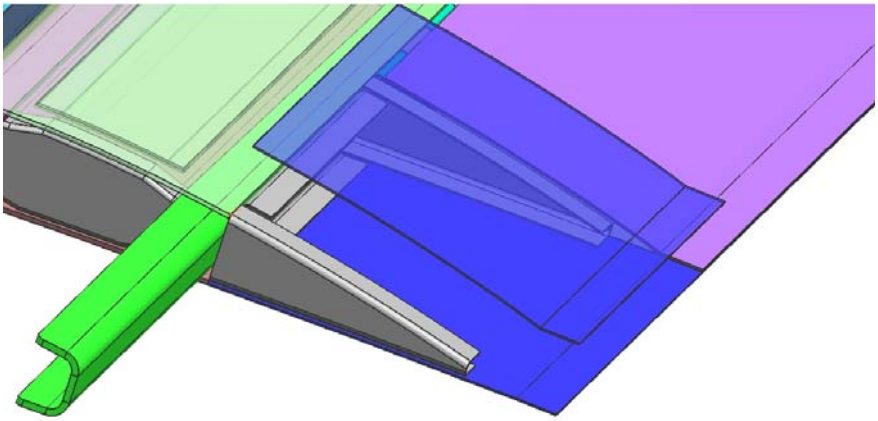

Figure 3.12 Trailing Edge Connection Concept

The sequence of the trailing edge skins are [45/0/0/45], the sequence of trailing edge brackets are [45/0/0/45] and the sequence of the trailing edge ribs are [45/0/45].

Table 3.9 The Ply Number and Thickness Information of the Structural Members in the Trailing Edge

	Trailing Edge Skin	Trailing Edge Brackets	Trailing Edge Ribs
Woven Number	4	4	3
Thickness (mm)	1.12	1.12	0.84

Doublers and Covers:

The doublers, shown in Figure 3.13, are bonded to lower skin by paste adhesive. The cover and doubler connection was done by nutplates MS21076. Cover and nutplates are shown in Figure 3.14 and Figure 3.15 respectively.

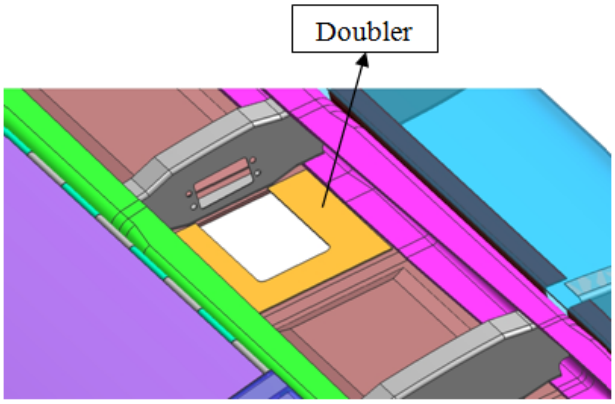

Figure 3.13 General View of a Doubler in Torque Box

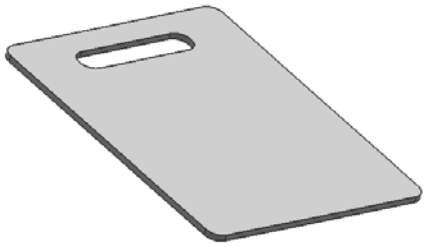

Figure 3.14 General View of Covers, Used in Lower Skin

Figure 3.15 MS21076: The Nutplate, Used in Doubler and Cover Connection

Schematic representation of the connection using nutplates is shown in Figure 3.16.

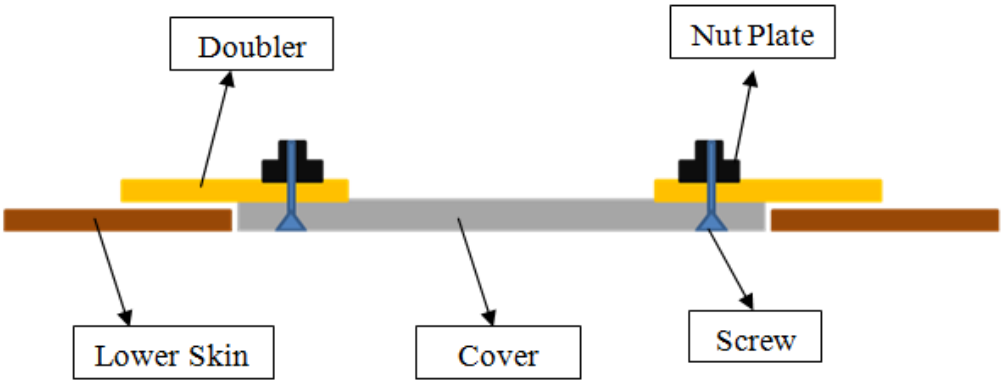

Figure 3.16 Doublers - Cover Connection Concept Used in Lower Skin

The ply sequence of the doublers are [45/0/0/45] with ply thickness given in Table 3.10. The ply sequence of Cover laminate and ply information is given in Table 3.11 and Table 3.12.

Table 3.10 The Ply Number and Thickness Information of the Doublers

	Doubler
Woven Number	4
Thickness (mm)	1.12

Table 3.11 The Ply Sequence of the Covers

Cover I	$[45/0/45/0]_S$
Cover II	[45/0/45/0/45]

Table 3.12 The Ply Number and Thickness Information of the Covers

	Cover I	Cover II
Fabric Number	8	5
Thickness (mm)	2.24	1.4

3.4.1.2 Control Surface of the Prepreg Wing Model

The detailed view of the control surface of prepreg wing model is given in Figure 3.17.

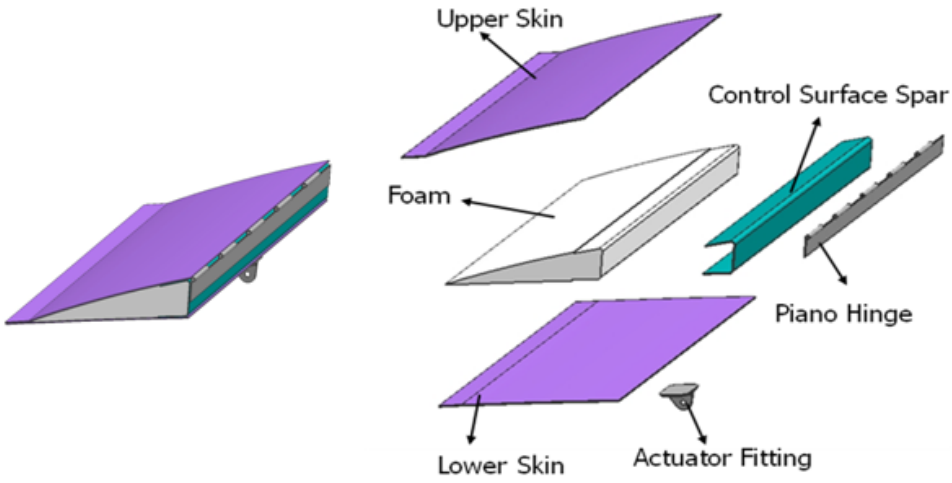

Figure 3.17 Detailed View of the Prepreg Control Surface Model

Structural members for control surface are upper skin, lower skin, control surface spar and actuator fitting.

In the scenario of manufacturing of control surface, control surface skin is manufactured in one cycle, since it doesn't have core. In order to provide adequate strength and reduce weight at the control surface, foam is used between the skins. The foam used is Rohacell 71 A [11]. All connections between the structure members are done by paste adhesive.

The ply sequences of the members are given in Table 3.13 and ply number and thickness are shown in Table 3.14.

Table 3.13 The Ply Sequences of Structural Members in Control Surface

Skins	[45/0/0/0/45]
Spar	[45/0/0/45]

Table 3.14 The Ply Number and Thickness Information of Structural Members in Control Surface

	Skins	Spar
Woven Number	4	4
UD Number	1	0
Thickness [mm]	1.304	1.12

3.4.2 Wet Lay-up Wing Model

In the wet lay-up model only glass fibers were used for structural members. The core material used was foam, which is Rohacell 71 A.

The general view of the wing is shown in Figure 3.18.

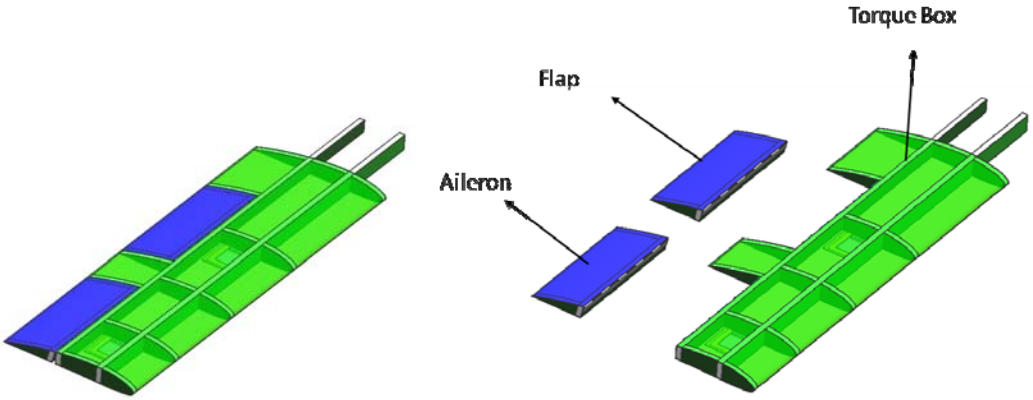

Figure 3.18 General View of Wet Lay-up UAV Wing Model

3.4.2.1 Torque Box of Wet Lay-up Wing Model

The detailed view of the torque box for the wet lay-up composite design is given in Figure 3.19.

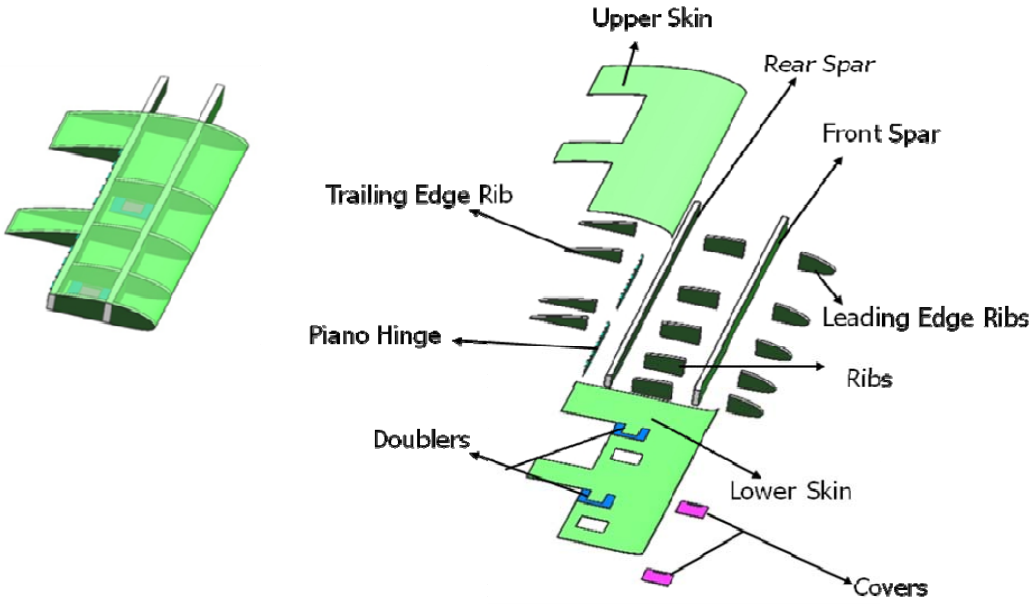

Figure 3.19 Detailed View of the Wet Lay-up Torque Box Model

The following paragraphs detail the structural members utilized in the design of wet lay-up composite UAV wing.

Lower and Upper Skin:

The general view of upper and lower skin is shown in Figure 3.20. The thicknesses of the skins were constant through the span.

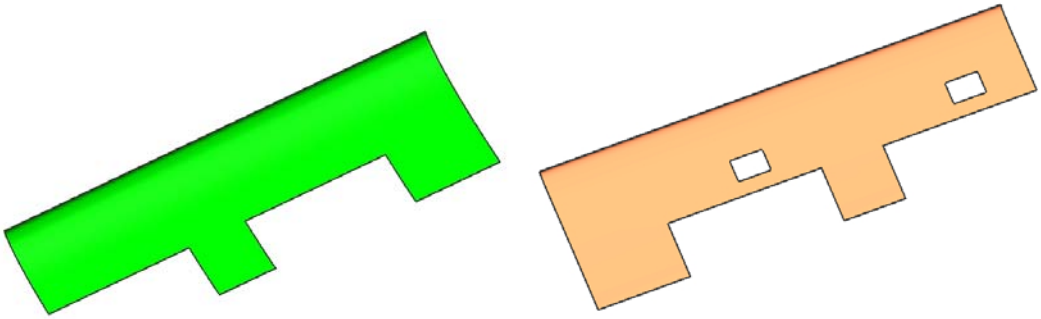

Figure 3.20 Upper and Lower Skin

In scenario of manufacturing of skins, upper and lower skins are manufactured in one cycle.

The laminates were symmetric with respect to middle axis. The ply sequences of the skins are [45/0/0/45], ply number and thickness information is given in Table 3.15.

Table 3.15 The Ply Number and Thickness Information of Upper and Lower Skin

	Upper and Lower Skin
Ply Number	4
Thickness (mm)	1.12

Spars and ribs:

Spars and ribs, shown in Figure 3.21 and Figure 3.22, were composed of foam core and ply.

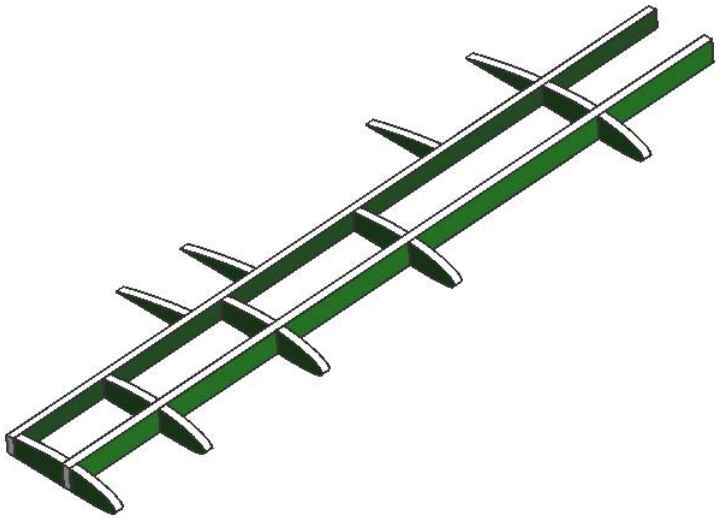

Figure 3.21 Front Spar, Rear Spar and Ribs

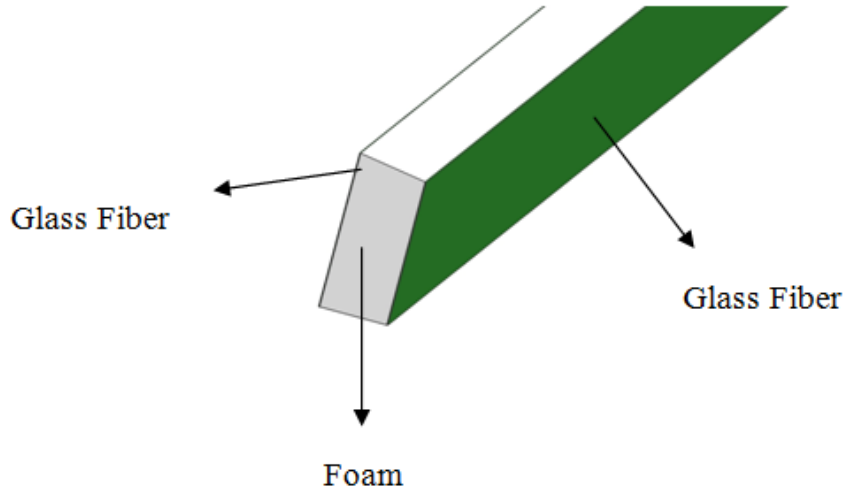

Figure 3.22 Composition of Spars and Ribs

The ply sequences of the members were [0/Core/0] and information is given in Table 3.16.

Table 3.16 The Ply Number, Core Thickness and Laminate Thickness Information

	Spars and Ribs
Ply Number	2
Core Thickness (mm)	10
Thickness (mm)	20.6

Doublers and Covers:

The general view of doubler and cover, used in the torque box of the wet lay-up wing model is shown in Figure 3.23.

Figure 3.23 General View of Doublers and Ribs, Used in Torque Box

Doubler and cover connection was done via the doubler and cover connection concept of the prepreg model, as explained in section 4.2.1.1.

The ply sequences of the members are [45/0/0/45] and ply thickness information is given in Table 3.17.

Table 3.17 The Ply Number and Laminate Thickness Information

	Covers and Doublers
Ply Number	4
Thickness (mm)	1.12

3.4.2.2 Control Surface of Wet Lay-up Model

The detailed view of the control surface of wet lay-up wing model is given in Figure 3.24 .

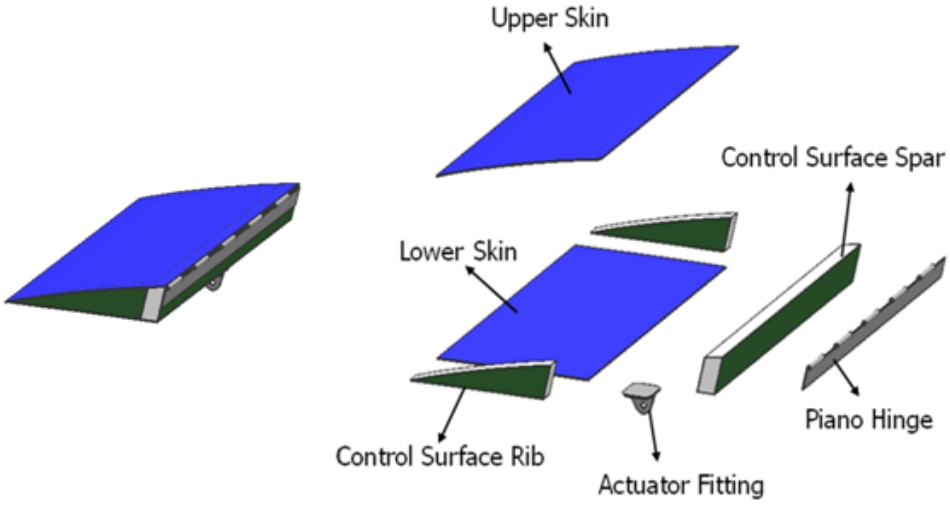

Figure 3.24 Detailed View of the Wet Lay-up Control Surface Model

Structural members for the control surface shown in Figure 3.24 are upper skin, lower skin, control surface, spar, control surface rib, actuator fitting.

The ply sequences of the control surface skins are [45/0/0/45] the ply sequences of the control surface spars and ribs are [0/Core/0]. Ply number, core thickness and laminate thicknesses information are given in Table 3.18.

Table 3.18 The Ply Number, Core Thickness and Laminate Thickness Information

	Upper and Lower Skin	Spars and Ribs
Ply Number	4	2
Thickness [mm]	1.12	20.6
Core Thickness [mm]	-	20

3.4.3 Aluminum Wing Model

Aluminum in 2XXX and 7XXX alloy series were used in modeling. 90% of structured members were designed from Aluminum Clad Sheet 2024 T3 and 10% of them were designed from Aluminum 7075-T651.

The general view of the aluminum wing is shown in Figure 3.25.

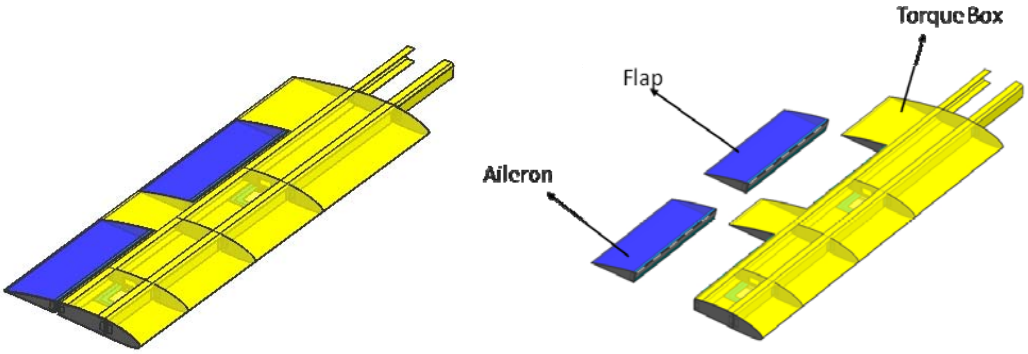

Figure 3.25 General View of Aluminum Model

3.4.3.1 Torque Box of Aluminum Wing Model

Detailed view of the torque box for is given in Figure 3.26.

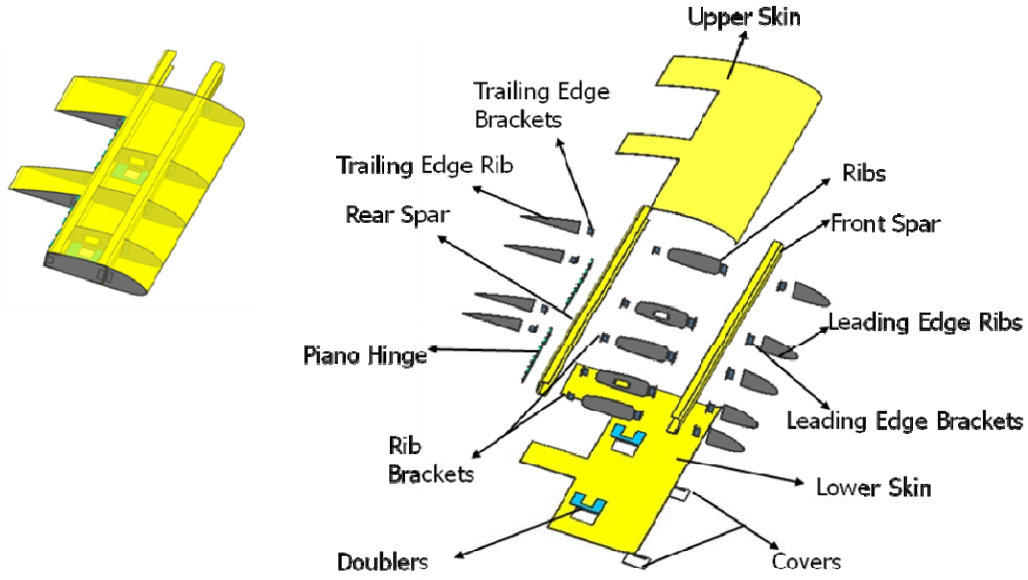

Figure 3.26 Aluminum Torque Box Design

The following paragraphs detail the structural members utilized in the design of aluminum UAV wing.

Lower and Upper Skin:

The upper and lower skins are shown in Figure 3.27.

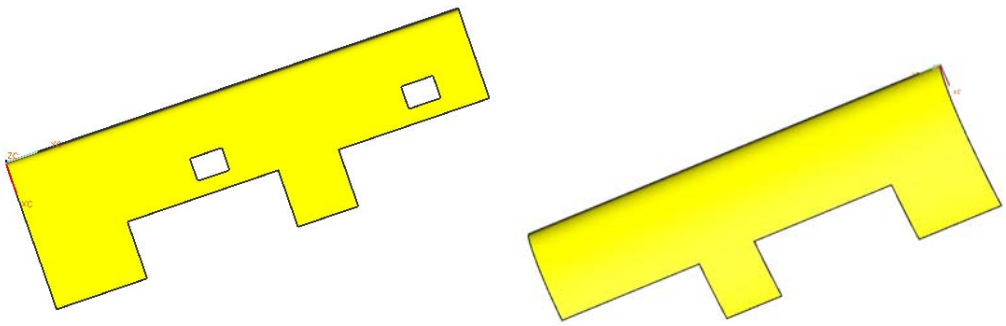

Figure 3.27 Lower and Upper Skins of Aluminum Wing Model

In the manufacturing scenario of the skins, they are manufactured from Aluminum Clad Sheet 2024 T3 by “drawing” method. The thickness is 1.42 mm.

Spars:

Figure 3.28 shows the front and rear spar of the aluminum wing model.

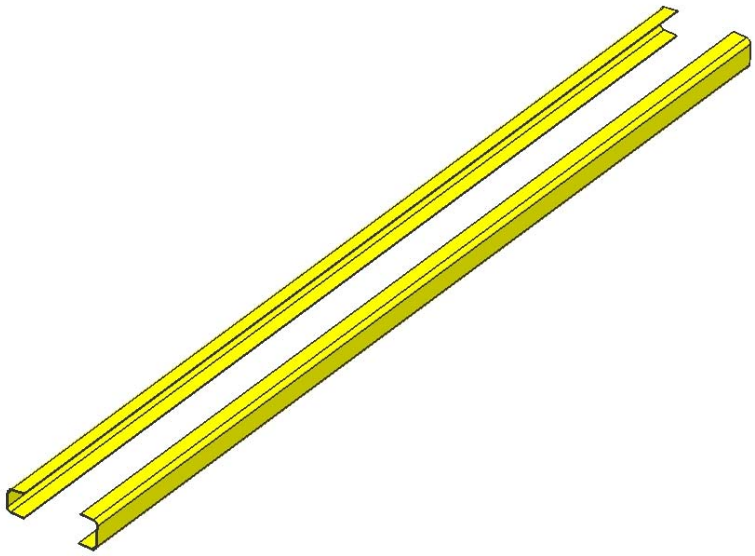

Figure 3.28 Front and Rear Spar of Aluminum Wing Model

They can be manufactured from Aluminum Clad Sheet 2024 T3 by “bending” method. The thickness is 1.803 mm, and cross section is shown in Figure 3.29.

Figure 3.29 Front and Rear Spar Cross-sections

Ribs:

Trailing edge rib, rib and leading edge rib of aluminum wing model are shown in Figure 3.30.

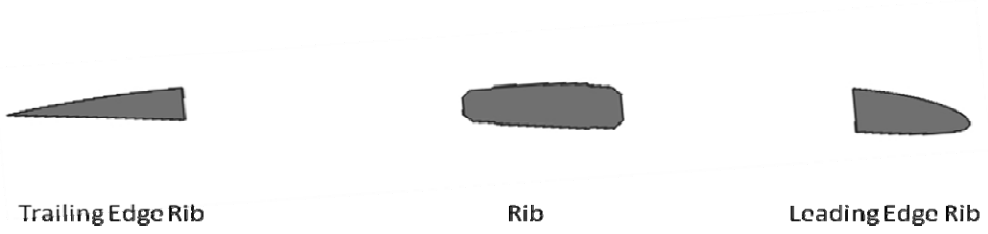

Figure 3.30 The Ribs of Aluminum Wing Model

They are assumed to be manufactured from Aluminum Clad Sheet 2024 T3 by cutting method. The thickness is 1.2 mm.

Doublers and Covers:

Figure 3.31 shows the doubler and cover of the torque box.

Figure 3.31 General View of Doubler and Cover

They can be manufactured from Aluminum Clad Sheet 2024 T3 by drawing method and cutting method. The doubler thickness is 1.06 mm and cover thickness is 1.42 mm. Doubler and cover connection was done via the doubler and cover connection concept of the prepreg model, as explained in section 4.2.1.1.

Brackets:

Brackets, shown in Figure 3.32 and Figure 3.33, provide the connection of ribs to front and rear spar.

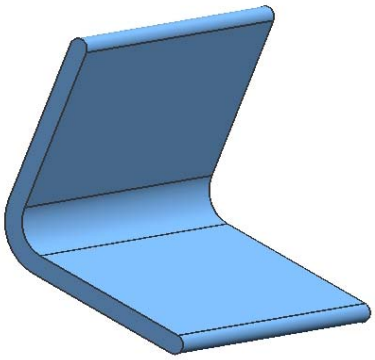

Figure 3.32 General View of Bracket, Used in Aluminum Wing Model

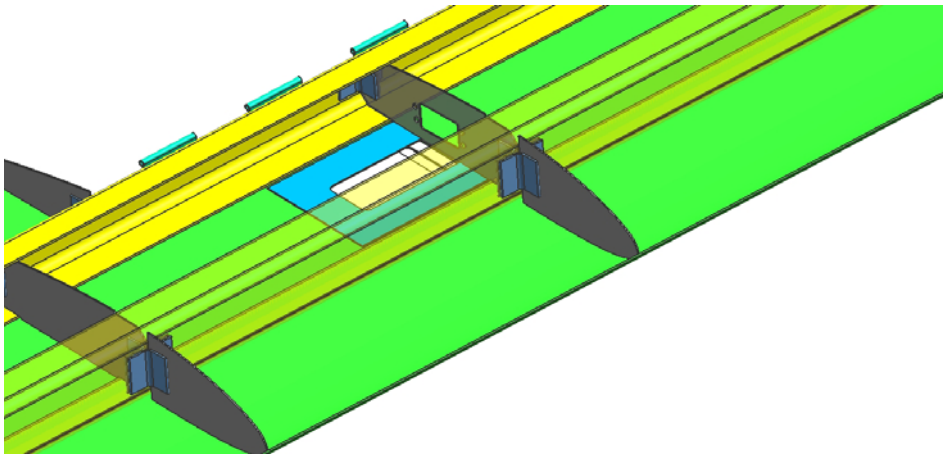

Figure 3.33 Connection Concept of Ribs to Spars

The brackets were manufactured from Aluminum 7075-T651 by “extrusion” method. The thickness is 1.65 mm. The cross section of the bracket is shown in Figure 3.34.

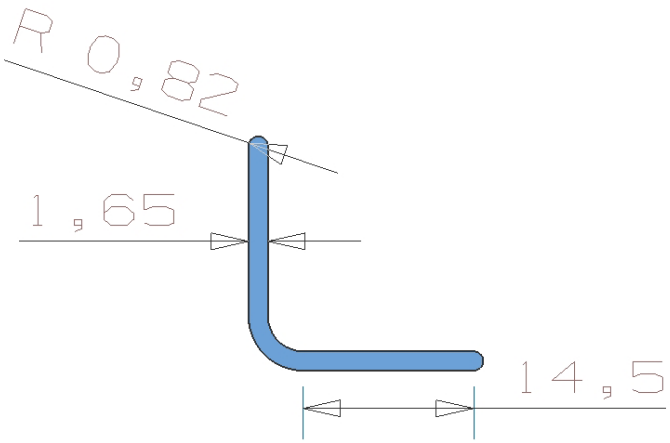

Figure 3.34 Bracket Dimension

3.4.3.2 Control Surfaces of Aluminum Wing Model

The detailed view of the control surface of wet lay-up wing model is given in Figure 3.35.

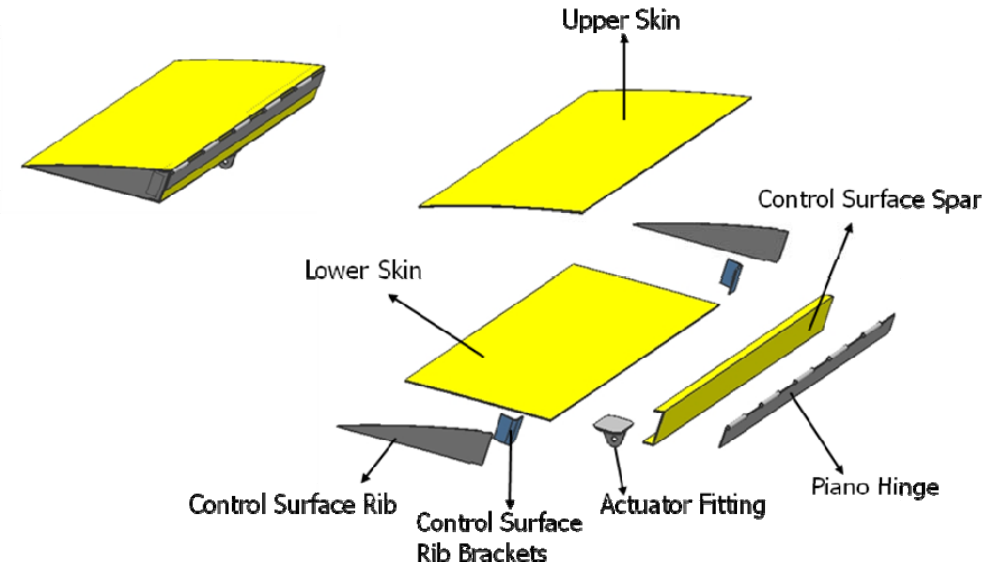

Figure 3.35 Detailed View of the Aluminum Control Surface Model

Structural members are upper skin, lower skin, control surface spar, control surface rib, control surface rib brackets and actuator fitting. The control surface skin, control surface spar and control surface rib are shown in Figure 3.36.

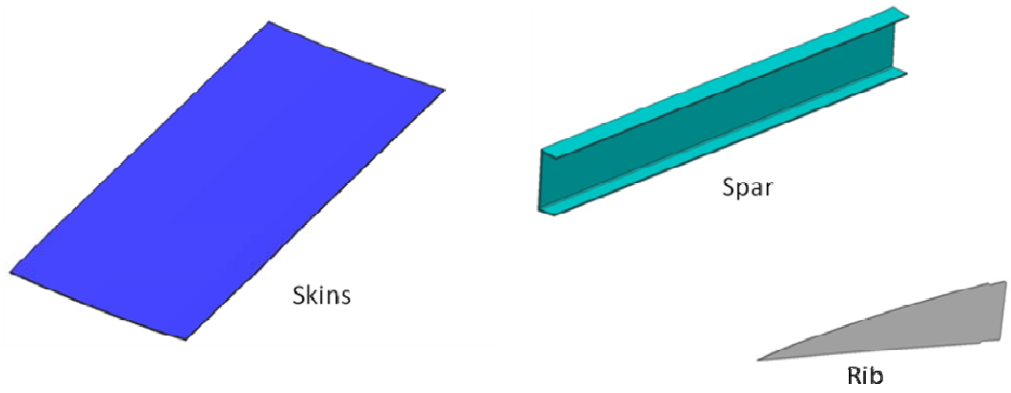

Figure 3.36 The Structural Members of Control Surface of Aluminum Wing Model

It is assumed that the upper and lower skins for control surfaces are manufactured from Aluminum Clad Sheet 2024 T3 by "drawing" method. Control surface spar and brackets are assumed to be manufactured from Aluminum 7075-T651 by "extrusion" method and the ribs are assumed to be manufactured from Aluminum Clad Sheet 2024 T3 by "cutting" method. Thickness for control surface components are given in Table 3.19.

Table 3.19 The Thickness Information of Structural Members in Control Surface

	Thickness (mm)
Skins	1.27
Spar	1.42
Ribs	1.2

3.5 Conclusion

3.5.1 Comparison between Composite Models:

Constraints lead to major differences in production between the wet lay-up model and prepreg model.

In the prepreg model; the leading edge skin, upper skin, lower skin and trailing edge skins are manufactured separately. The leading edge skin is manufactured in one piece with smooth surface by female tool. Then, the upper skin and lower skin, which are sandwich laminates, are manufactured. Finally trailing edge skins are manufactured.

In the wet lay-up model, the upper and lower skin are manufactured as one piece by using female tools in order to obtain smooth aerodynamic surface as shown in Figure 3.37. However the connection upper and lower skin, requires the lay ups of extra patch plies on the leading edge as shown in Figure 3.38. This brings extra weight penalty and also causes rough leading edge surface which is not a desirable aerodynamic property.

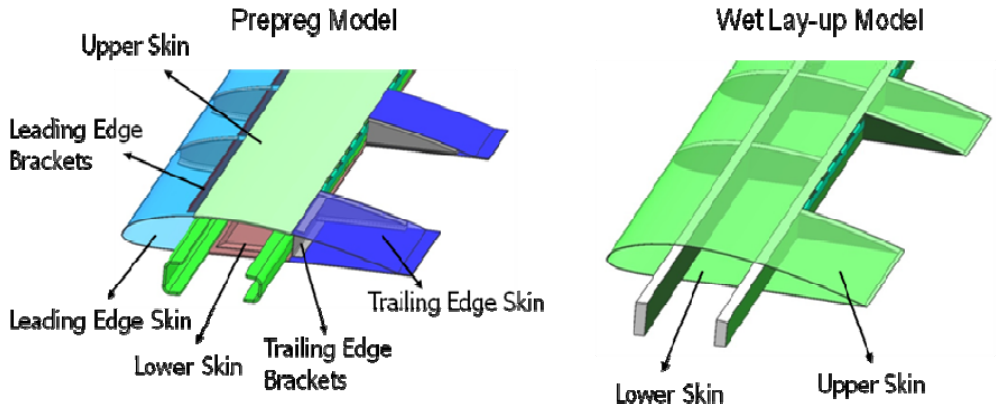

Figure 3.37 Comparison of the Skins of Composite Wing Models

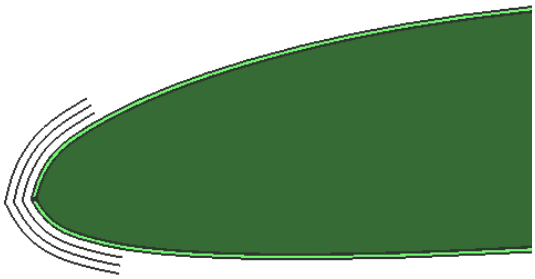

Figure 3.38 Patch Plies of Leading Edge in the Wet Lay-up Model

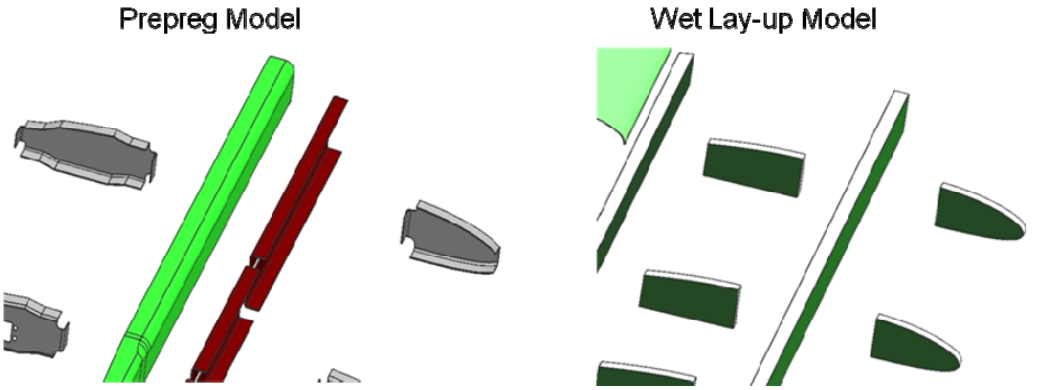

Figure 3.39 Comparison of the Spars and Ribs of Composite Wing Models, Close-up View

The composite structural members with U profiles, such as spars and ribs, can be manufactured with prepreg material. The wet lay-up approach cannot be used for this type of members because of the excess resin build-up in corners. Thus, in order to account for the loss of inertia provided by spar and rib caps, the core materials are used to generate the thickness to increase the inertia. Figure 3.39 shows these differences in a close-up view of spars and ribs for these wing models.

3.5.2 General Comparison

According to initial sizing, the mass of the wing each model is calculated. Table 3.20 gives the total mass of each wing model according to the results of initial sizing. For wet lay-up wing model, about the 0.5 kg change was attributed to the resin applicant.

Table 3.20 The Total Mass of Different Wing Structural Models after the Initial Sizing

	Mass (kg)
Prepreg	6.7
Aluminum	8.9
Wet Lay-up	5-5.5

As it can be seen from Table 3.20 that aluminum model was the heaviest one. Hence the aluminum model was eliminated and therefore no structural analysis will be conducted for the aluminum model.

CHAPTER 4

FINITE ELEMENT MODELING AND LOAD APPLICATION

4.1 Introduction

In this chapter, Finite Element Modeling and Analysis of wing which was conducted by using MSC Patran and Nastran [8, 9] is presented. In addition, application of the aerodynamic loads which was obtained by considering the cruise condition and gust conditions, were interpolated to finite element mesh and applied to the wing [1, 2].

4.2 Finite Element Model Preparation

In order to perform Finite Element Modeling of the wing, the mold surfaces of the wing should be created, because composite modeling is based on first ply being the first one lyed on the mold. The mold surfaces were obtained by using Unigraphics NX. Figure 4.1 shows the mold surfaces in Unigraphics NX.

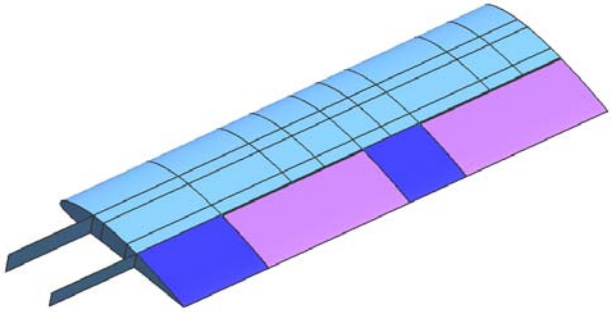

Figure 4.1 The Mold Surface created in Unigraphics NX

After the creation of mold surfaces, they were imported to MSC Patran, as seen in Figure 4.2.

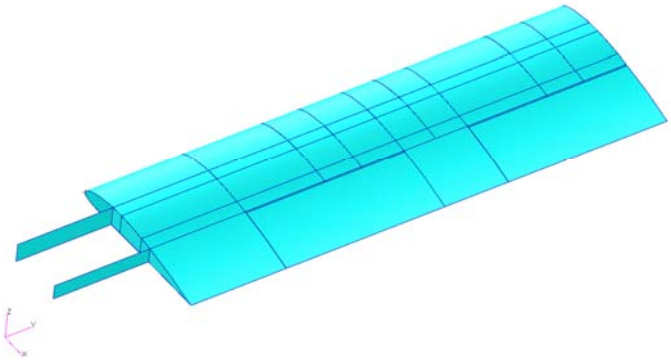

Figure 4.2 The Mold Surfaces in MSC Patran

The meshes were created, after the mold surfaces were obtained. The structural members in the wing are thin walled structures. Therefore, two dimensional (2D) elements were used. Skins, spars webs, ribs were modeled as 2D shell elements,

which have orthotropic properties. 3D type elements were not used. Figure 4.3 to Figure 4.5 show the meshed finite element model of the wing.

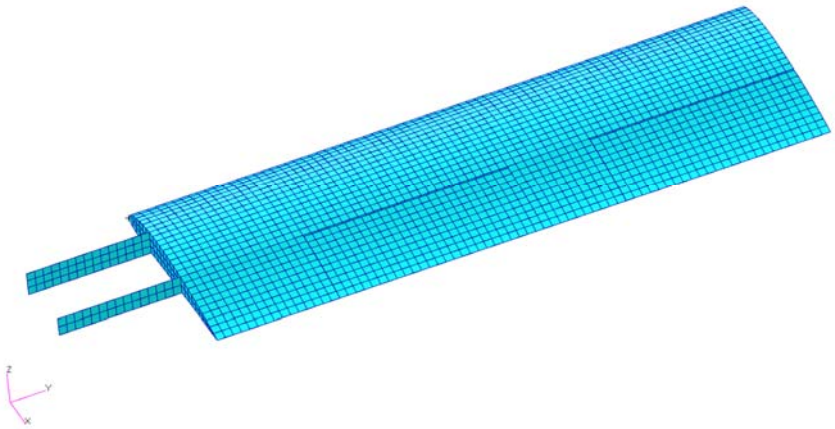

Figure 4.3 The General View of the Finite Element Model

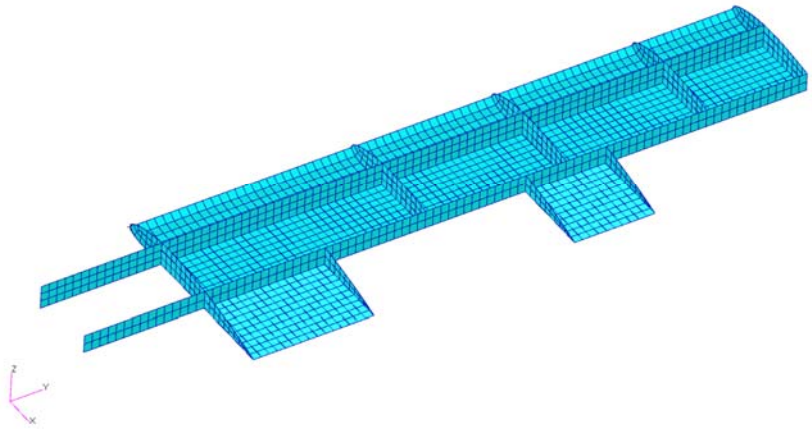

Figure 4.4 The Meshed Torque Box

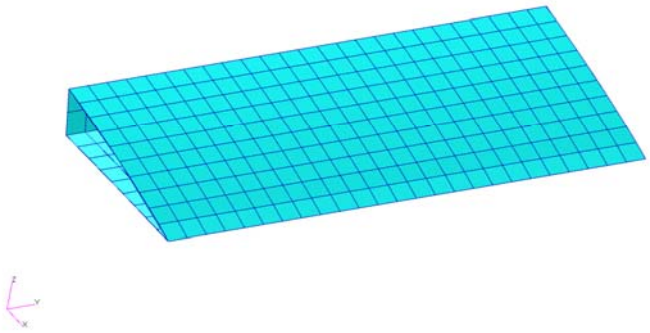

Figure 4.5 The Meshed Control Surface

Afterwards, the piano hinge connections were modeled. RBE2, multi point constraint elements were used in the modeling to connect nodes of control surface to rear spar to simulate rotating motion. This connection is shown in Figure 4.6.

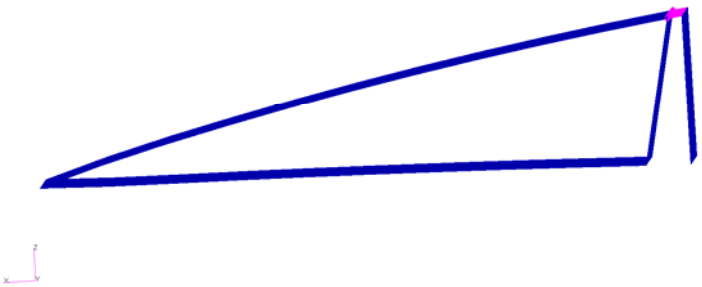

Figure 4.6 Finite Element Model of Piano Hinge

In order to identify and check each part, main parts of the wing were grouped. The structural elements were grouped as Upper Skin, Lower Skin, Front Spar, Rear

Spar, Ribs, Flap and Aileron. Figure 4.7 shows the colored meshes of the wing as result of grouping the structural members.

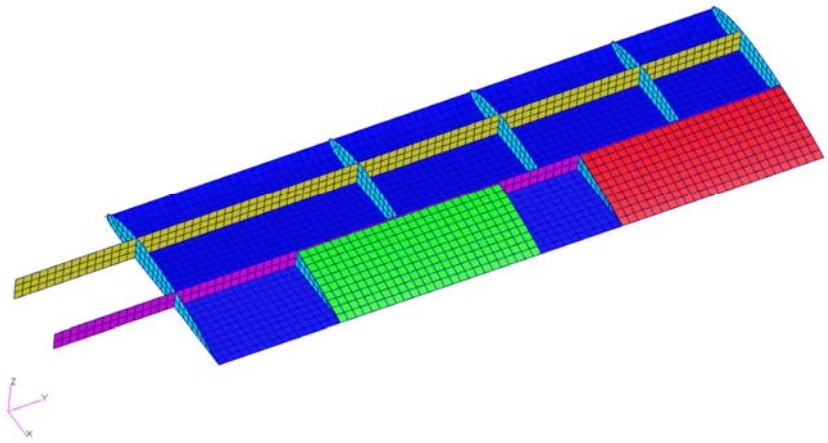

Figure 4.7 The Grouped Structural Members in Finite Element Model (Upper Skin was Removed for Better Visibility)

Finally, the Boundary Conditions to fix spar extensions in six degrees of freedom were created, as seen in Figure 4.8.

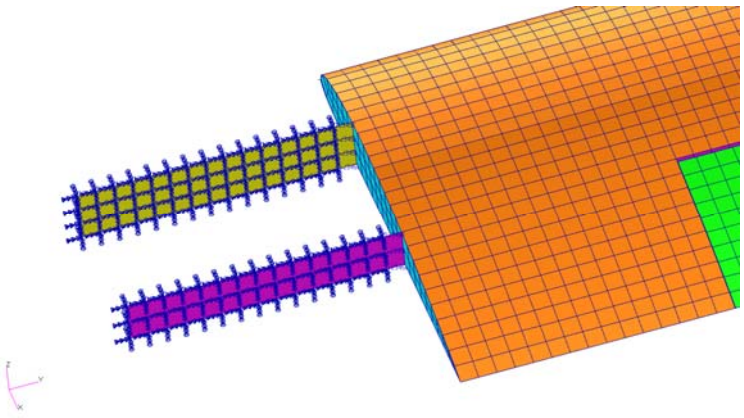

Figure 4.8 The Boundary Conditions of The Wing

4.3 Finite Element Model Properties

Up to this point wet lay-up and prepreg models have the same features, surface meshes, boundary conditions and control surface connection is modeled in the same manner. There are two main differences in further modeling; one is the material properties for structural members and the other one is that prepreg model has spar caps while wet lay-up doesn't.

2D orthotropic materials were created in order to determine the materials of wet lay-up and prepreg. The wet lay-up model was designed by using 7781 E-Glass Fabric, Araldite LY5052 Resin, Aradur HY5052 Hardener and Rohacell 71 A Foam. The material properties are given in Table 4.1.

Table 4.1 Material Properties for Wet Lay-up Design [1]

	7781 E-Glass Fabric, Araldite LY5052 Resin, Aradur HY5052 Hardener	Rohacell 71 A
Density	1772 [kg/m^3]	75 [kg/m^3]
Young's Modulus, E11	22.1 [GPa]	92 [MPa]
Young's Modulus, E22	22.4 [GPa]	92 [MPa]
Shear Modulus, G12	3.79 [GPa]	29 [MPa]
Shear Modulus, G23	2.96 [GPa]	29 [MPa]
Shear Modulus, G13	2.96 [GPa]	29 [MPa]
Ultimate Compression Strength	249 [MPa]	1.5 [MPa]
Ultimate Tensile Strength	369 [MPa]	2.8 [MPa]
Inter-laminar Shear Strength	33.21 [MPa]	-

Prepreg wing model was designed by using HexPly 8552 AS4 UD Carbon Prepregs and HexPly 8552 AGP 280-5H Woven Carbon Prepreg. The material properties of UD carbon prepreg and woven carbon prepreg are given in Table 4.2.

Table 4.2 Material Properties for Prepreg Design [10]

	HexPly 8552 AS4	HexPly 8552 AGP 280-5H
Density	1580 [kg/m^3]	1570 [kg/m^3]
Young's Modulus, E11	141 [GPa]	67 [GPa]
Young's Modulus, E22	8 [GPa]	66 [GPa]
Shear Modulus, G12	3.3 [GPa]	3.6 [GPa]
Shear Modulus, G23	2.6 [GPa]	2.8 [GPa]
Shear Modulus, G13	2.6 [GPa]	2.8 [GPa]
Ultimate Compression Strength	1531 [MPa]	924 [MPa]
Ultimate Tensile Strength	2207 [MPa]	876 [MPa]
Inter-laminar Shear Strength	128 [MPa]	79 [MPa]

The spar caps of the pregreg model were modeled as 1D elements, as shown in Figure 4.9 and Figure 4.10. Caps are modeled as rod elements to carry bending loads only.

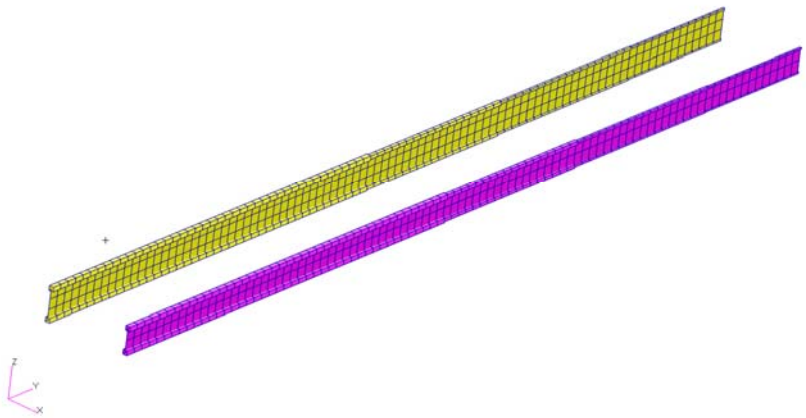

Figure 4.9 The General View of The Meshed Spars

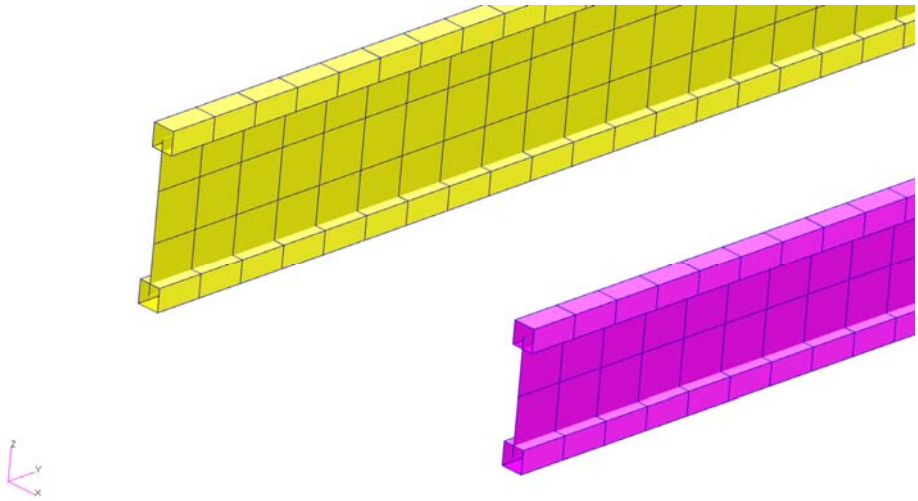

Figure 4.10 The Beam Elements of The Spar Caps

4.4 Aerodynamic Loading

The cruise condition and gust condition of aerodynamic loading was applied to the wing as element uniform pressure [1, 2]. Gust loading and pull-down

maneuver loading for the wing is obtained as five times cruise loading [1, 2]. Figure 4.11, Figure 4.12 and Figure 4.13 show the cruise condition load on the wing with aerodynamic meshes. This pressure distribution is obtained by CFD solution via ANSYS/FLUENT [2].

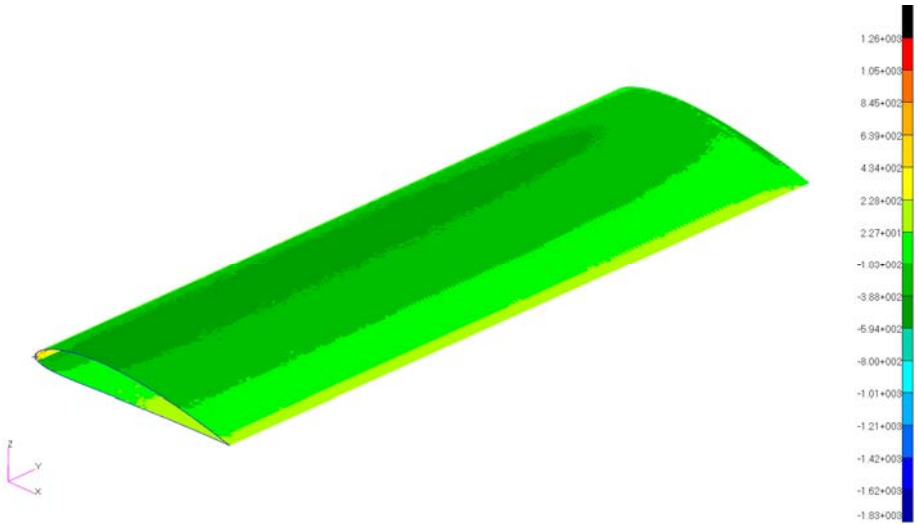

Figure 4.11 General View of Cruise Condition Pressure Load Contours, Aerodynamic Mesh [Pa]

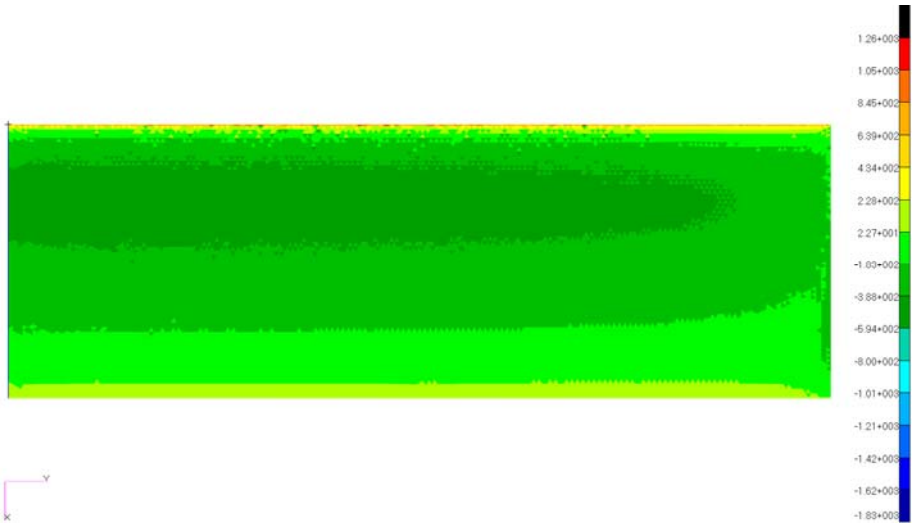

Figure 4.12 Cruise Condition Pressure Load Contours for Upper Skin, Aerodynamic Mesh [Pa]

Figure 4.13 Cruise Condition Pressure Load Contours for Lower Skin, Aerodynamic Mesh [Pa]

Pressure loading is imported into Patran with aerodynamic meshes. Aerodynamic mesh is formed with tria elements much smaller in size compared to quad elements used in finite element mesh, shown in Figure 4.14 and Figure 4.15. Thus an interpolation is employed in order to transfer loads into finite element model.

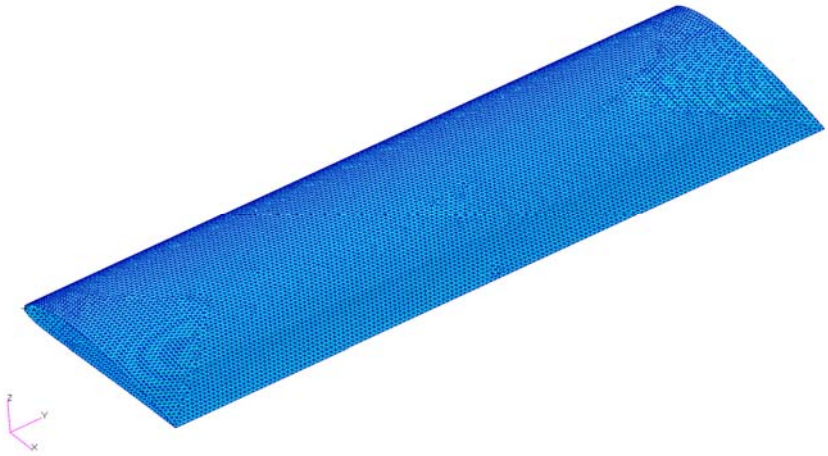

Figure 4.14 Aerodynamic Mesh for Wing

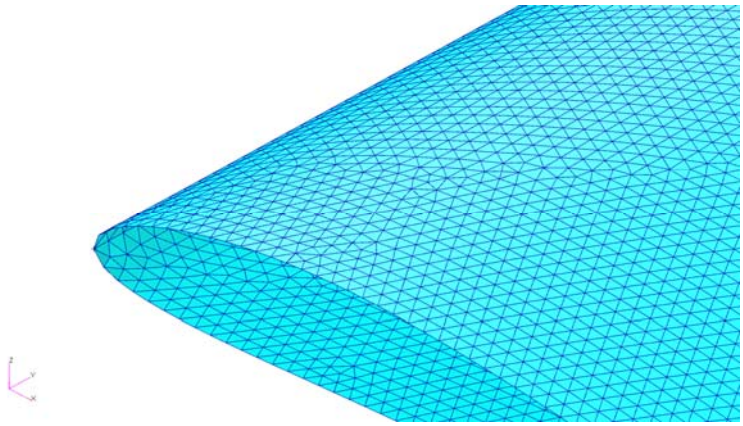

Figure 4.15 Aerodynamic Mesh for Wing (Close-up View of Leading Edge)

Interpolation is done with the help of Patran FEM fields. Scalar, continous interpolation function is calculated by Patran for a spatial field, shown in Figure 4.16.

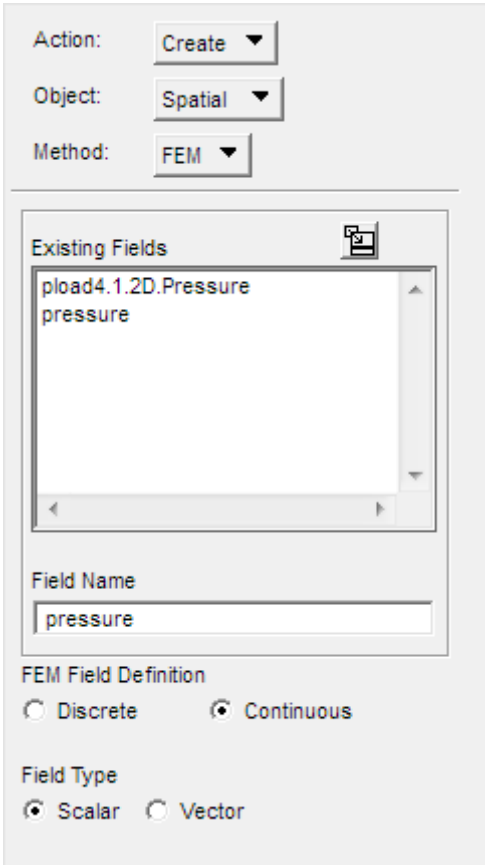

Figure 4.16 Spatial Field Creation for Interpolation

When the field carrying interpolation data is formed, this field can be selected in the element uniform pressure application as shown in Figure 4.17 and Figure 4.18.

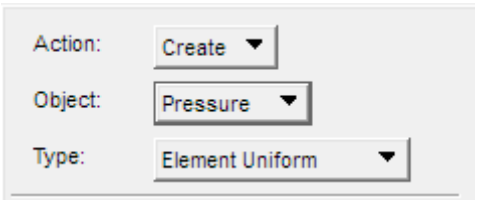

Figure 4.17 Element Uniform Pressure Creation

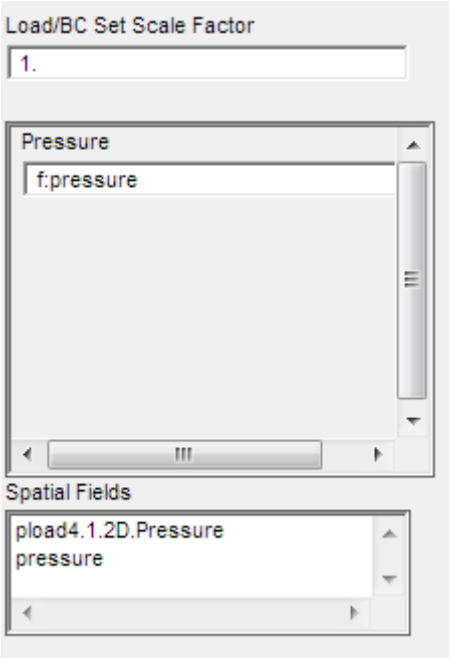

Figure 4.18 Element Uniform Pressure, Spatial Field Selection

Pressure field is interpolated to finite element meshes and applied to elements. Pressure distribution applied to finite element wing model is shown in Figure 4.19 to Figure 4.21.

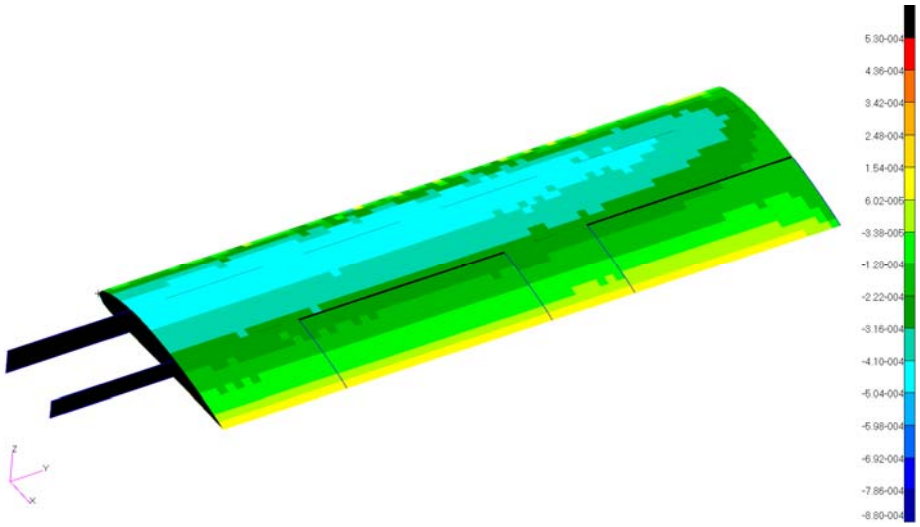

Figure 4.19 General View of Cruise Condition Pressure Load Contours, Finite Element Mesh [MPa]

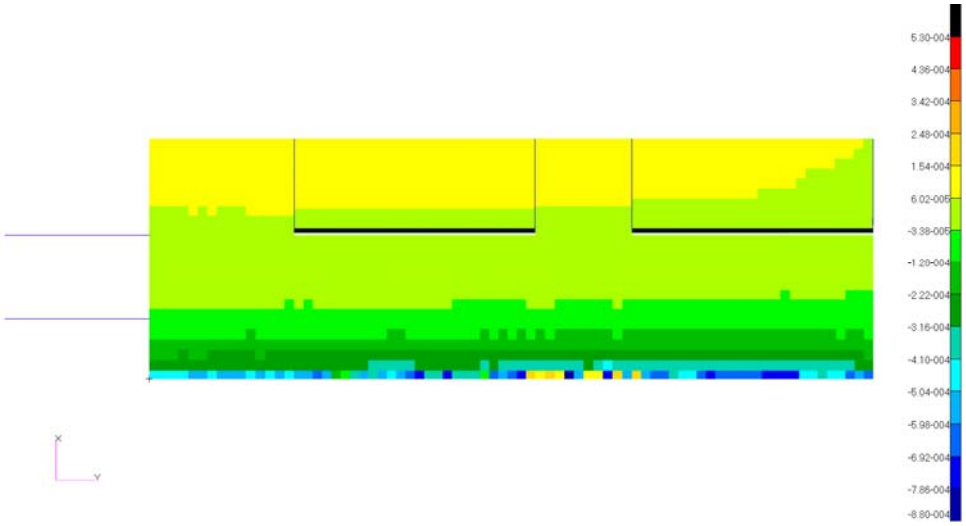

Figure 4.20 Cruise Condition Pressure Load Contours for Lower Skin, Finite Element Mesh [MPa]

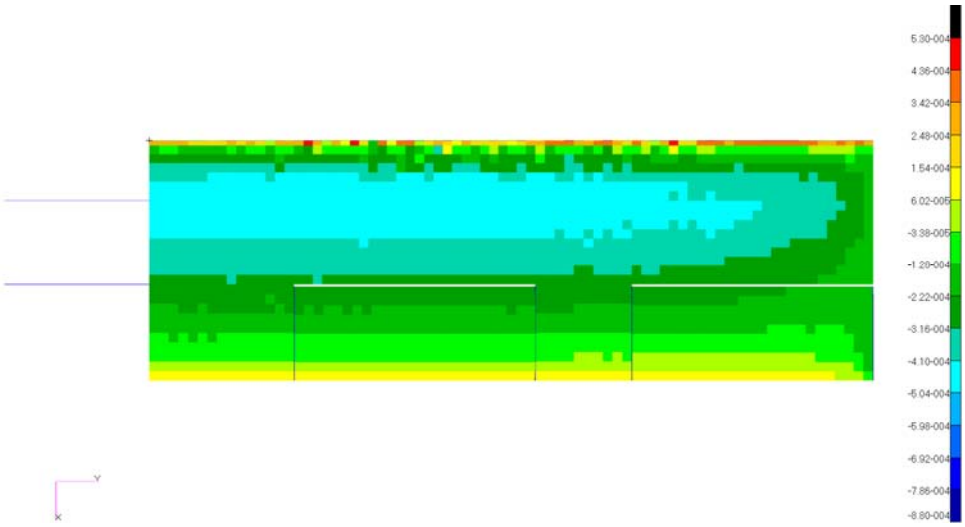

Figure 4.21 Cruise Condition Pressure Load Contours for Upper Skin, Finite Element Mesh [MPa]

4.5 Conclusion

The finite element models of wet lay-up wing model and prepreg wing model were created. The aerodinamic loads, which are under cruise flight condition and gust condition, were interpolated from aerodynamic mesh to finite element mesh.

CHAPTER 5

STRUCTURAL ANALYSIS

5.1 Introduction

The structural static stress analysis of wet lay-up wing model and prepreg wing model were performed in this chapter. MSC Patran and Nastran [8, 9] were used during the analysis. The optimum design was chosen.

5.2 The Structural Analysis of Wet Lay-up Wing Model

Finite Element Model of Wet Lay-up Wing was analyzed with the ply sequences, which were assumed before, for cruise and gust conditions.

Figure 5.1 shows the displacement result of the wet lay-up wing model under the cruise condition. The maximum displacement at the tip was 92.8 mm. As can be seen from the displacement results, it is highly likely that the wing may undergo failure.

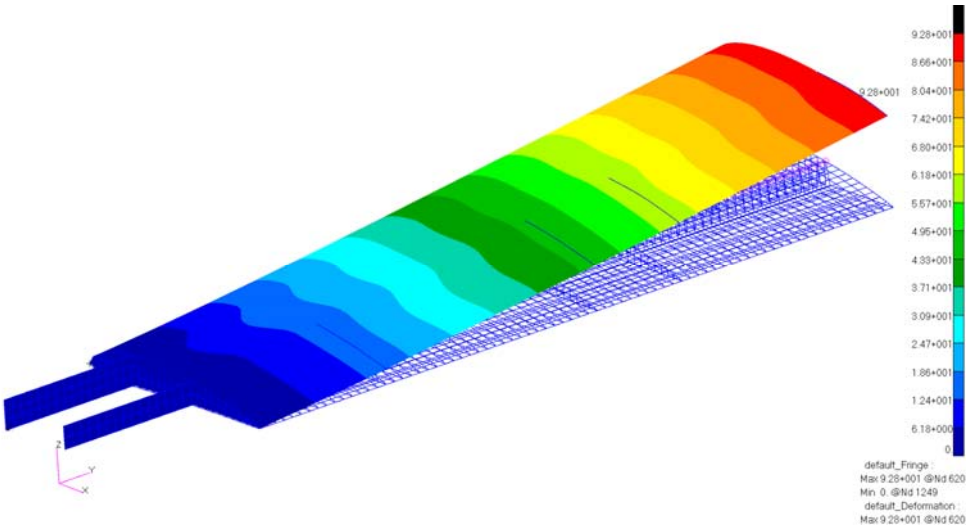

Figure 5.1 Displacement Result of Initial Wet Lay-up Wing Model in Cruise Condition [mm]

The failure can be checked by the stress distribution on the structural members. The Ultimate Tensile Strength of the 7781 E-Glass Fabric is 369 MPa. The maximum stress on the spars and ribs were 177 MPa, as seen in Figure 5.2 and the maximum stress on second and third layers of the lower skin was 305 MPa, as seen in Figure 5.3. However, Figure 5.4 shows that the maximum stress on second and third layers of upper skin was 742 MPa. Hence it can be concluded that the design may fail.

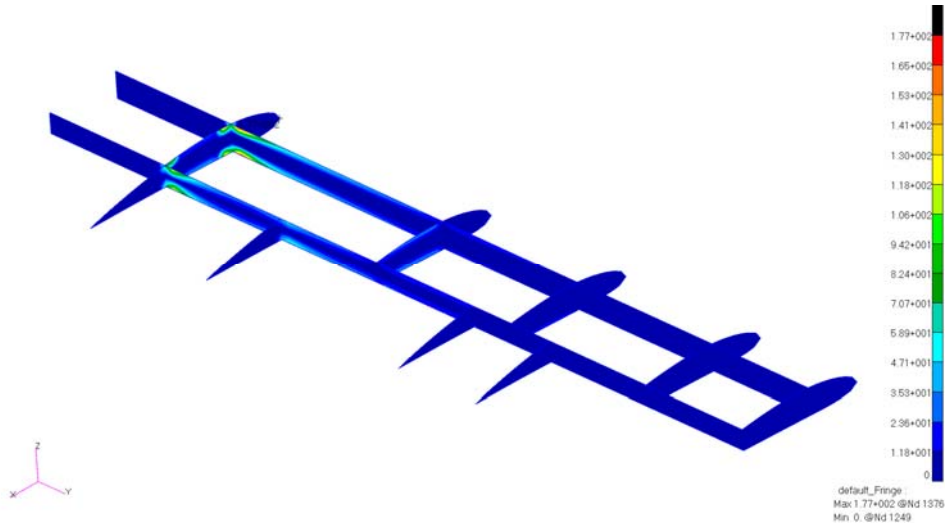

Figure 5.2 Stress Distribution on Spar and Ribs of Initial Wet Lay-up Wing Model in Cruise Condition [MPa]

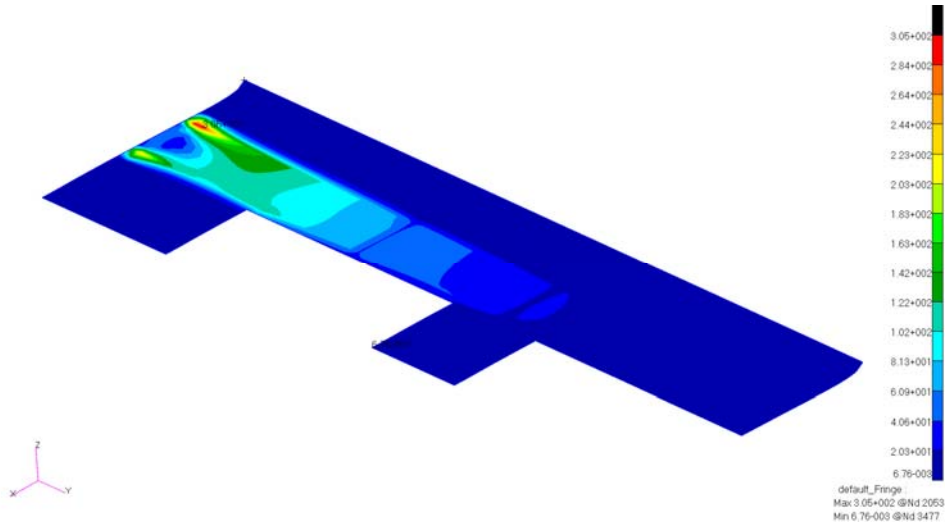

Figure 5.3 Stress Distribution on Lower Skin of Initial Wet Lay-up Wing Model in Cruise Condition [MPa]

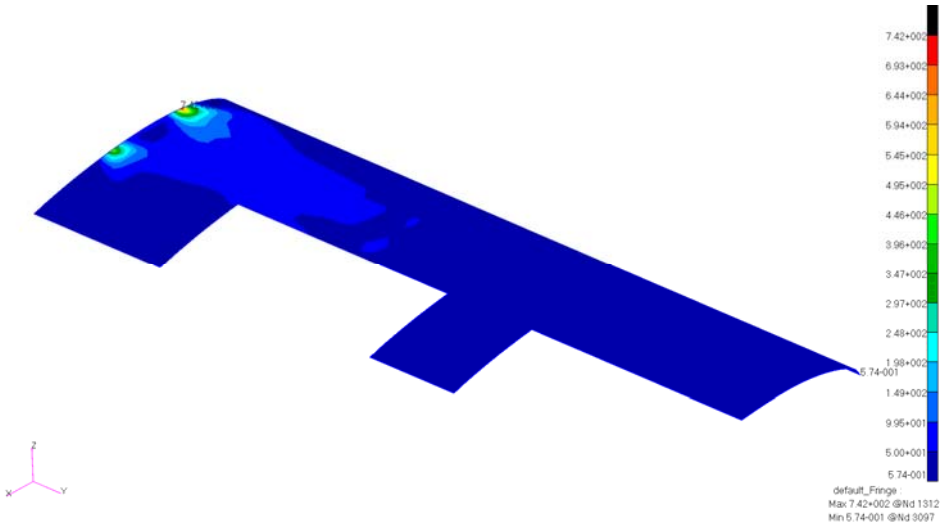

Figure 5.4 Stress Distribution on Upper Skin of Initial Wet Lay-up Wing Model in Cruise Condition [MPa]

Since the initial model failed due to stress criteria, some modifications should be done in order to strengthen the wet lay-up wing. First, one 0° glass fabric layer was added but its additional stiffness effect was not evaluated as being proper. Hence, two 0° oriented glass fabric was added to skins, so the new ply sequence was obtained as [45/0/0/0/0/45]. Also, the spars and ribs were similarly strengthened by adding six new plies; four 45° oriented glass fabric and two 0° oriented glass fabric. The new sequence of spars and ribs became as [45/0/0/45/Core/45/0/0/45].

After the analysis of modified wing model, the maximum displacement at tip of wing decreased from 92.8 mm to 29.3 mm. Figure 5.5 shows the maximum displacement of the modified wet lay-up wing model.

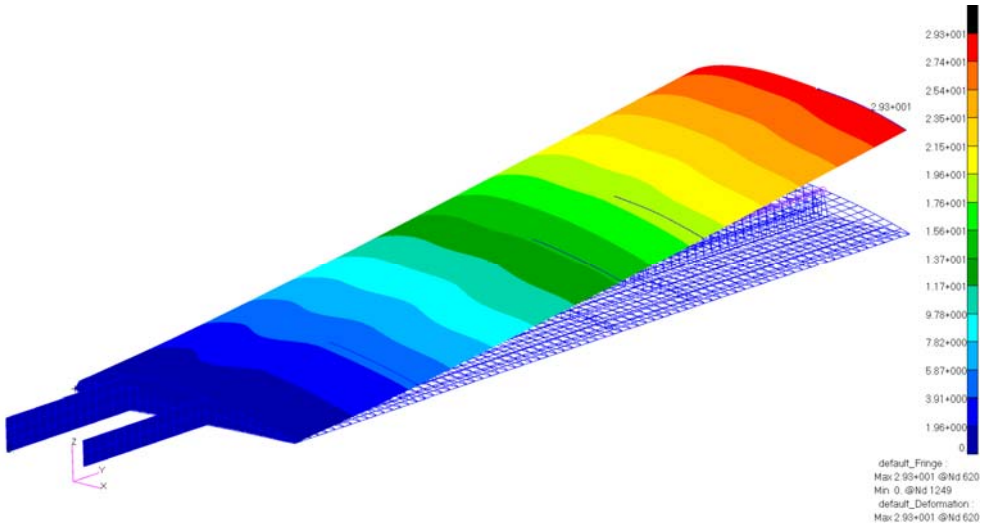

Figure 5.5 Displacement Result of Modified Wet Lay-up Wing Model in Cruise Condition [mm]

The stress distribution is also checked in order to see whether the wing can operate with the loading. Figure 5.6, Figure 5.7 and Figure 5.8 show that the maximum stresses on the structural members of the wet lay-up wing model were under the Ultimate Tensile strength of the material, used in the wing.

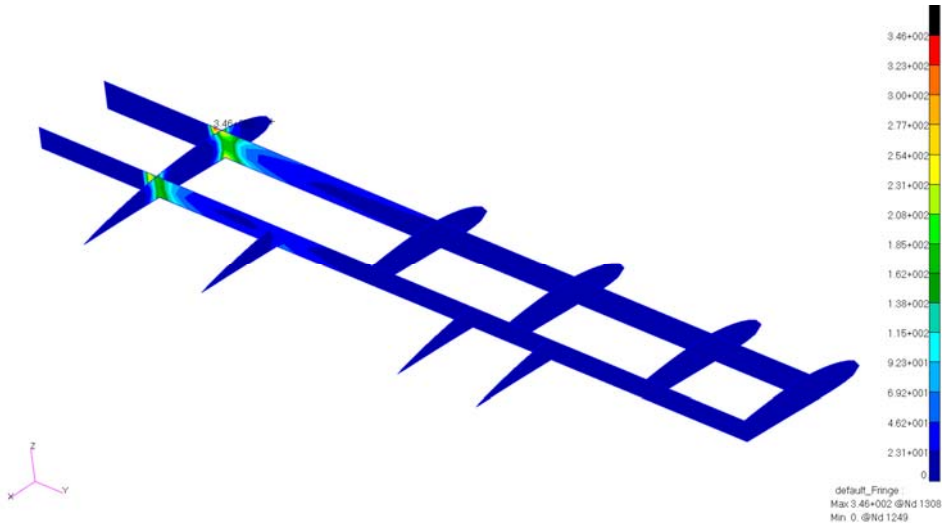

Figure 5.6 Stress Distribution on Spar and Ribs of Modified Wet Lay-up Wing Model in Cruise Condition [MPa]

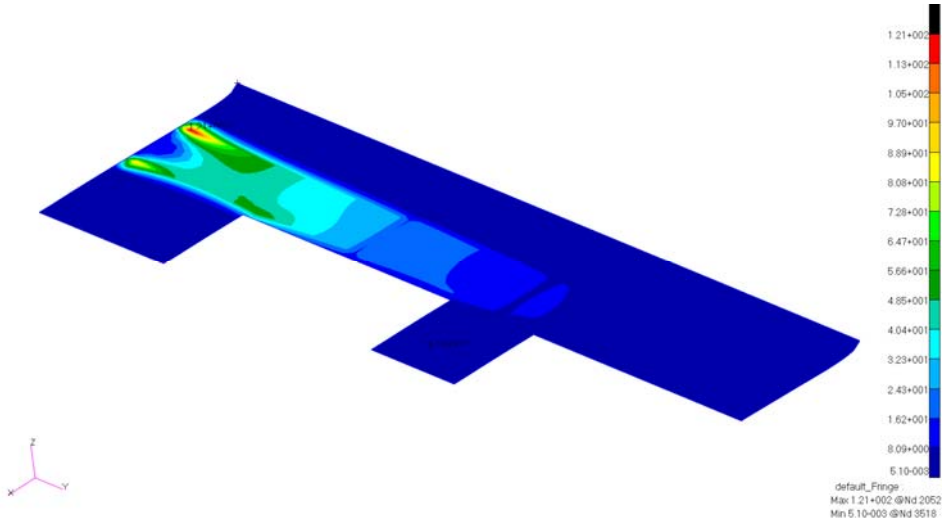

Figure 5.7 Stress Distribution on Lower Skin of Modified Wet Lay-up Wing Model in Cruise Condition [MPa]

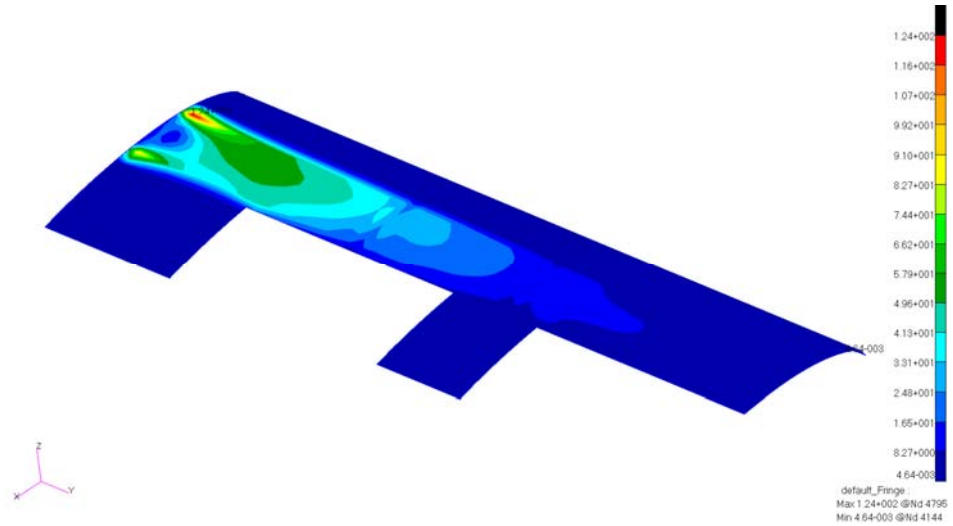

Figure 5.8 Stress Distribution on Upper Skin of Modified Wet Lay-up Wing Model in Cruise Condition [MPa]

Although the displacement and stress distribution was decreased, the strengthening the wing brought the weight penalty. The total mass of initial model was approximately calculated as 5-5.5 kg. After modification on the wet lay-up wing model, the total mass increased to approximately 8.7-9.2 kg. The new calculated mass was very close to the aluminum wing model.

5.3 The Structural Analysis of the Prepreg Wing Model

In this subsection of this study, finite Element Model of Prepreg Wing was analyzed with the initial ply sequence.

Figure 5.9 shows the maximum displacement result at tip as 1.04 mm in cruise flight condition. The maximum displacement in gust condition was also calculated as 6.42 mm, as shown in Figure 5.10.

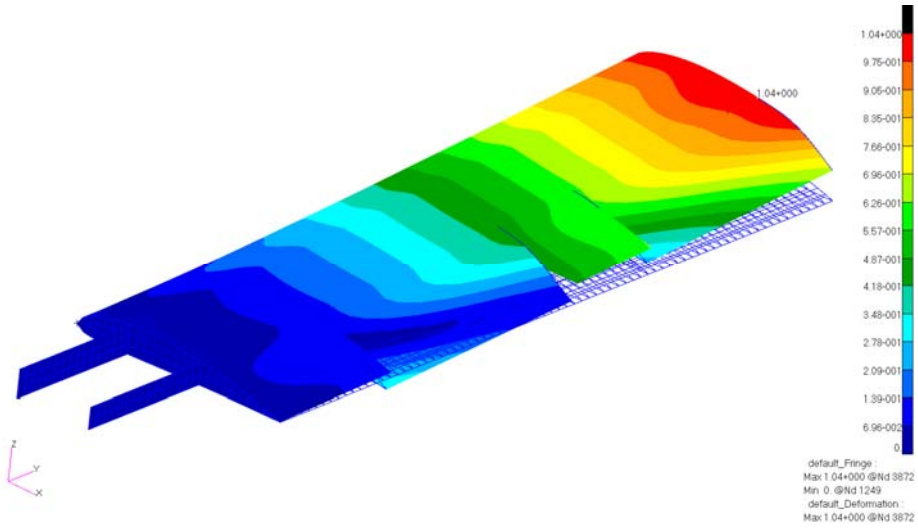

Figure 5.9 Displacement Result of Initial Prepreg Wing Model in Cruise Condition [mm]

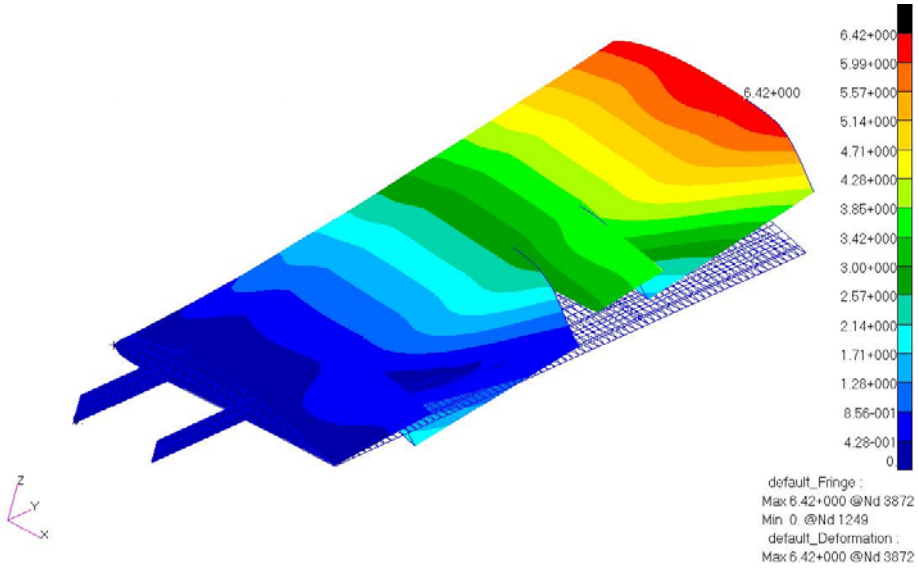

Figure 5.10 Displacement Result of Initial Prepare Wing Model in Gust Condition [mm]

The maximum stresses on the structural members, spars and ribs, lower skin and upper skin, were also checked. Figure 5.11, Figure 5.12 and Figure 5.13 show example stress distributions for different members.

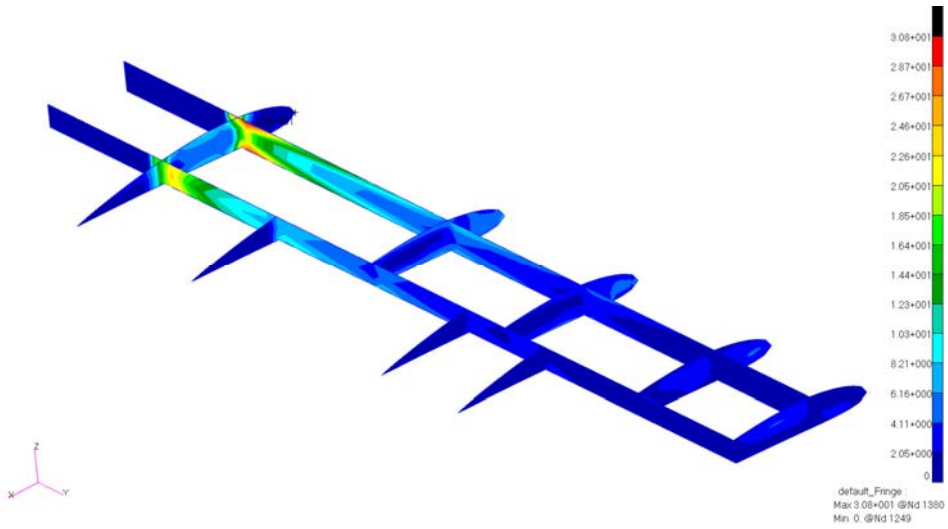

Figure 5.11 Stress Distribution on Spar and Ribs of Initial Prepreg Wing Model in Gust Condition [MPa]

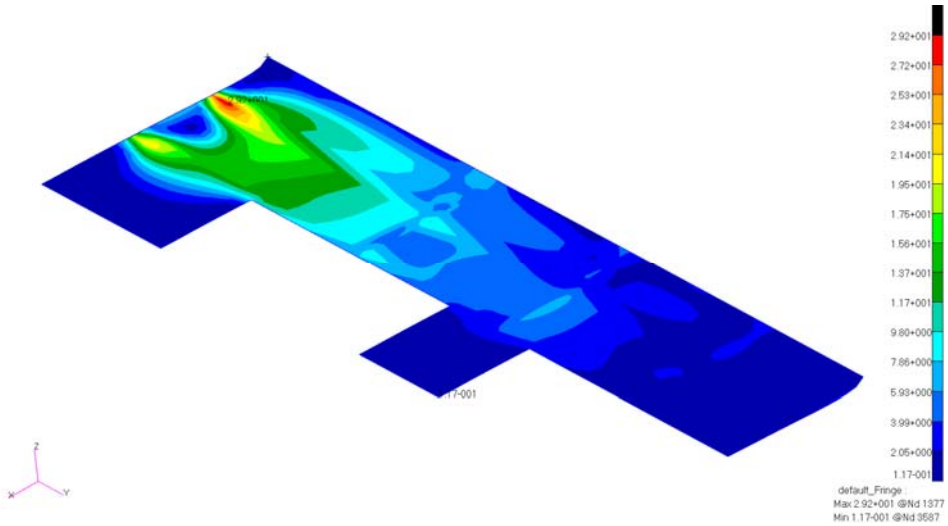

Figure 5.12 Stress Distribution on Lower Skin of Initial Prepreg Wing Model in Gust Condition [MPa]

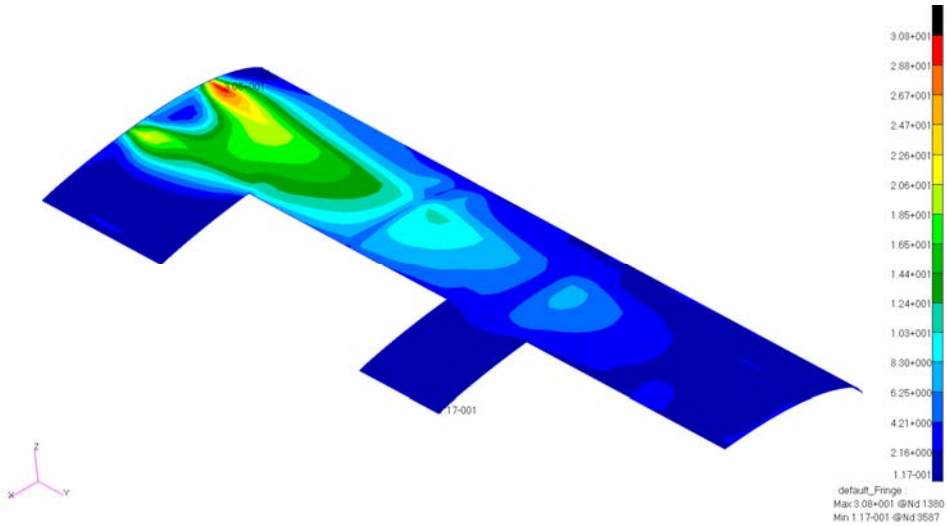

Figure 5.13 Stress Distribution on Upper of Initial Prepreg Wing Model in Gust Condition [MPa]

As seen from the results that the initial prepreg model was too stiff and heavy for the flight conditions of this moderate unmanned aerial vehicle. Therefore modifications to ply sequences were done in order to lower the total mass of the prepreg wing.

Composite materials provide a tailored design in order to find the optimum one. Ten trials, which satisfy stress check (maximum stress failure criteria), are presented. In trials, ply sequences of some components were kept constant while sequences for other components were changed.

Table 5.1 to Table 5.5 show the ply sequences of lower and upper skin for each trial. In ply sequences “C” stands for honeycomb core.

Table 5.6 and Table 5.7 give the ply sequences of front and rear spar for all trials.

Table 5.1 The Ply Sequences of Lower Skin for Trial 1 to 7

	Trial 1	Trial 2	Trial 3, 4, 5, 6, 7
BAY 1	45/0/45/0/45/C/45/0/0/45	45/0/45/45/0/45/C/45/0/0/45	45/0/45/0/45/C/45/0/0/45
BAY 2	45/0/0/45/C/45/0/45	45/0/0/45/C/45/0/0/45	45/0/0/45/C/45/0/45
BAY 3	45/0/45/C/45/45	45/0/45/C/45/0/45	45/0/45/C/45/45
BAY 4	45/45/45/45	45/45/45/45	45/45/45/45

Table 5.2 The Ply Sequences of Lower Skin for Trial 8 to 10

	Trial 8	Trial 9	Trial 10
BAY 1	45/0/0/45/C/45/0/45	45/0/0/45/C/45/0/45	45/0/45/C/45/0/45
BAY 2	45/0/0/45/C/45/0/45	45/0/45/C/45/0/45	45/45/C/45/45
BAY 3	45/0/45/C/45/45	45/0/45/45/45	45/45/45/45
BAY 4	45/45/45/45	45/45/45/45	45/45/45/45

Table 5.3 The Ply Sequences of Upper Skin for Trial 1 to 5

	Trial 1	Trial 2	Trial 3, 4 ,5
BAY 1	45/0/45/0/45/C/45/0/0/45	45/0/45/45/0/45/C/45/0/0/45	45/0/45/0/45/C/45/0/0/45
BAY 2	45/0/0/45/C/45/0/45	45/0/0/45/C/45/0/0/45	45/0/0/45/C/45/0/45
BAY 3	45/0/45/C/45/45	45/0/45/C/45/0/45	45/0/45/C/45/45
BAY 4	45/45/45/45	45/45/45/45	45/45/45/45

Table 5.4 The Ply Sequences of Upper Skin for Trial 6 to 8

	Trial 6	Trial 7	Trial 8
BAY 1	45/0/0/45/C/45/0/0/45	45/0/0/45/C/45/0/0/45	45/0/45/C/45/0/45
BAY 2	45/0/45/C/45/0/45	45/0/45/45/0/45	45/0/45/45/0/45
BAY 3	45/0/45/C/45/45	45/0/45/45/45	45/0/45/45/45
BAY 4	45/45/45/45	45/45/45/45	45/45/45/45

Table 5.5 The Ply Sequences of Upper Skin for Trial 9, 10

	Trial 9	Trial 10
BAY 1	45/0/0/45/C/45/0/45	45/0/0/45/C/45/0/45
BAY 2	45/0/45/C/45/45	45/0/45/C/45/45
BAY 3	45/0/45/45/45	45/45/45/45
BAY 4	45/45/45/45	45/45/45/45

Table 5.6 The Ply Sequences of Front and Rear Spar for Trial 1 to 5

	Trial 1	Trial 2, 3, 4	Trial 5
BAY 1	$[45/0/45/0/0/0/45/0/45]_S$	$[45/0/45/0/0/45/0/45]_S$	$[45/0/45/0/45/0/45]_S$
BAY 2	$[45/0/0/0/45/0]_S$	$[45/0/0/45/0]_S$	$[45/0/45/0]_S$
BAY 3	[45/0/0/0/0/45]	[45/0/0/45]	[45/0/0/45]
BAY 4	[45/0/45]	[45/0/45]	[45/0/45]

Table 5.7 The Ply Sequences of Front and Rear Spar for Trial 6 to 10

	Trial 6	Trial 7	Trial 8	Trial 9, 10
BAY 1	$[45/0/45/0/45]_S$	$[45/0/45/0]_S$	$[45/0/45]_S$	[45/0/0/45]
BAY 2	$[45/0/45]_S$	$[45/0/45]_S$	[45/0/0/45]	[45/0/0/45]
BAY 3	[45/0/0/45]	[45/0/0/45]	[45/0/0/45]	[45/0/45]
BAY 4	[45/0/45]	[45/0/45]	[45/0/45]	[45/0/45]

In order to manufacture a composite part, minimum three ply is needed, otherwise warping can occur after curing [4]. Therefore, the ply number of leading edge bracket and ribs were not decreased.

Table 5.8 and Table 5.9 show the ply sequences of other structural members for each trial. Displacements in cruise flight and gust flight conditions were calculated for each trial model. Table 5.10 shows the displacement results of finite element analysis of each trial.

Table 5.8 The Ply Sequences of Other Structural Members for Trial 1 to 4

	Trial 1	Trial 2	Trial 3	Trial 4
Leading Edge Skin	No Change	No Change	No Change	[45/0/45]
Cover I	[45/0/45/0/45/0/45]	$[45/0/45/0]_S$	[45/0/45/0/45/0/45]	No Change
Cover II	[45/0/45/0/45]	[45/0/45/0/45]	[45/0/45/0/45]	No Change
Trailing Edge Skin	No Change	No Change	No Change	[45/0/45]
Trailing Edge Bracket	No Change	No Change	No Change	[45/0/45]
Control Surface Skin	No Change	No Change	No Change	No Change
Control Surface Spar	No Change	No Change	No Change	No Change

Table 5.9 The Ply Sequences of Other Structural Members for Trial 5 to 10

	Trial 5	Trial 6	Trial 7, 8	Trial 9	Trial 10
Leading Edge Skin	No Change	No Change	No Change	No Change	No Change
Cover I	No Change	No Change	No Change	[45/0/45/45/0/45]	[45/0/45/0/45]
Cover II	No Change	No Change	No Change	No Change	No Change
Trailing Edge Skin	No Change	No Change	No Change	No Change	No Change
Trailing Edge Bracket	No Change	No Change	No Change	No Change	No Change
Control Surface Skin	No Change	[45/0/0/45]	[45/0/45]	No Change	No Change
Control Surface Spar	[45/0/45]	No Change	No Change	No Change	No Change

The optimum design, considering cruise and gust displacement and total mass, which was calculated as 4.5 kg, was chosen as Trial 9. Although Trial 8 had slightly larger displacement then Trial 9; it also had greater mass when compared to Trial 9.

Table 5.10 Displacement Results for Each Trial under Cruise and Gust Flight Condition

	Displacement for Cruise Condition [mm]	Displacement for Gust Condition [mm]
Initial Model	1.04	6.42
Trial 1	1.08	6.66
Trial 2	1.09	6.71
Trial 3	1.15	7.1
Trial 4	1.21	7.44
Trial 5	1.36	8.34
Trial 6	1.55	9.51
Trial 7	1.67	10.3
Trial 8	2.03	12.5
Trial 9	1.84	11.3
Trial 10	1.93	11.9

Figure 5.14 and Figure 5.15 show the displacement results of selected prepreg wing model under cruise and gust flight conditions. Stress distribution on spars, ribs, lower and upper skin can be seen from Figure 5.16, Figure 5.17 and Figure 5.18.

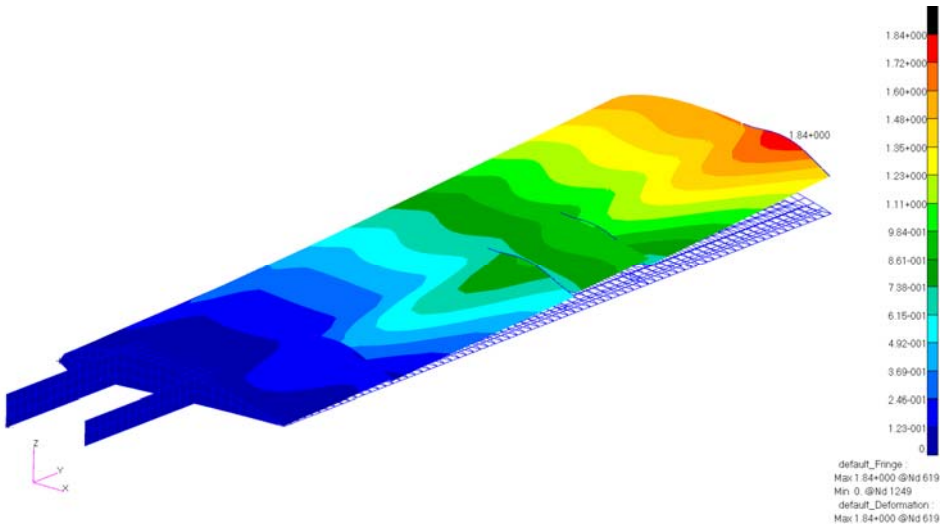

Figure 5.14 Displacement Result of Selected Prepreg Wing Model in Cruise Condition [mm]

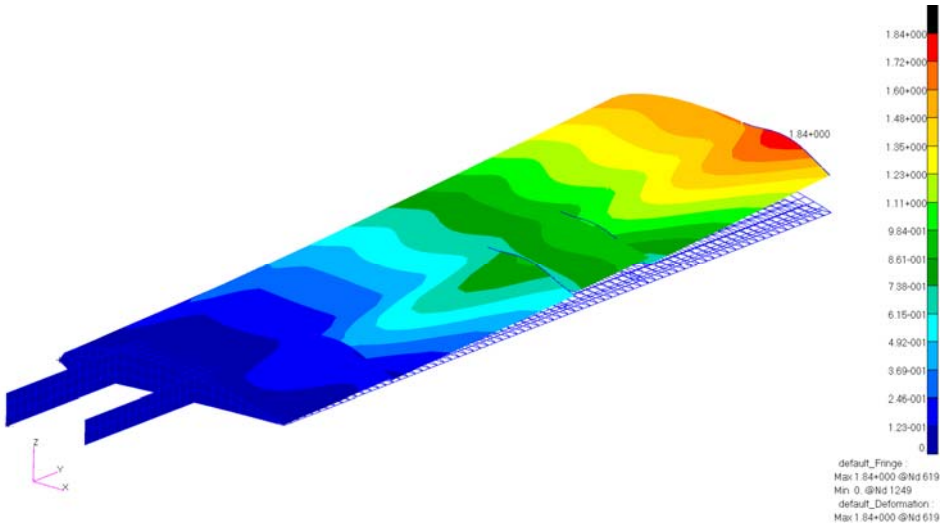

Figure 5.15 Displacement Result of Selected Prepreg Wing Model in Gust Condition [mm]

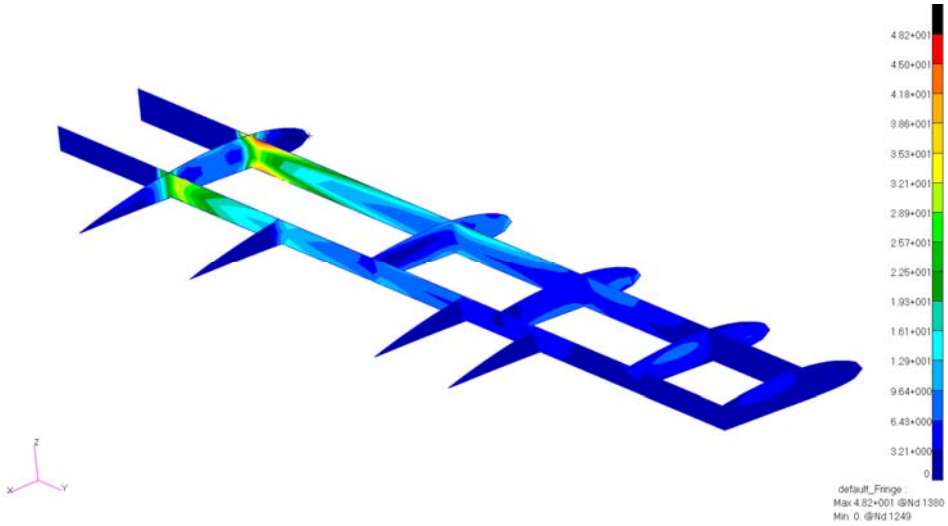

Figure 5.16 Stress Distribution on Spar and Ribs of Selected Prepreg Wing Model in Gust Condition [MPa]

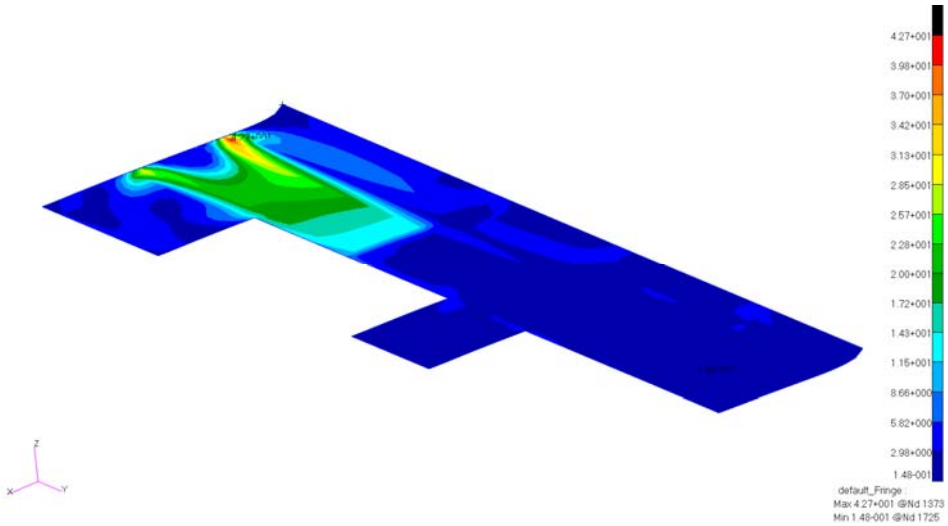

Figure 5.17 Stress Distribution on Lower Skin of Selected Prepreg Wing Model in Gust Condition [MPa]

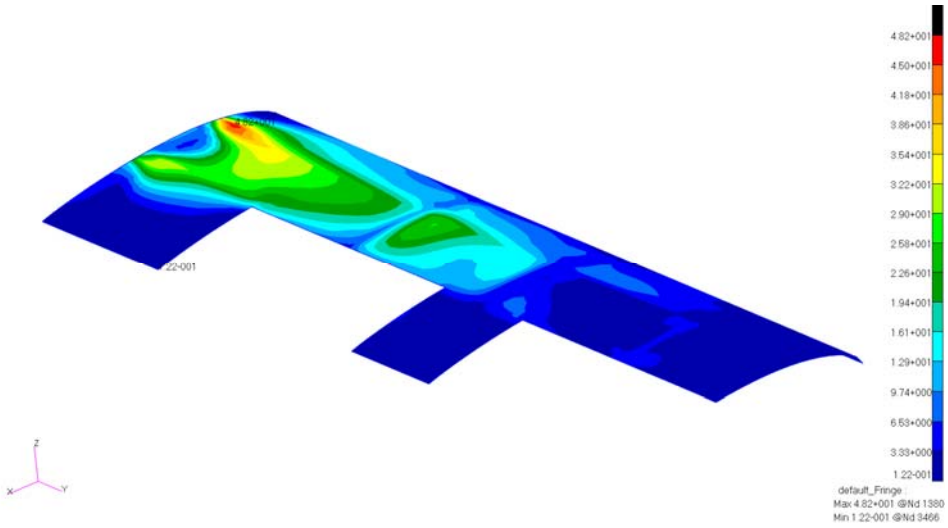

Figure 5.18 Stress Distribution on Upper of Selected Prepreg Wing Model in Gust Condition [MPa]

5.4 Conclusion

The finite element wing models of wet lay-up and prepreg were analyzed for cruise and gust conditions. The initial wet lay-up wing model seemed to fail under cruise condition by maximum stress failure criteria. The addition of plies had to be done, but this brought a weight penalty. On the other hand, the analysis result of prepreg wing model showed that initial model is too stiff for the mission of a moderate UAV wing. The excess plies in the model were removed and modifications to plies were done. The optimum prepreg design was selected. The total mass of prepreg model dropped from 6.7 kg to 4.5 kg. Since wet lay-up model is much heavier compared to prepreg model, only prepreg model will be used for further analysis.

CHAPTER 6

PRODUCIBILITY

6.1 Introduction

Producibility analysis for the prepreg composite materials was conducted using FiberSIM program [6]. FiberSIM is an add-on for CAD programs. It is used by aerospace, automotive, marine and medical equipment industries. FiberSIM enables the correct design and manufacturing approach for the composite parts. It simulates laying up of the plies on tools in order to show whether the part is producible or not by using a given material. If a problem of producibility occurs on simulation due to the characteristic of the given material, the designer uses another method in order to make an accurate design. Guillermin determines in his study that in early stages of the design of a composite part fabric deformations can be seen by the lay-up simulation of the plies in FiberSIM [15]. Therefore, the composite part's manufacturing process is done correctly. This application of this program is believed to decrease the manufacturing time and cost.

Figure 6.1 gives the parts of FiberSIM. They are Composite Engineering Environment (CEE), Advanced Composite Engineering Environment (ACEE), Automated Deposition Design (ADD), Documentation, and Interfaces; which are Analysis Interface, Flat Pattern Export, Laser Projection, Fiber Placement Interface, Tape Laying Interface and Composite Quality Connector.

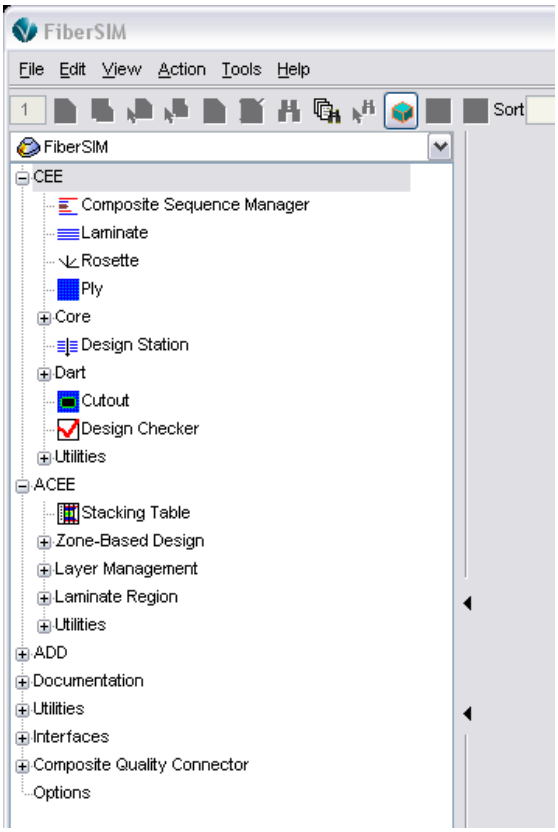

Figure 6.1 Parts of FiberSIM Package Program

In this thesis, Composite Engineering Environment (CEE), Advanced Composite Engineering Environment (ACEE) and Documentation parts are used. The information of the composite part, like material, tool surface, sequence, fiber direction, core, etc., is given in the CEE. Producibility, flat pattern, laser projection, laminate property, automated cutting data can be generated by the data defined in CEE. Flat pattern shows the real shapes of the plies and then the data is exported to the automated cutting machine. Laser projection machine shows the boundaries of the plies on the lay-up tool of composite part while manufacturing and this ensures the ply is laid up in accurate position. All the data enables the correct information to be transferred to manufacture department. ACEE provides the users advanced methods in order to make design changes in a short time.

6.2 Producibility Analysis

In this study, FiberSIM 2009 was used with Unigraphics NX. The FiberSIM window is opened in Unigraphics NX as an add-on. In the producibility analysis, the required procedure is explained by using initial prepreg model.

6.2.1 Skin Producibility Analysis

The model of upper skin was chosen for the demonstration of FiberSIM analysis. Before starting an analysis, first a model should be set-up for FiberSIM. The required input data were the tool surface, net boundary of the laminate, boundaries of bays, boundaries of the cores and 0° fiber direction; those are shown in the Figure 6.2.

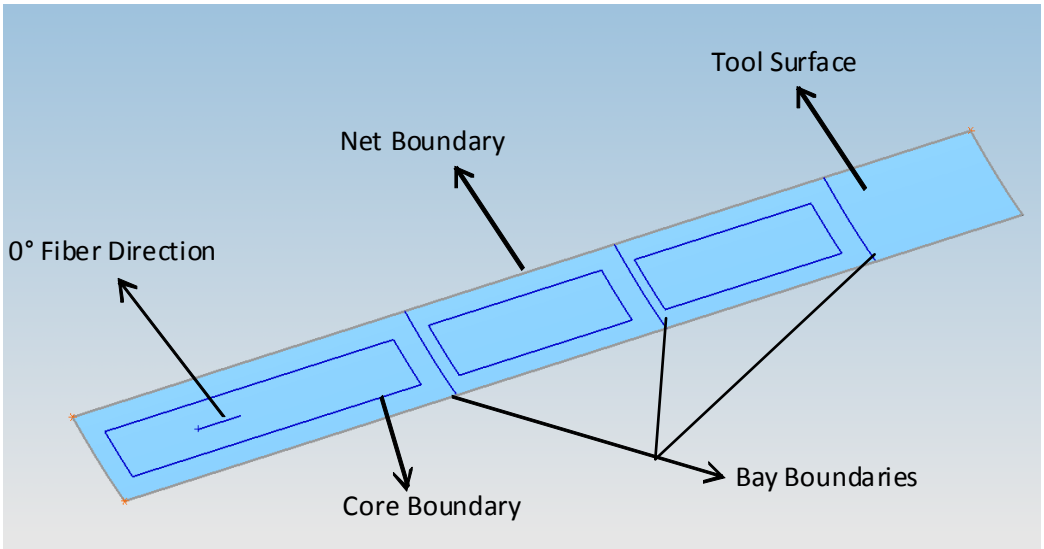

Figure 6.2 FiberSIM Model of the Upper Skin

A laminate was created with the name Upper Skin 1st Cycle in the laminate part. The tool surface was determined from the laminate section shown in Figure 6.3.

The direction of the arrow is important because plies will be lay-up through the direction of the arrow. Also this selection determines whether the tool is female or male.

For the upper skin, aerodynamic surface was selected as the tool surface and the arrow direction was through the torque box. As a consequence, the tool for this part was determined as a female tool by arranging the direction of the tool. Then the net boundary information was selected in laminate properties, which is shown in Figure 6.4.

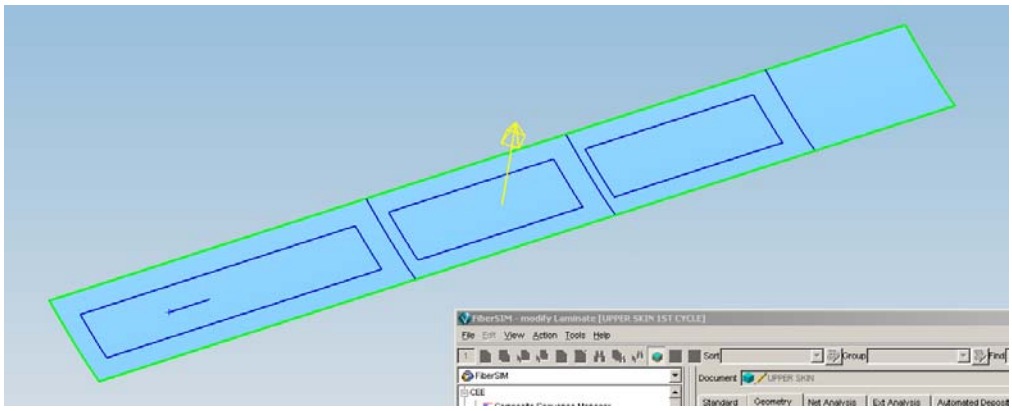

Figure 6.3 Determination of the Tool Surface in FiberSIM

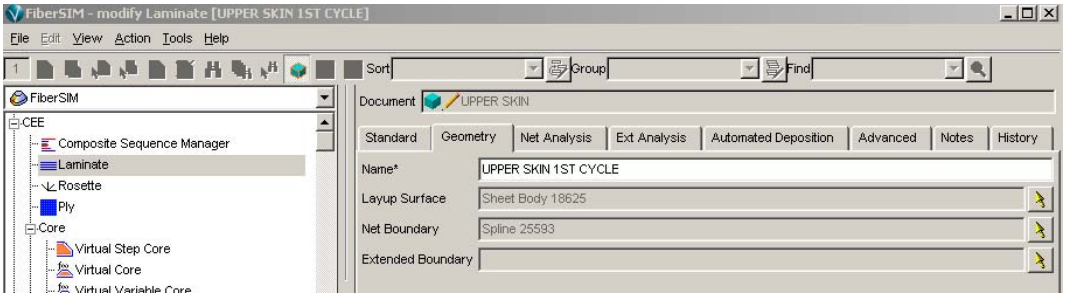

Figure 6.4 Creating the Laminate " Upper Skin 1st Cycle"

A rosette must be created for “determining the fiber orientations” [6]. The rosette was created using “Rosette” by defining the origin and direction, shown in Figure 6.5. The created rosette, which gives 0°, 45°, 90° and -45° directions of the plies, is shown in Figure 6.6.

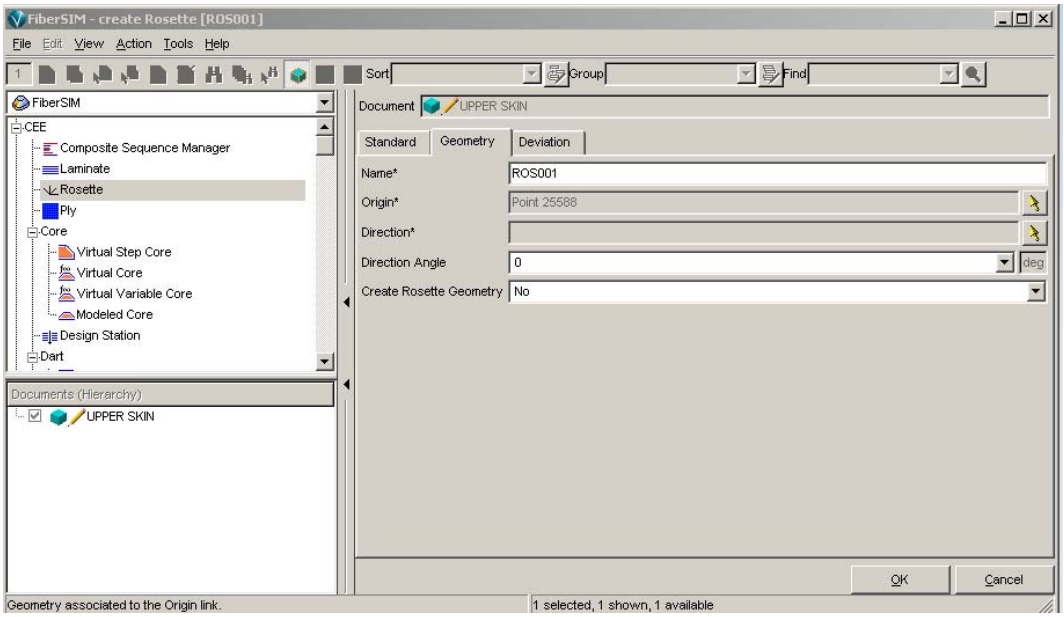

Figure 6.5 The Creation of Rosette for the Upper Skin

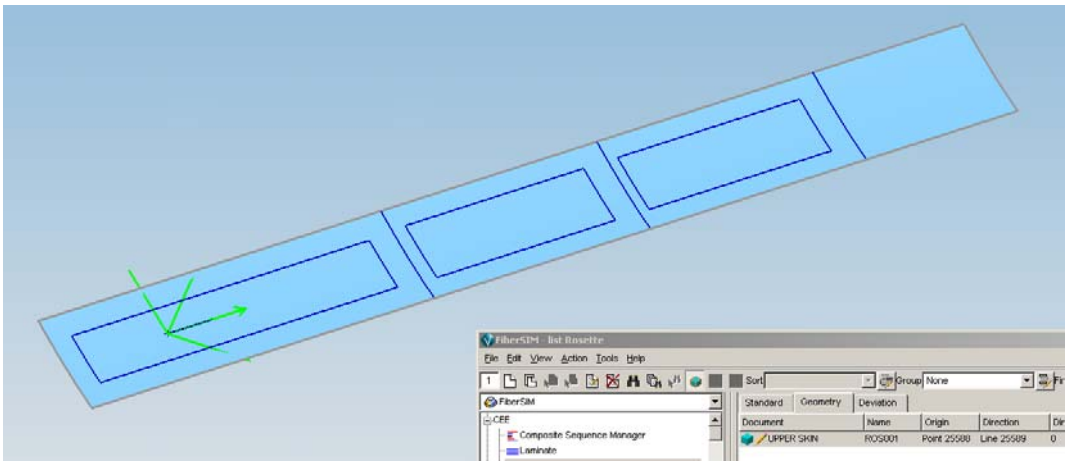

Figure 6.6 The Created Rosette Directions

There are two methods in FiberSIM for the analysis of a composite par. They are called Ply-Based Design and Zone-Based Design. In the skin producibility analysis, the Zone-Based Design Method is generally used for the analysis of plies under the core and Ply-Based Design Method is prefered for the analysis of plies above the core.

The skins consist of 4 bays. In the Zone-Based Design, the bays would be defined in the Zone part after the sequence of plies under the core of each bay was determined in the laminate specification part. That part is shown in Figure 6.7.

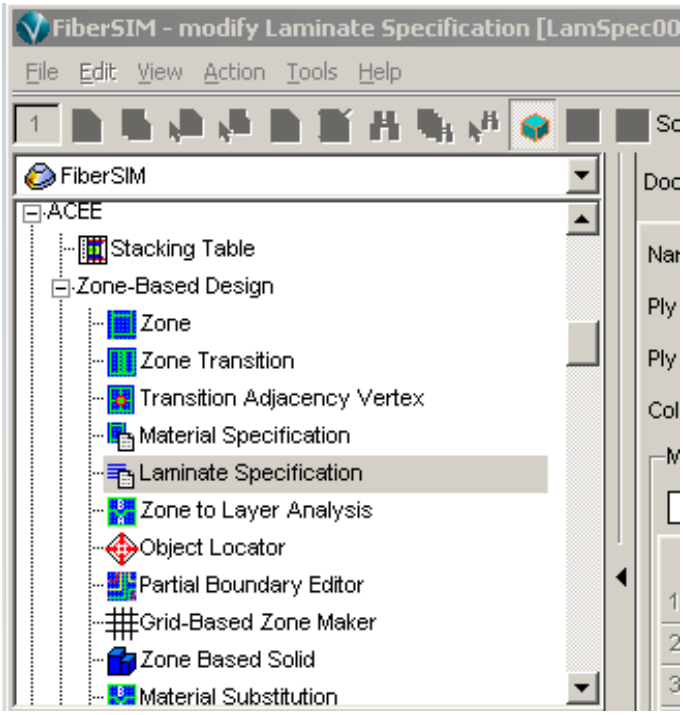

Figure 6.7 Laminate Specification in Zone-Based Design

In the Laminate Specification, each ply can be determined with material information, orientation and ordering information with step number of the upper skin with step numbers of the plies. Figure 6.8 - Figure 6.12 show the created laminate specification part for each of the four bays. They were created by using the undercore laminate information.

Table 6.1 gives the sequence of the upper skin with step numbers of the plies. Figure 6.8 - Figure 6.12 show the created laminate specification part for each of the four bays. They were created by using the undercore laminate information, which is given in Table 6.1. Ply Name determines the name each ply in the sequence as P1, P2, and P3 and so on.

Table 6.1 Laminate Sequence of Upper Skin with Step Number

	STEP NO	PLY NAME	BAY 1	BAY 2	BAY 3	BAY 4
UNDER CORE	10	P 1	45˚	45˚	45˚	45˚
	20	P 2	0˚	0˚	0˚	
	30	P 3	45˚			
	40	P 4	45˚			
	50	P 5	0˚	0˚		
	60	P 6	45˚	45˚	45˚	45˚
OVER CORE	70	P 7				
	65					
	80	P 8				
	80	P 9				
	80	P 10				
	90	P 11	45˚	45˚	45˚	45˚
	100	P 12	0˚	0˚	0˚	
	110	P 13	0˚	0˚		
	120	P 14	45˚	45˚	45˚	45˚

45˚ Woven Fabric
0˚ UD Fabric
0˚ Woven Fabric
Film Adhesive
Honeycomb

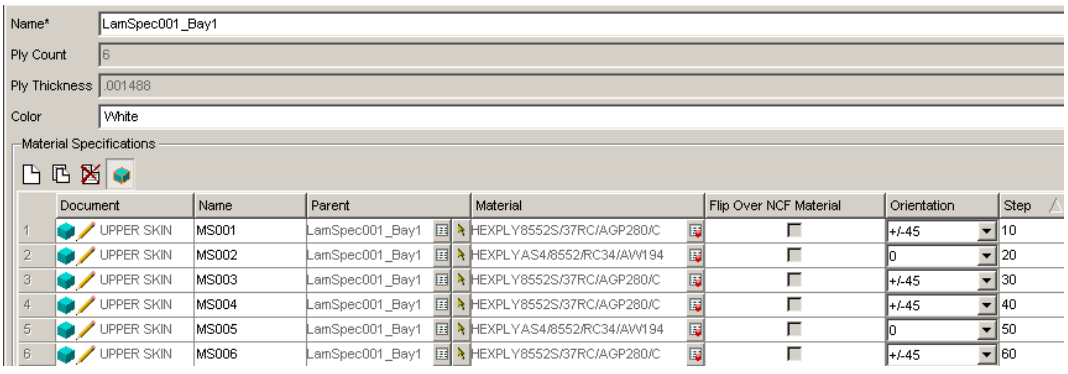

Figure 6.8 Laminate Specification for Bay 1

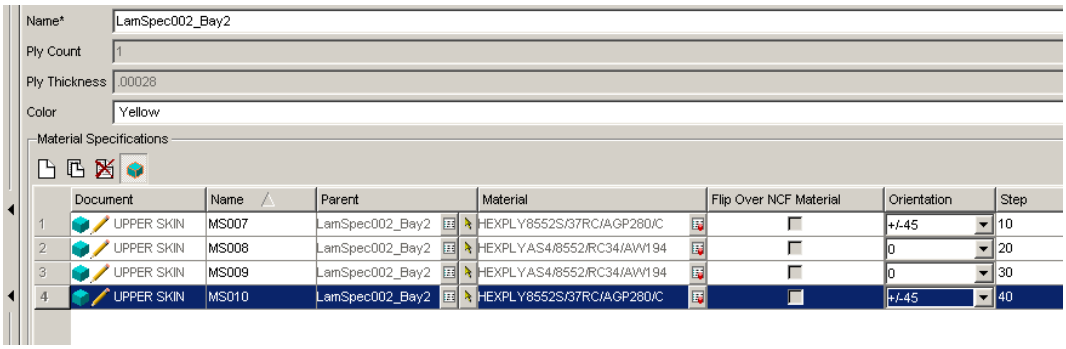

Figure 6.9 Laminate Specification for Bay 2

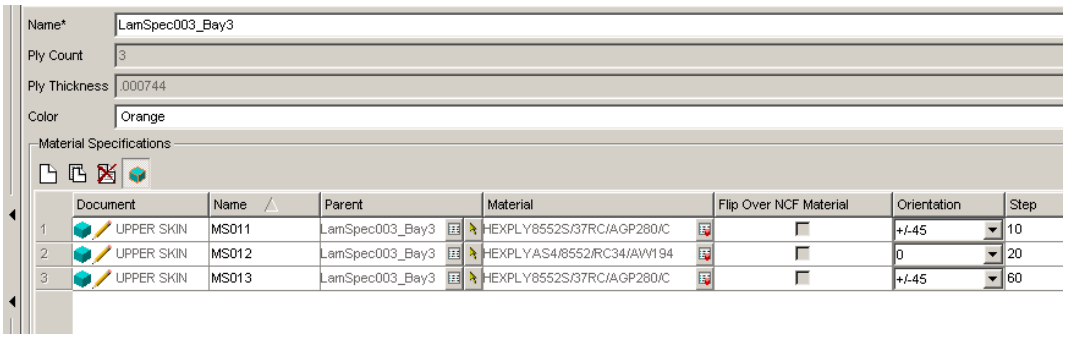

Figure 6.10 Laminate Specifications for Bay 3

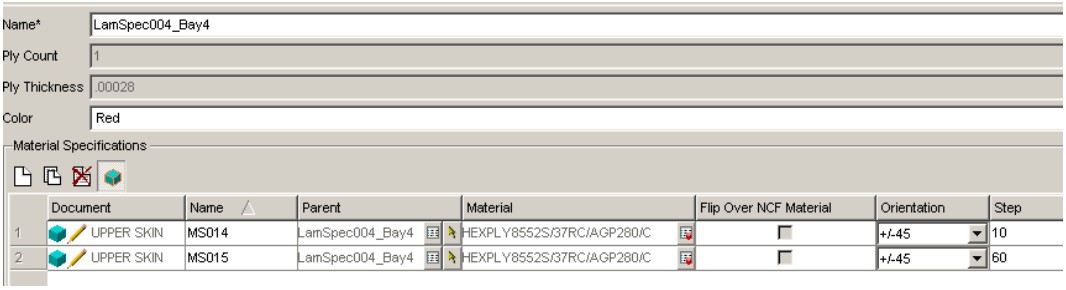

Figure 6.11 Laminate Specifications for Bay 4

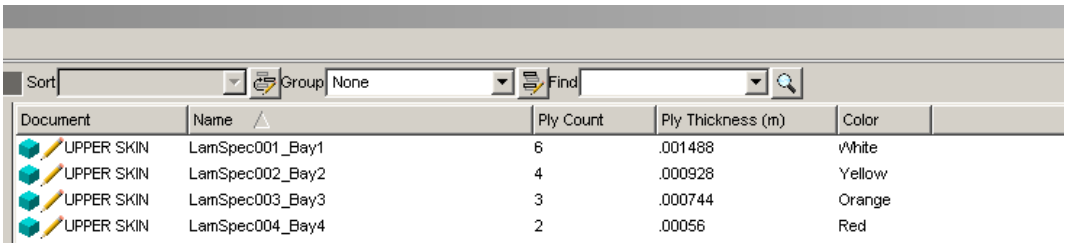

Figure 6.12 The List of Laminate Specifications of 4 Bays

After determining the laminate specifications, the bays were determined from the Zone part. In the Standard tab, laminate information, rosette information, origin of the zone information and boundary information can be defined, shown in Figure 6.13.

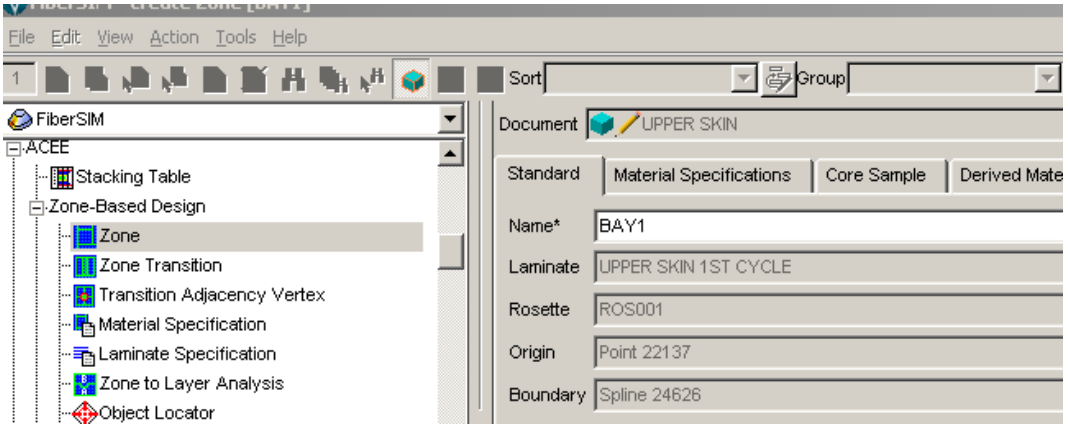

Figure 6.13 Creating Bay 1 from Zone Part

From Material Specifications tab, Target Ply Count and Laminate Specification information for the given bay was defined. An example for Bay 1 is given in Figure 6.14. All other bays were also determined by this method. The final condition of the created bays can be seen in Figure 6.15.

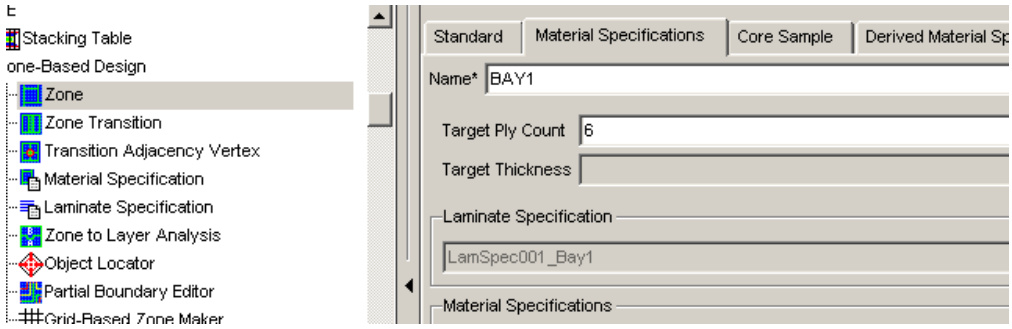

Figure 6.14 Selecting Laminate Specification of Bay 1 in Zone Part

Specifications | Derived Material Specifications

Name	Target Ply Count	Target Thickness (m)	Actual Ply Count	Actual Ply Thickness (m)	Laminate Specification
BAY1	6		6	.001488	LamSpec001_Bay1
BAY2	4		4	.000928	LamSpec002_Bay2
BAY3	3		3	.000744	LamSpec003_Bay3
BAY4	2		2	.00056	LamSpec004_Bay4

Figure 6.15 Final Condition of the Created Bays

After bays were created in the zone part, 'Zone to Layer Analysis' was done in order to obtain the plies, shown in Figure 6.16. In the analysis stagger profile and offset specification should be determined. The stagger profile determines the cross sectional shape of a drop-off and on the other hand the offset specification gives the distance between two plies in the drop-off. Examples of Stagger Profiles and Offset Specifications are given in Figure 6.17 and Figure 6.18 [6].

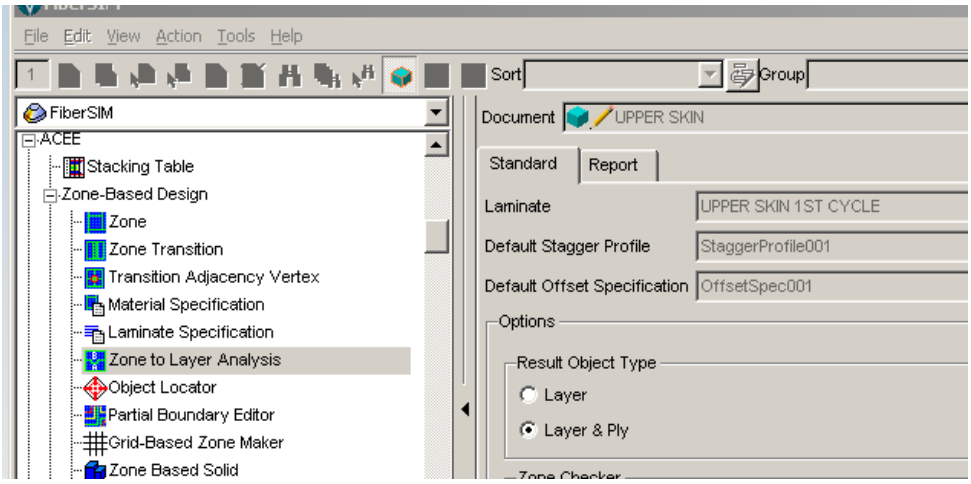

Figure 6.16 Zone to Layer Analysis Part

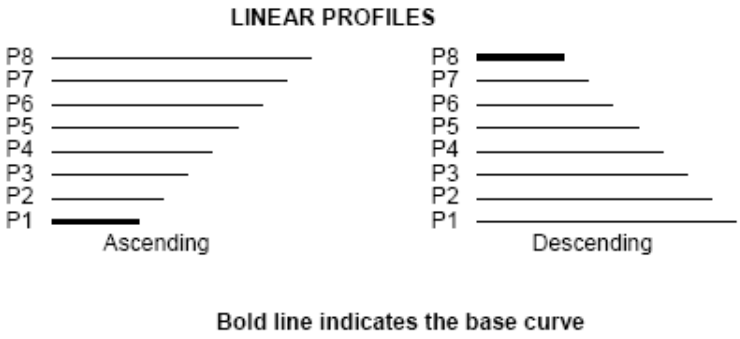

Figure 6.17 Stagger Profiles

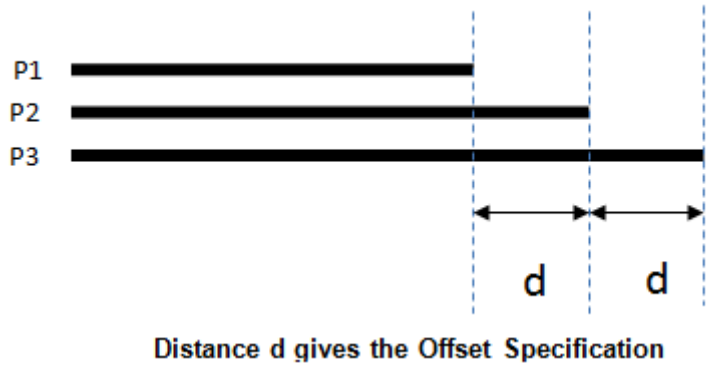

Figure 6.18 Offset Specification

The Stagger Profile Menu and Offset Specification Menu are shown in the Figure 6.19 and Figure 6.20 respectively.

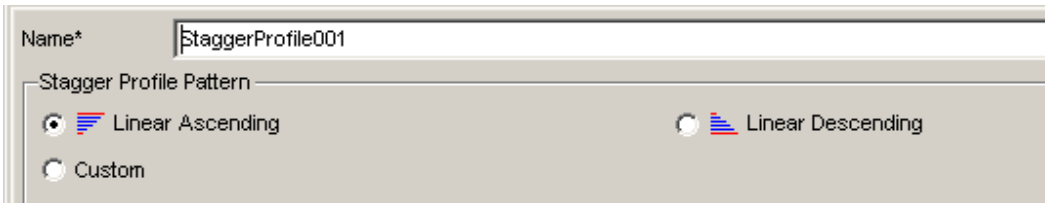

Figure 6.19 Stagger Profile Menu

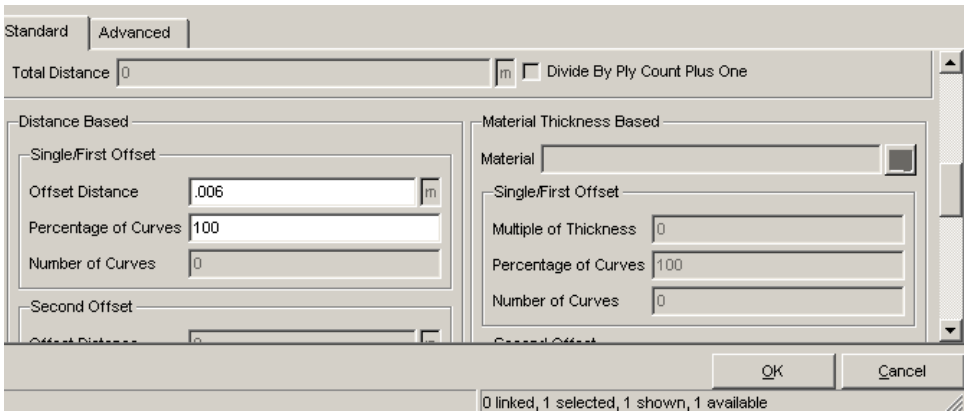

Figure 6.20 Offset Specification Menu

After stagger and offset characteristics were determined, the model was ready for the analysis. Figure 6.21 shows the relevant success message for Zone to Layer Analysis.

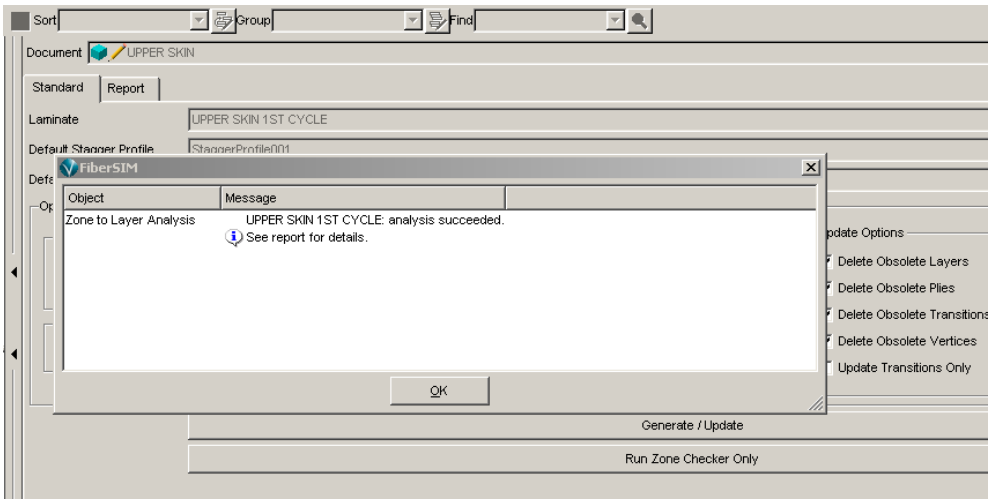

Figure 6.21 The Succeeded Zone to Layer Analysis

Figure 6.22 shows the analysis report. In the report, number of layers and transitions should be checked. Figure 6.23 gives all the layers, created after the analysis.

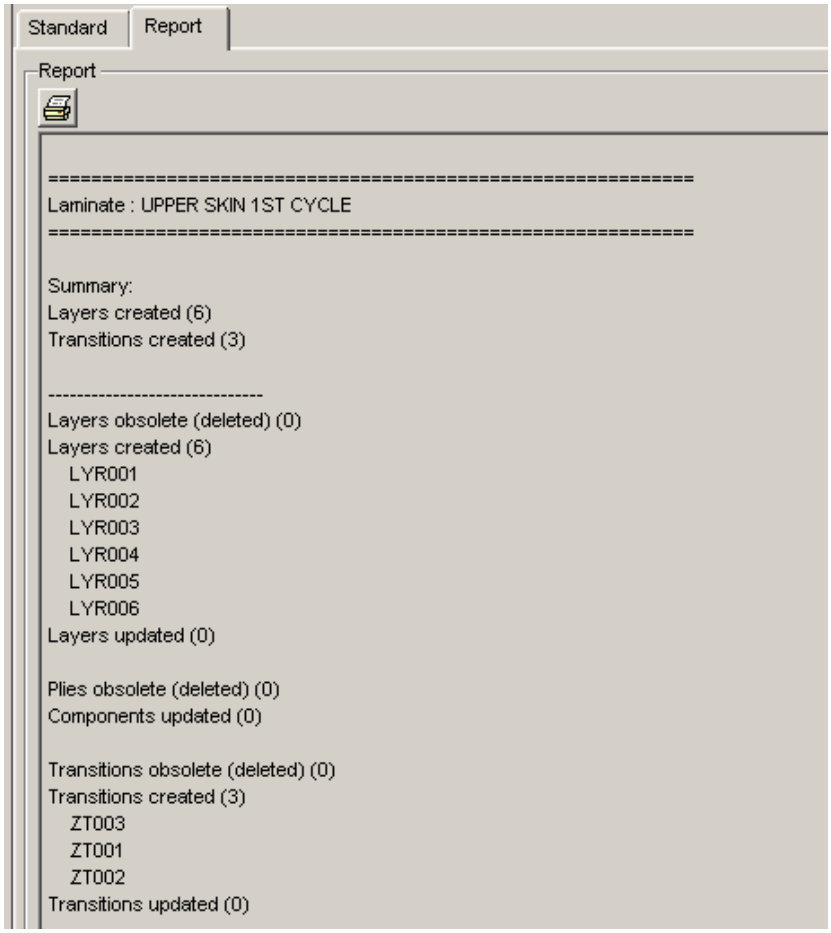

Figure 6.22 Zone to Layer Analysis Report

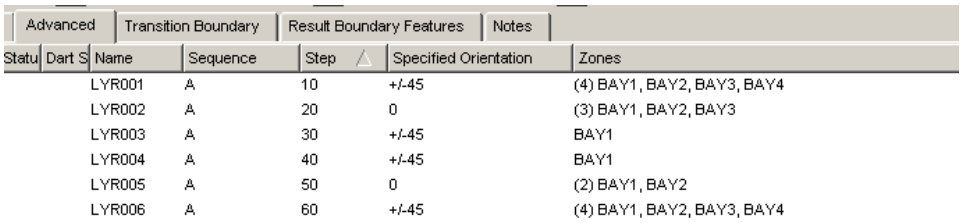

Figure 6.23 Layers Under Core, Upper Skin

After the layers were created, the plies could be created from the layers. This is shown in Figure 6.24.

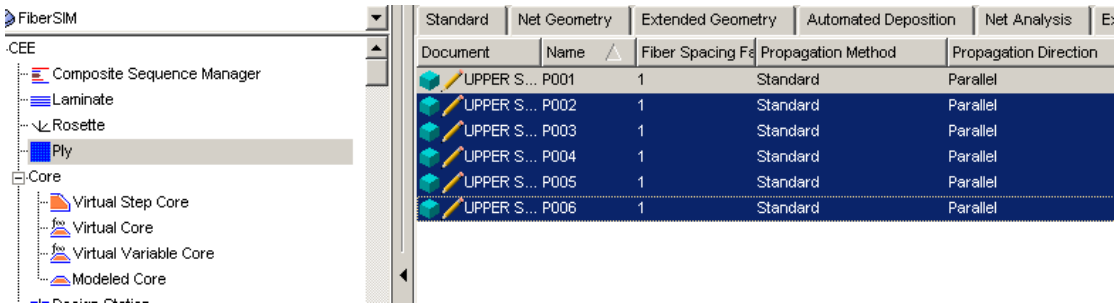

Figure 6.24 Plies Under Core, Upper Skin

The required producibility analysis of each ply was conducted separately. The results of producibility analysis of under core plies can be seen from in Figure 6.25 to Figure 6.30.

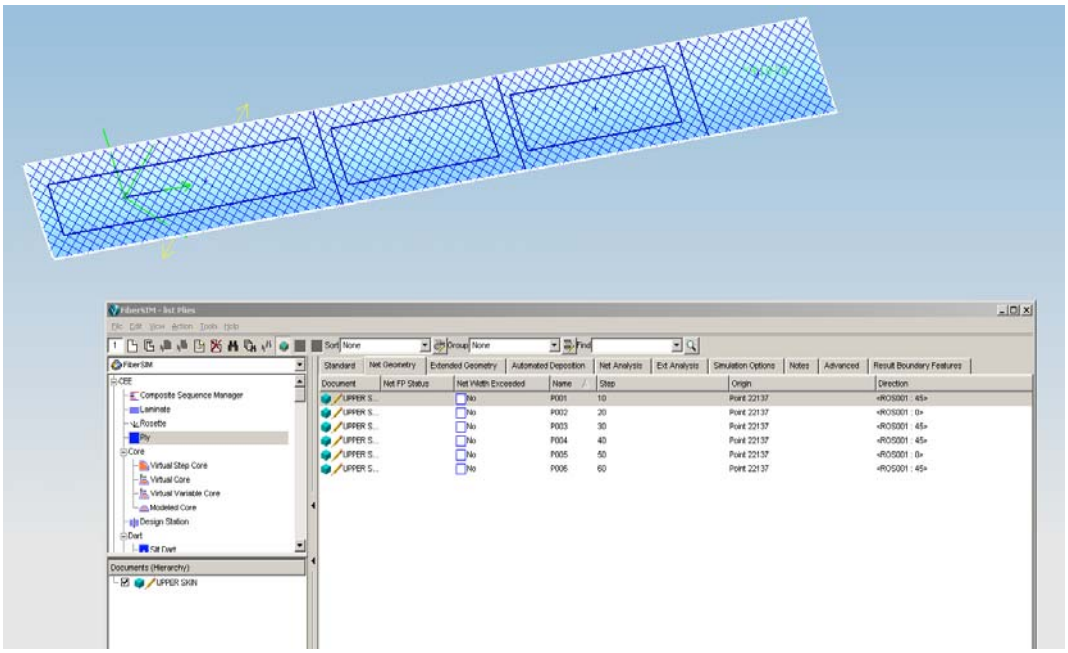

Figure 6.25 The Producibility Analysis of Ply 1

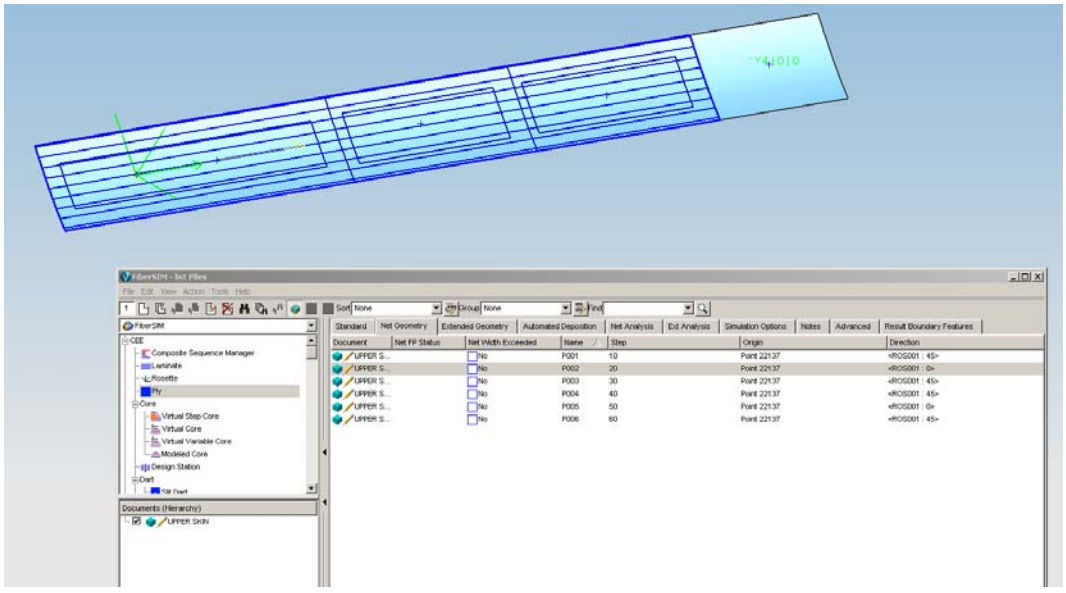

Figure 6.26 The Producibility Analysis of Ply 2

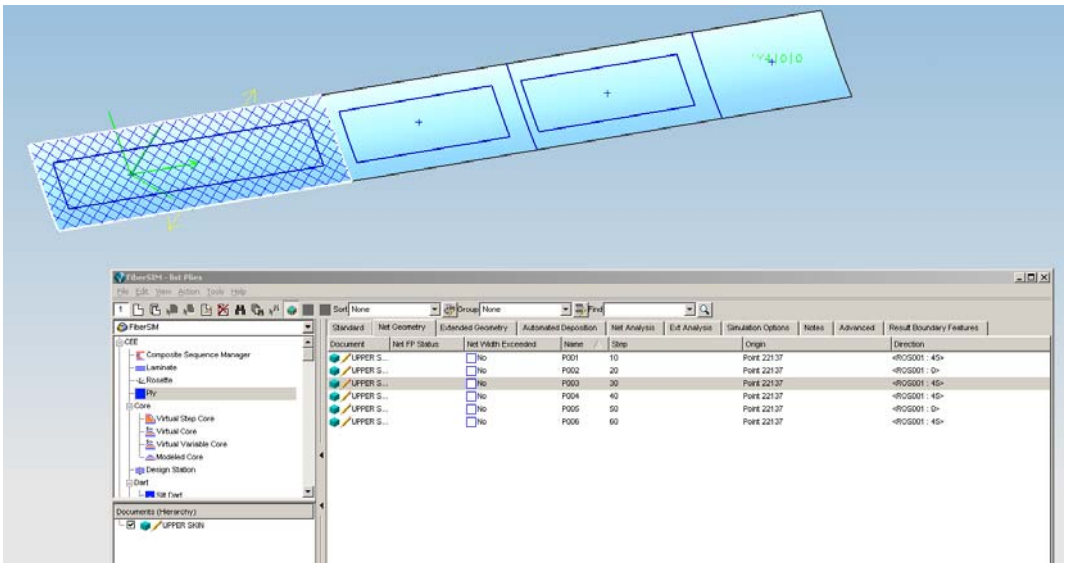

Figure 6.27 The Producibility Analysis of Ply 3

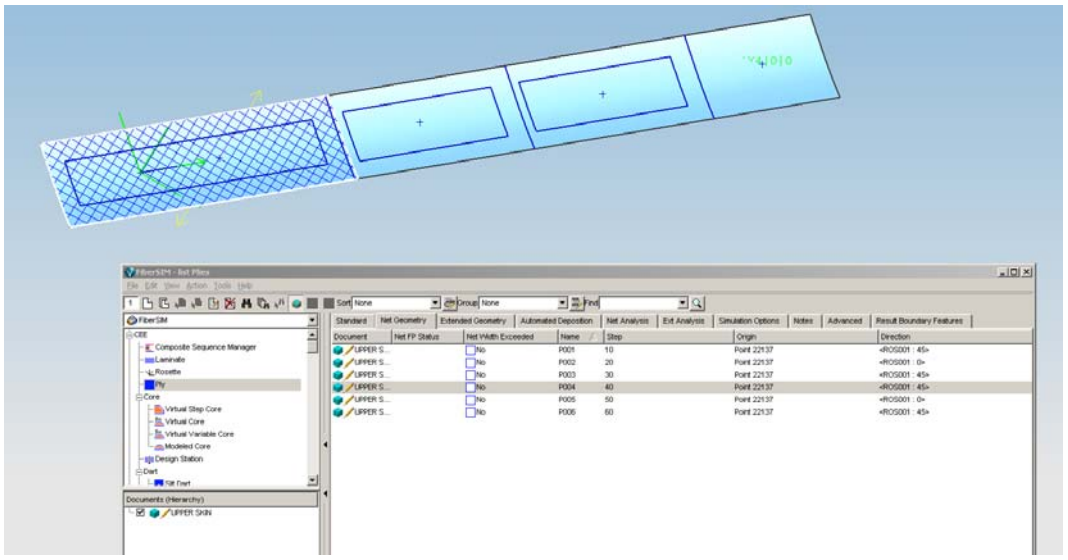

Figure 6.28 The Producibility Analysis of Ply 4

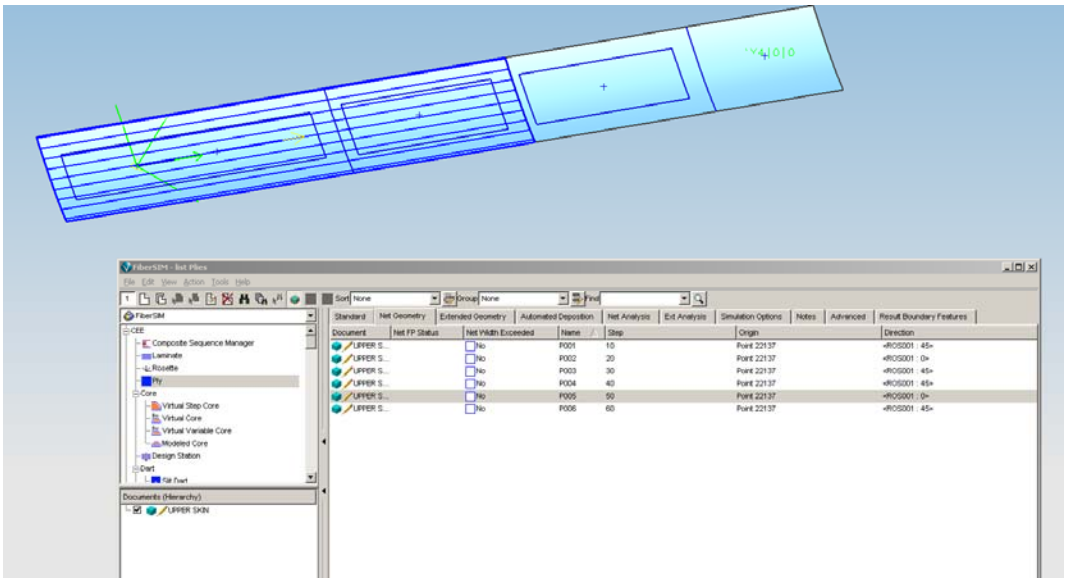

Figure 6.29 The Producibility Analysis of Ply 5

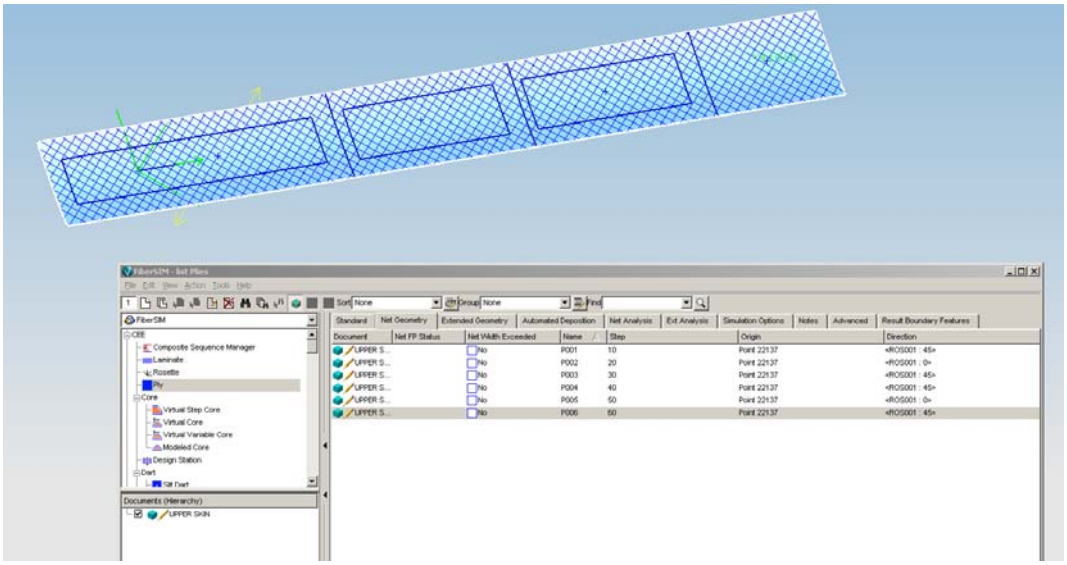

Figure 6.30 The Producibility Analysis of Ply 6

After the producibility analysis of under core plies; the cores and the plies over the cores were created by using Ply-Based Design. First, the film adhesive ply was created with step number 70, as shown in Figure 6.31.

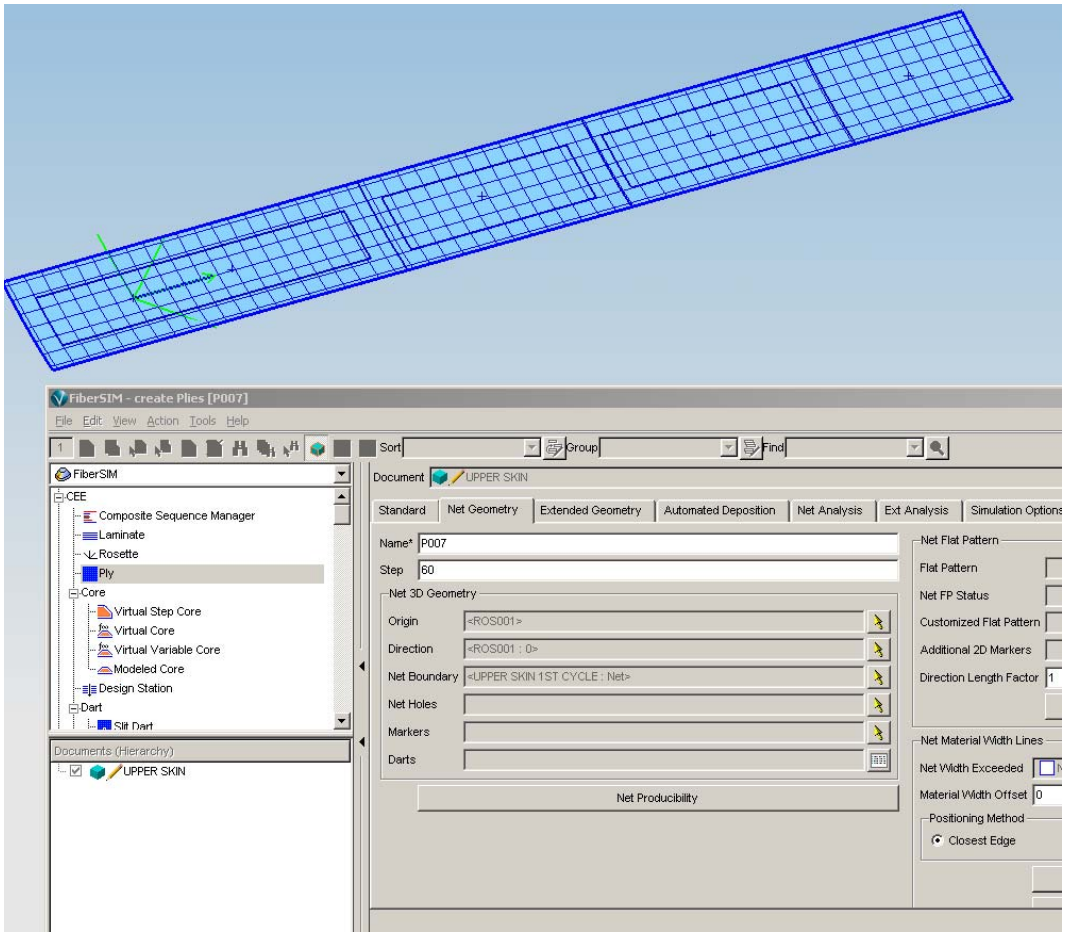

Figure 6.31 The Producibility Analysis of Ply 7 Film Adhesive

Figure 6.32 shows the over core surface, which was created in Unigraphics NX for over core plies producibility analysis.

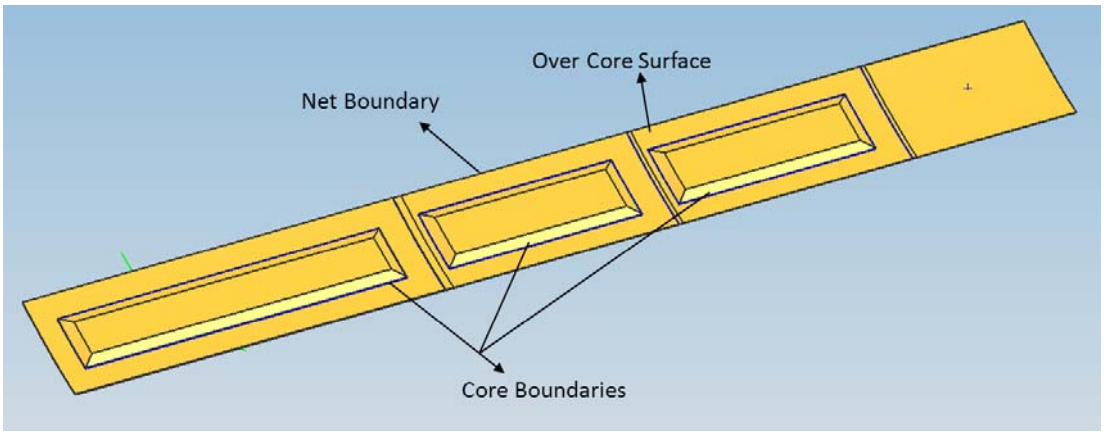

Figure 6.32 Overcore Surface of Upper Skin

A new laminate was created in the laminate part as the of Upperskin 2nd Cycle. The tool surface and net boundary were determined in this laminate, as seen from Figure 6.33. The arrow direction was still important even though new layers were laid up on other part of the skin.

After creating a new laminate, the cores were created. The cores are shown in Figure 6.34. The step number, core thickness (1), Top Bevel Angle (2), Step Height (3) were provided and Figure 6.35 displays three honeycombs created by this method.

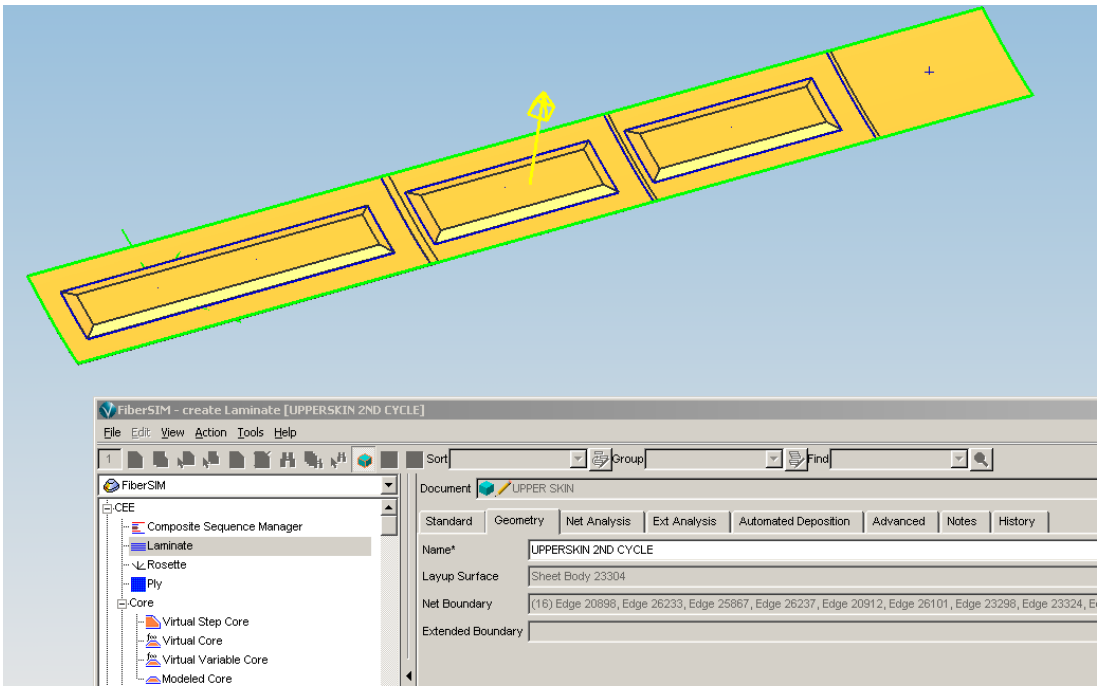

Figure 6.33 Creating the laminate "Upper Skin 2nd Cycle"

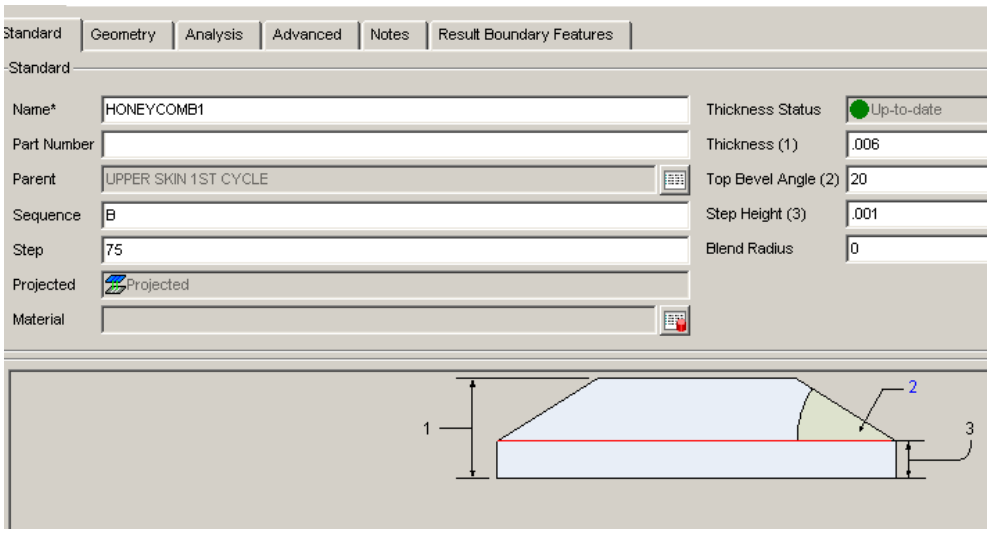

Figure 6.34 Creating Honeycomb1

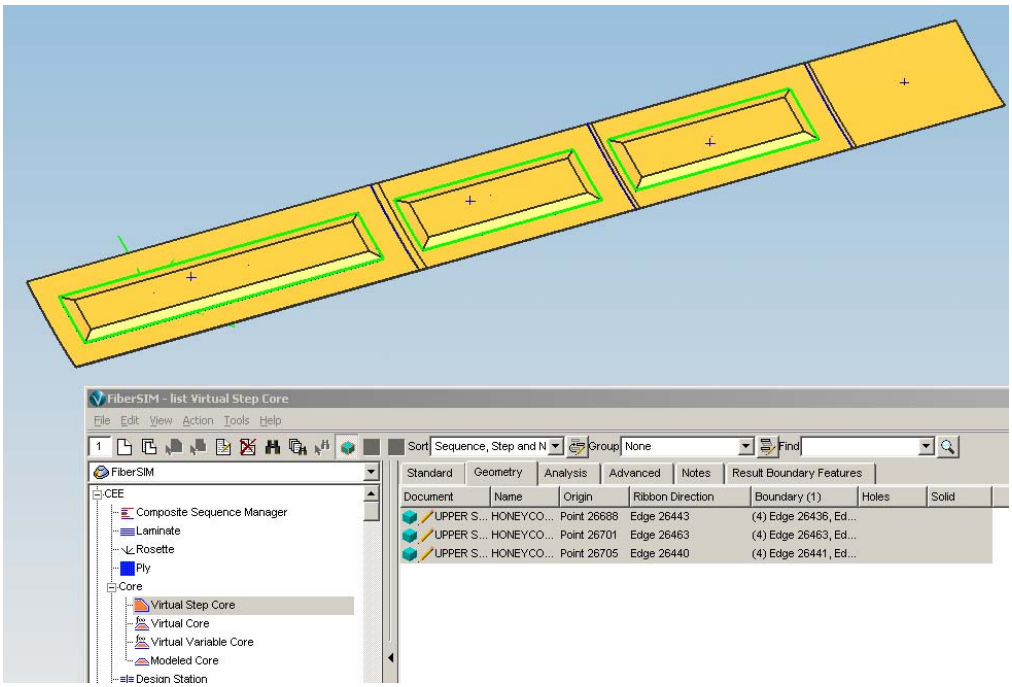

Figure 6.35 Created Honeycombs

The film adhesive plies over the cores were created by defining the origin and boundaries of the plies. Figure 6.36 shows the film adhesive ply over Honeycomb1.

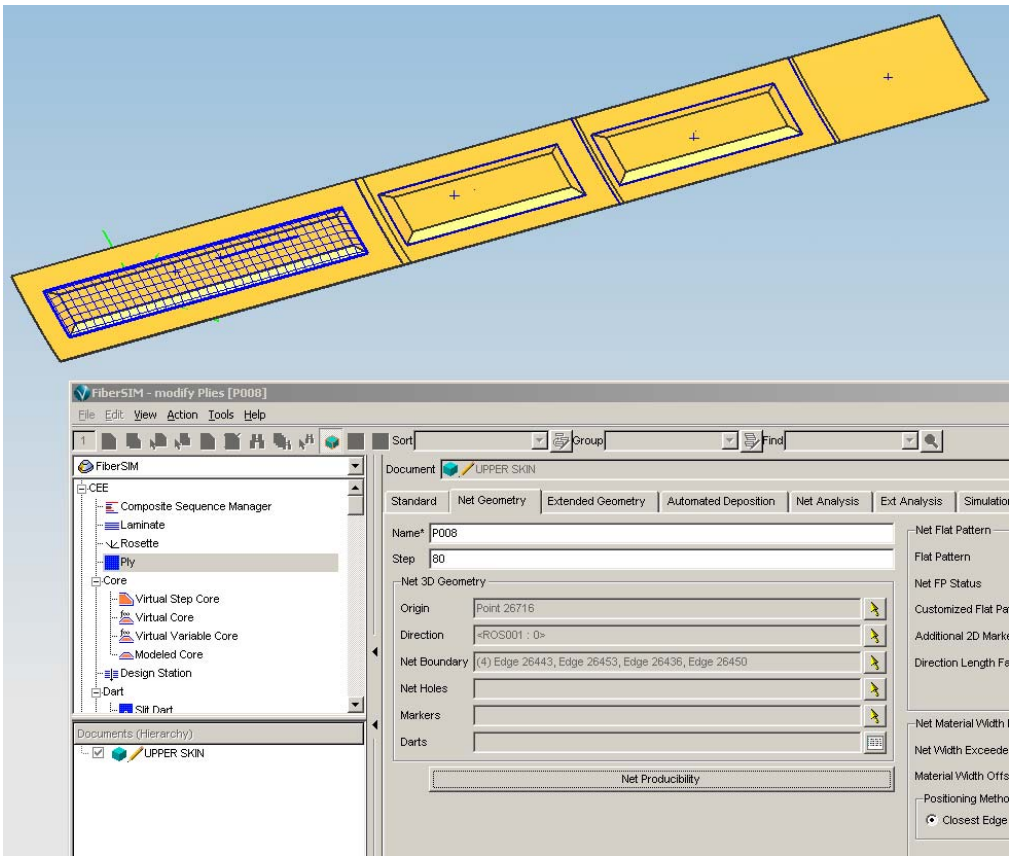

Figure 6.36 The Producibility Analysis of Ply 8, Film Adhesive

The Ply 11, which has 45° direction, was created with correct step number. The producibility analysis of Ply 11 can be seen in Figure 6.37.

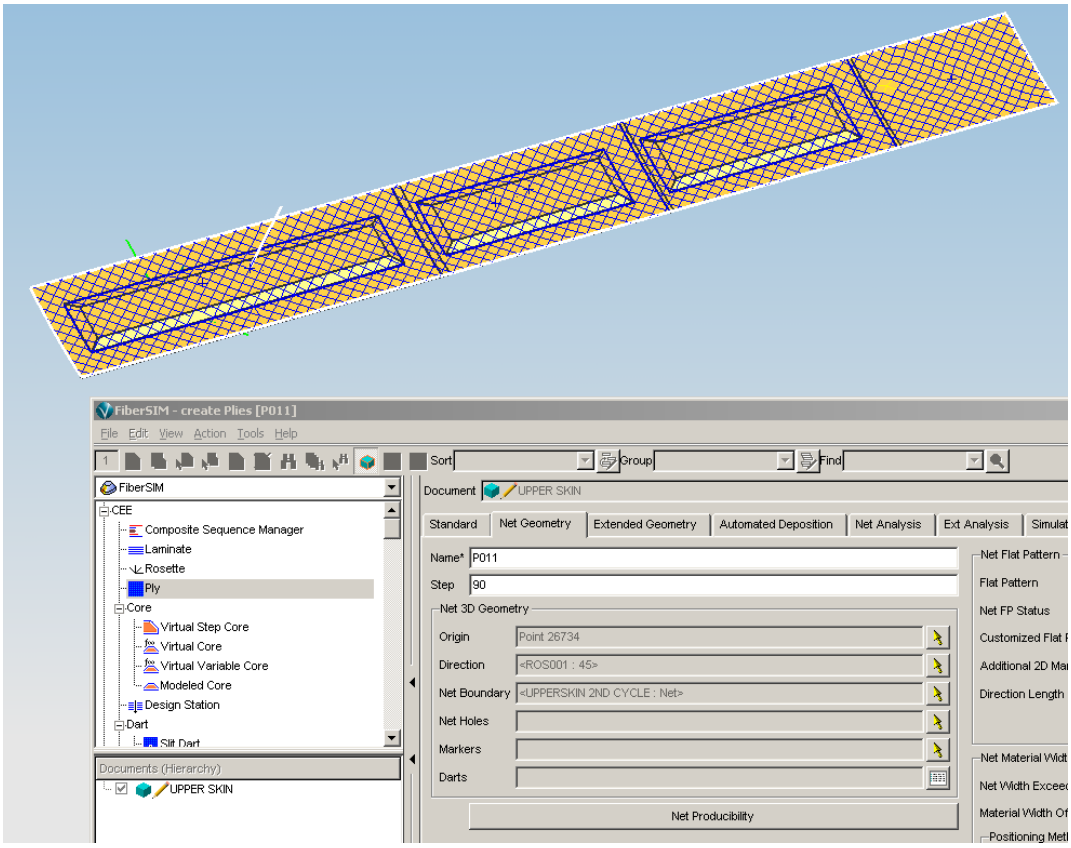

Figure 6.37 The Producibility Analysis of Ply 11

Figure 6.38 shows the Ply 12, which has 0° direction, created with correct step number. However, as it can be seen from the Net Producibility Analysis, the 0° woven fabric cannot be layed up on the tool.

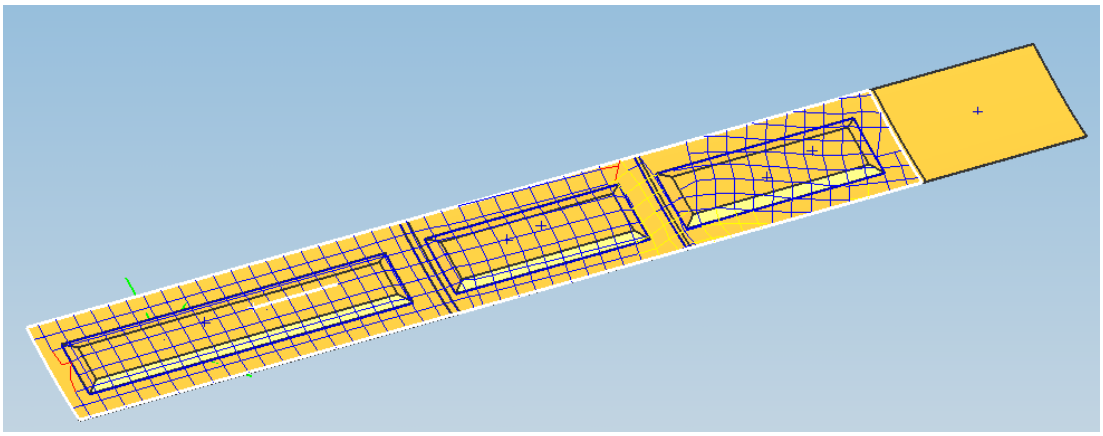

Figure 6.38 The Producibility Analysis of Ply 12

The solution for this problem was to use the 'Splice Ply' Part, as shown in the Figure 6.39. The ply will be divided into two pieces in order to be layed up on the tool appropriately.

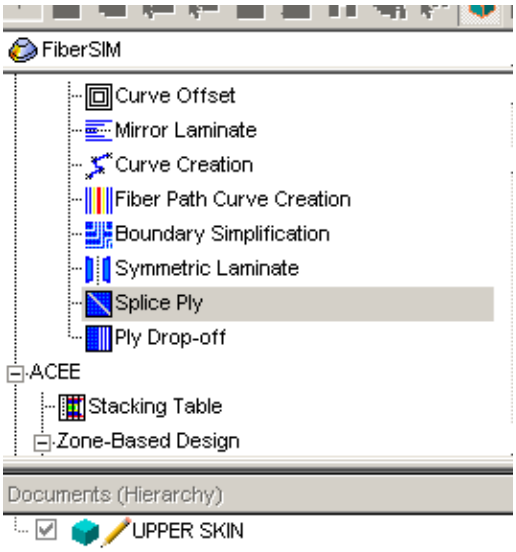

Figure 6.39 Splice Ply Part in Composite Engineering Environment

Two plies, which were called Ply 12-A and Ply 12-B, were created by using the Splice Ply. Created plies are shown in Figure 6.40 and Figure 6.41.

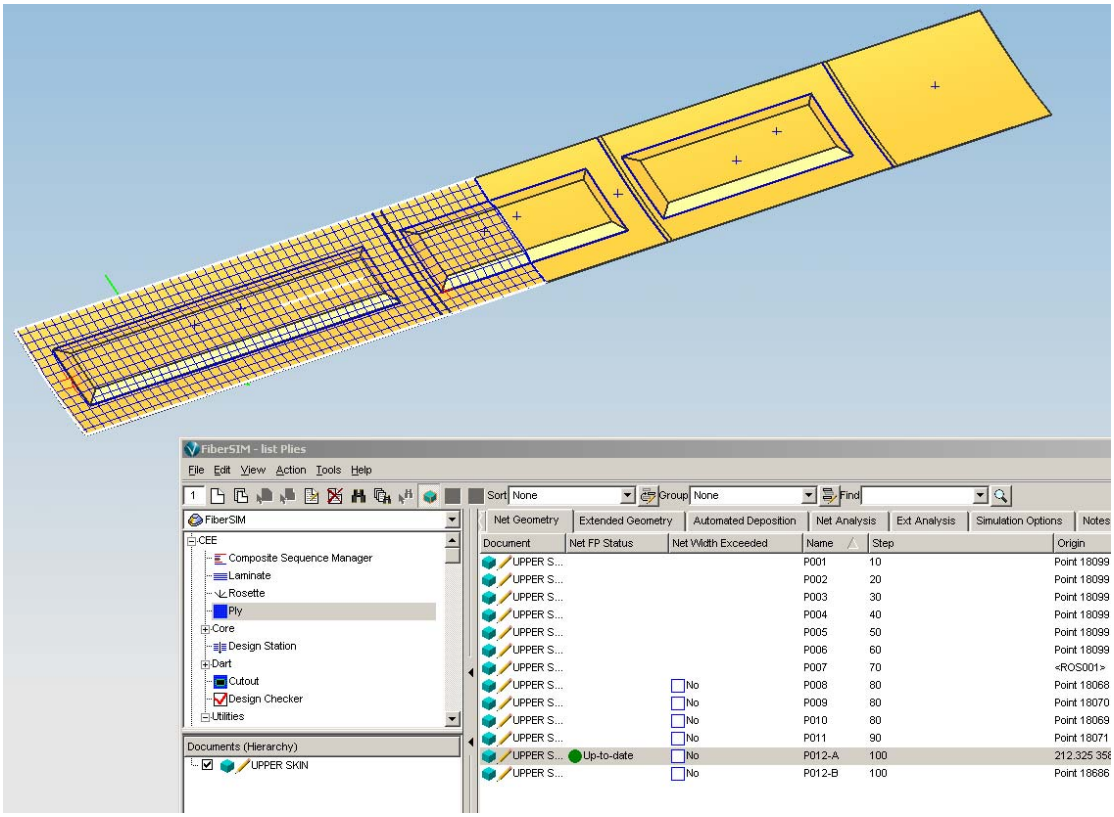

Figure 6.40 The Producibility Analysis of Ply 12-A

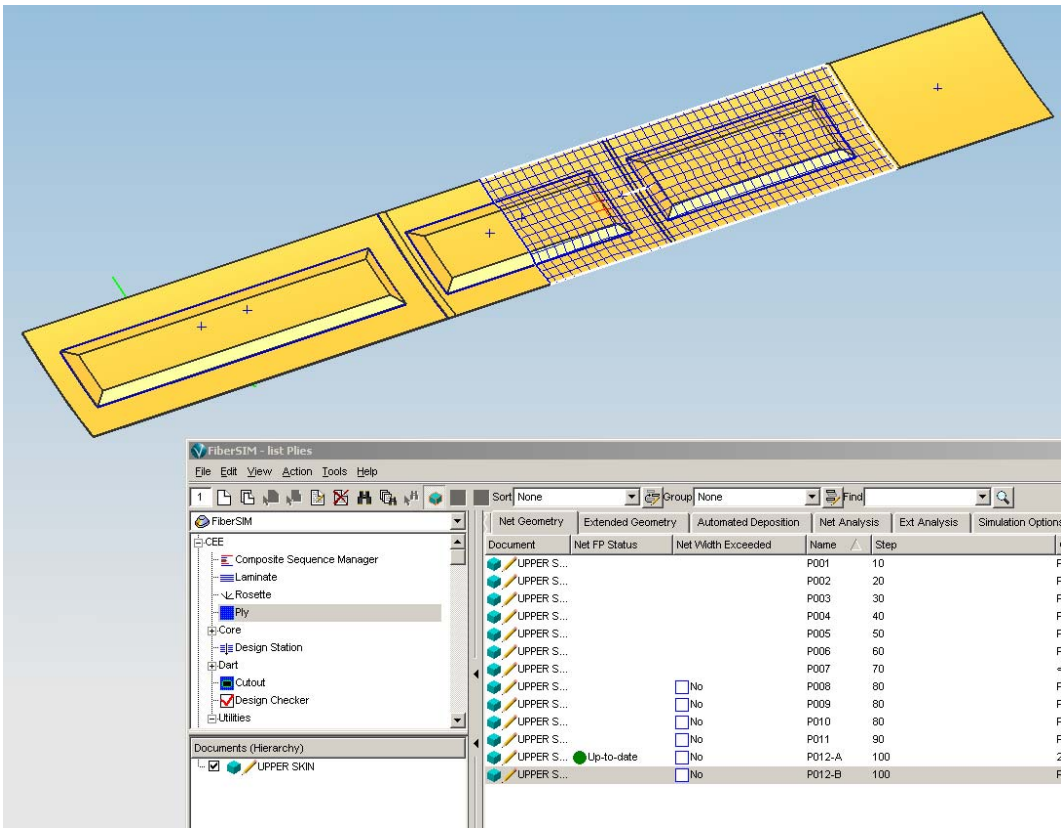

Figure 6.41 The Producibility Analysis of Ply 12-B

The Ply 13, which has 0° direction, was created with correct step number. The similar problem to Ply 12 had occurred from net producibility analysis, as seen in Figure 6.42. The same solution method was applied on the ply 13 and two plies, Ply 13-A and Ply 13-B, were created, as shown in Figure 6.43 and Figure 6.44 respectively.

Figure 6.45 shows Ply 14, which has 45° direction, was created without encountering any producibility problem.

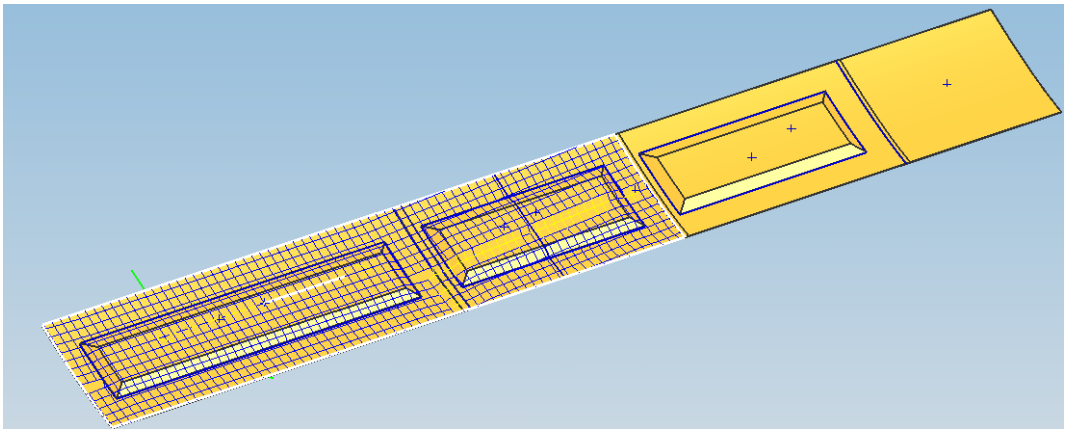

Figure 6.42 The Producibility Analysis of Ply 13

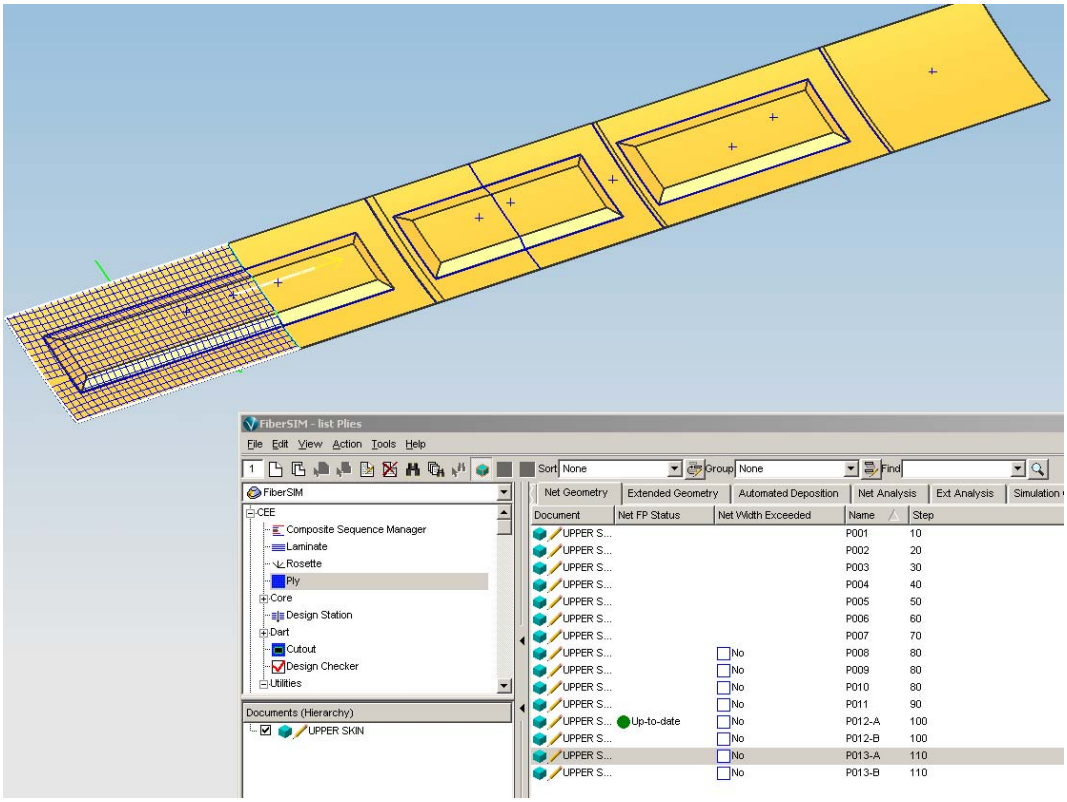

Figure 6.43 The Producibility Analysis of Ply 13-A

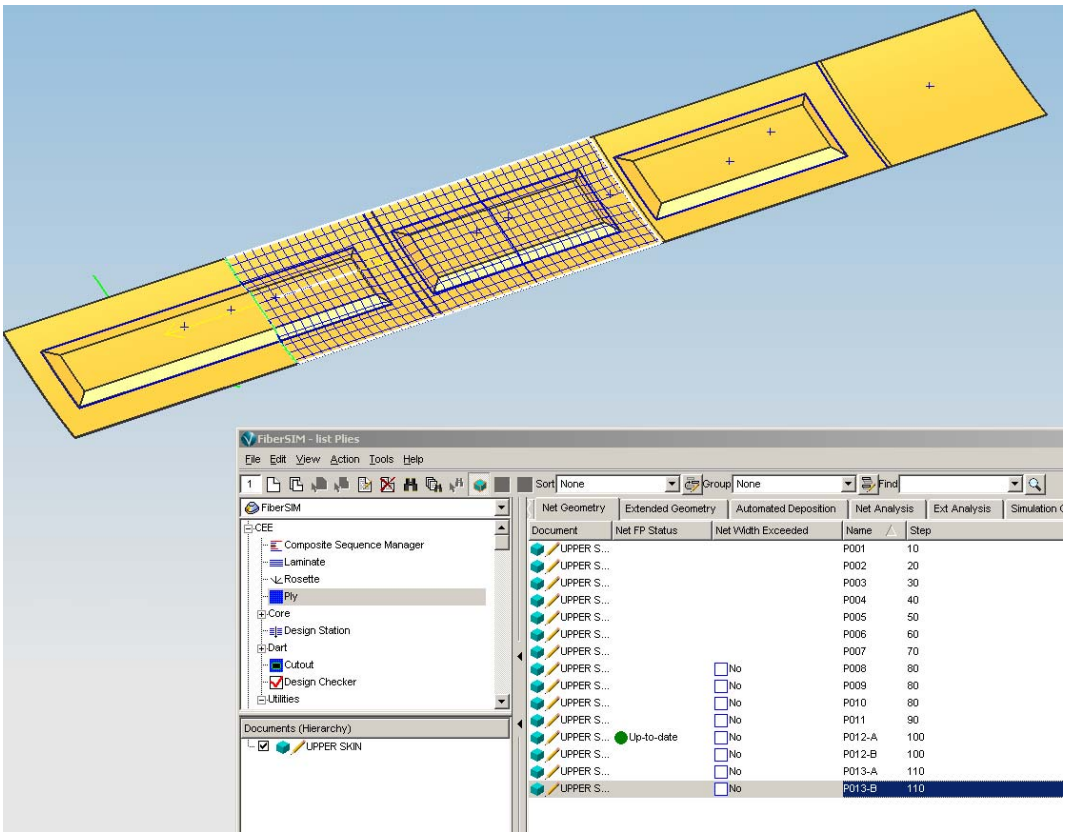

Figure 6.44 The Producibility Analysis of Ply 13-B

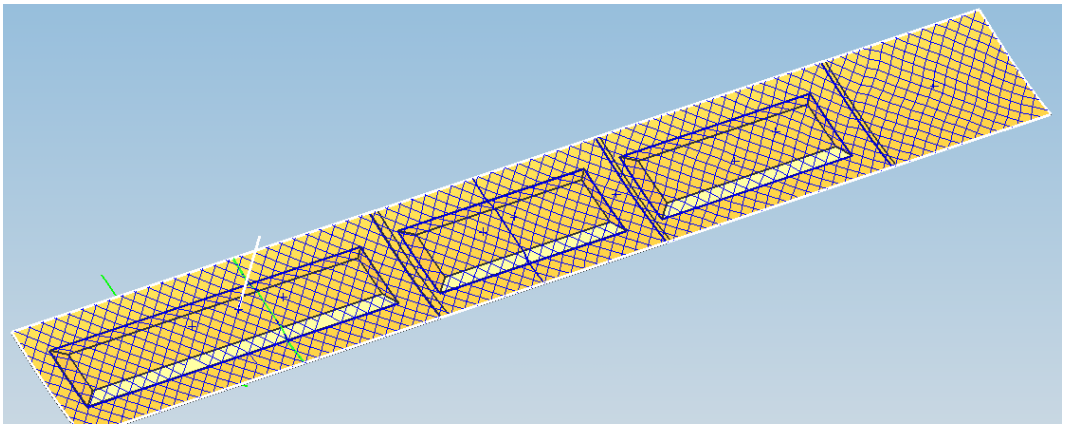

Figure 6.45 The Producibility Analysis of Ply 14

After creating all the plies, the flat patterns of the 14 plies were created. This was given in Figure 6.46. The flat pattern data would be transferred to automatic cutting machine as it was described previously on chapter introduction.

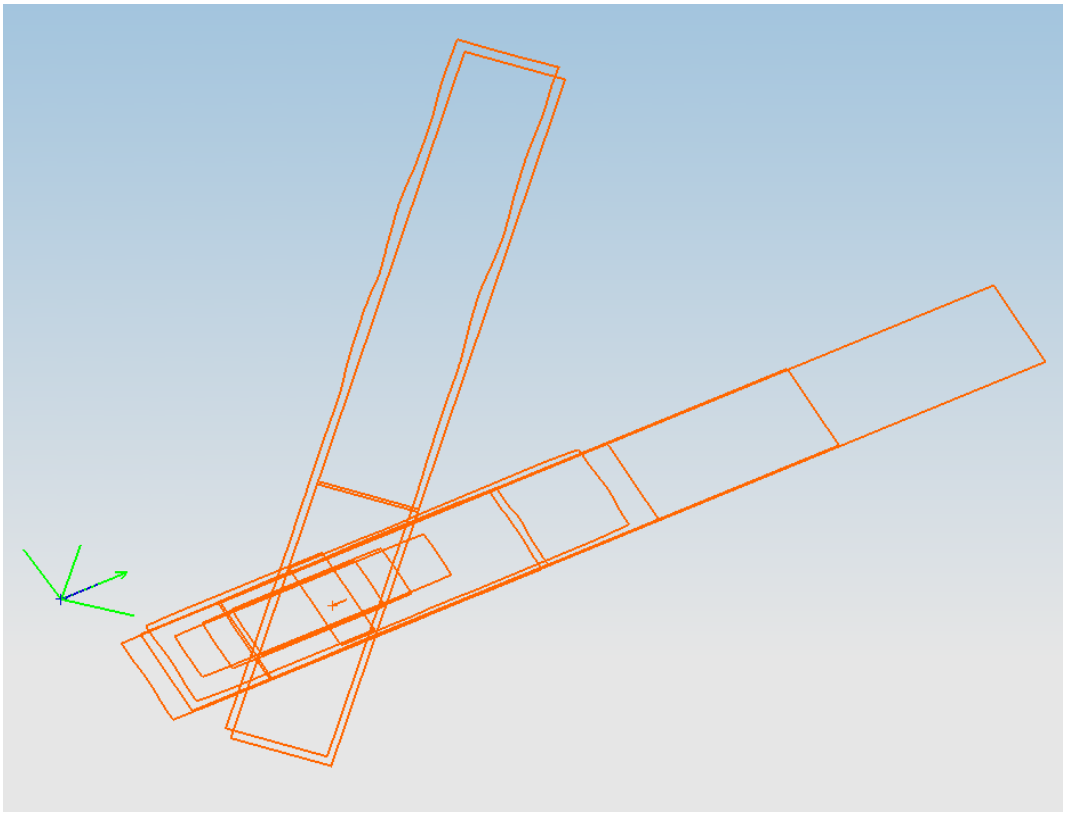

Figure 6.46 The Flat Patterns of 14 Plies

The boundaries of 14 plies were created from Boundary Simplication part, shown in Figure 6.47. The created boundaries of all plies can be seen in Figure 6.48.

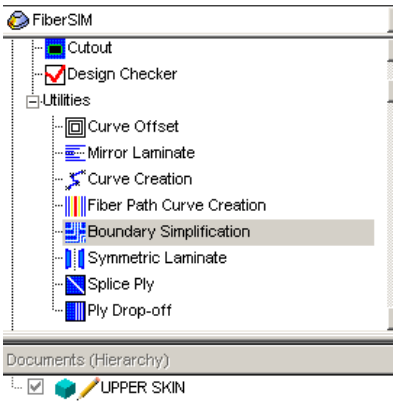

Figure 6.47 Boundary Simplification Part in Composite Engineering Environment

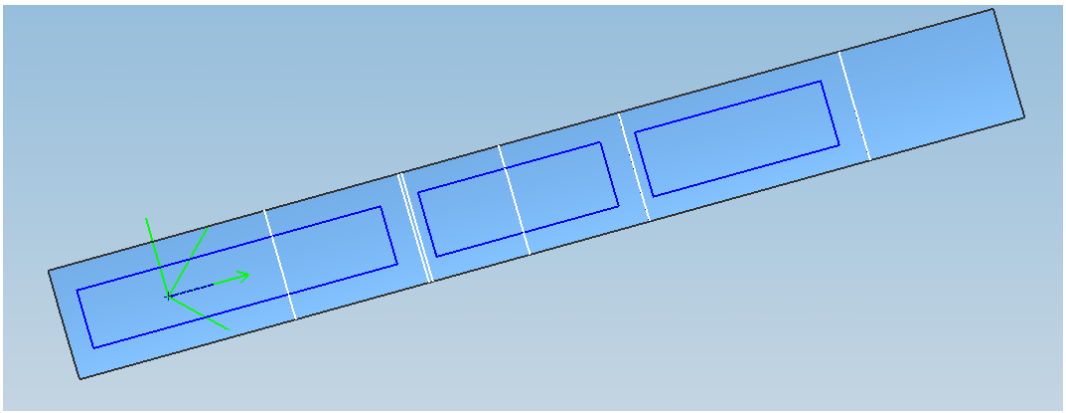

Figure 6.48 Boundary Simplification Result for the Upper Skin

Before all the data transferred to the manufacturing department, the cross section of the laminate was obtained from 3D Cross Section in the Documentation part. This procedure is shown in Figure 6.49.

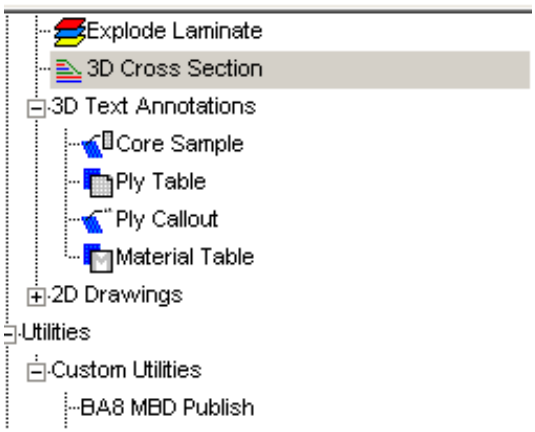

Figure 6.49 3D Cross Section in Documentation

The results of 3D Cross Section of the Upper Skin can be seen in Figure 6.50 to Figure 6.55.

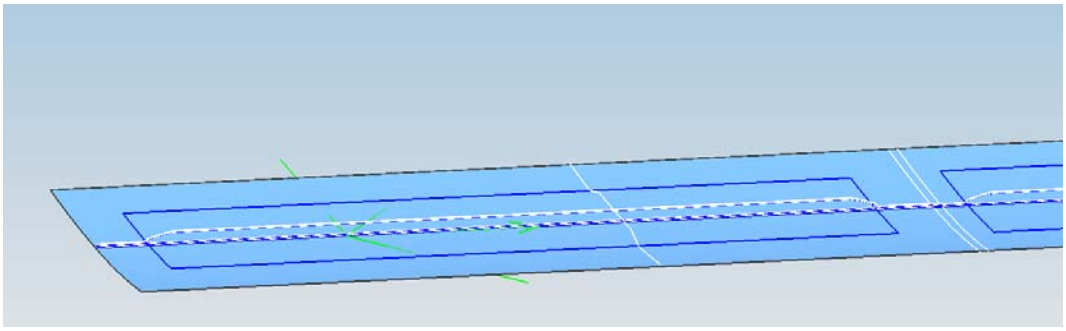

Figure 6.50 The General View of 3D Cross Section Result

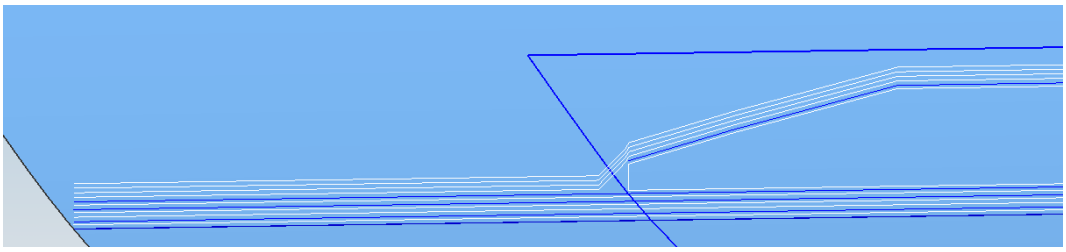

Figure 6.51 3D Cross Section Result of Honeycomb1 Near Tip of the Ting

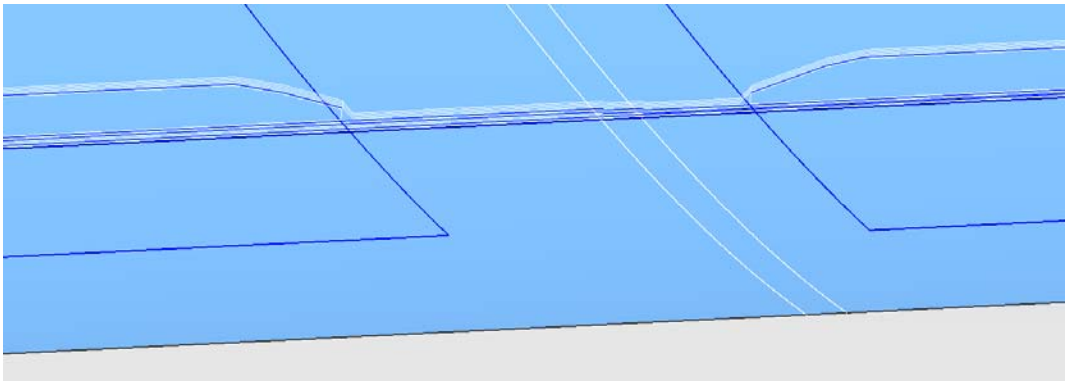

Figure 6.52 3D Cross Section Result of Drop-off from Bay 1 to Bay 2

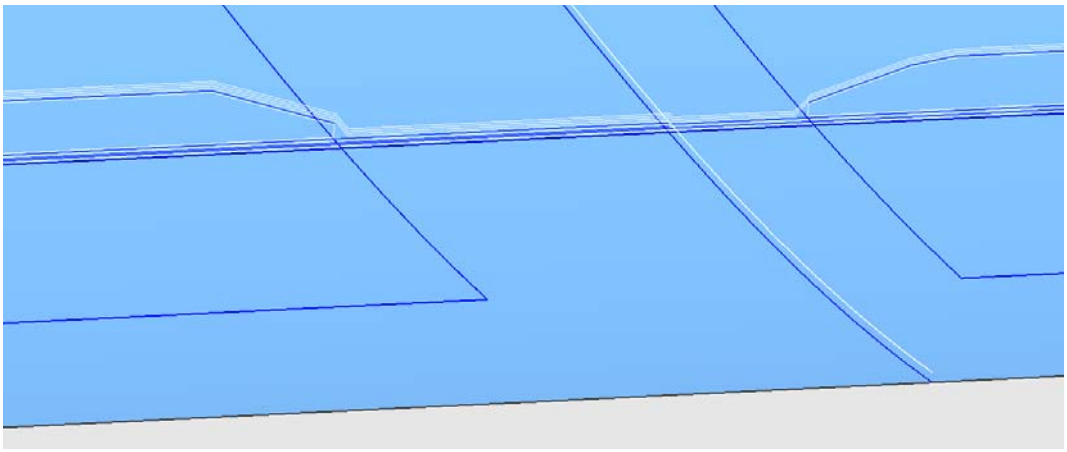

Figure 6.53 3D Cross Section Result of Drop-off from Bay 2 to Bay 3

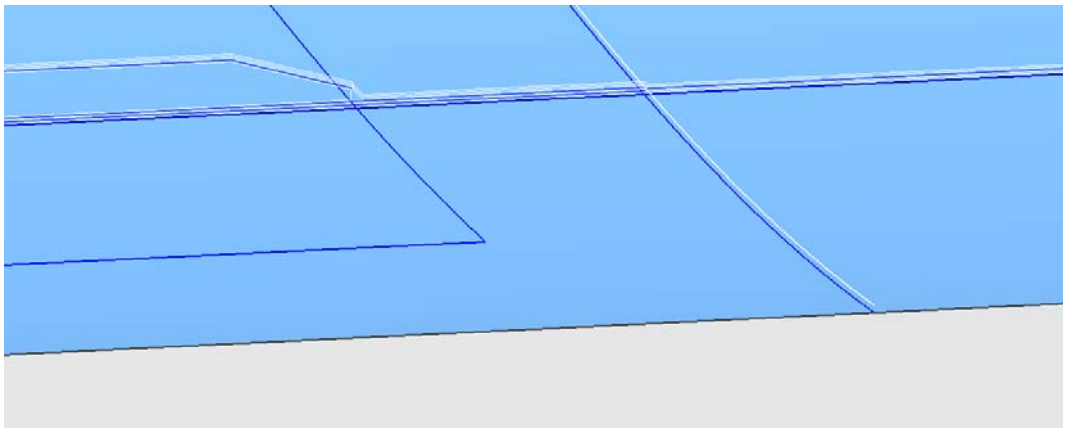

Figure 6.54 3D Cross Section Result of Drop-off from Bay 3 to Bay 4

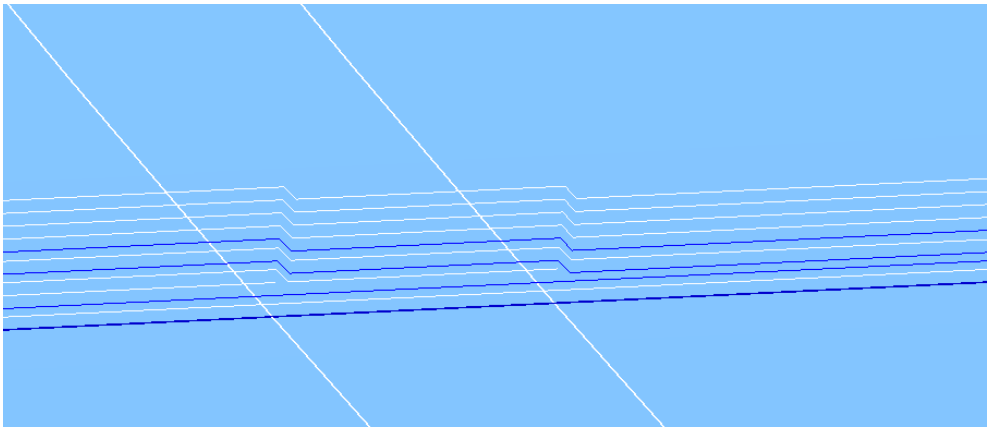

Figure 6.55 Cross Sectional Shape of the Drop-off from Bay 1 to Bay 2

6.2.2 Spar Producibility Analysis

The model of the rear spar was chosen for the FiberSIM analysis. Figure 6.56 shows the model tool surface, net boundary of the laminate, and the boundaries of the bays for the rear spar.

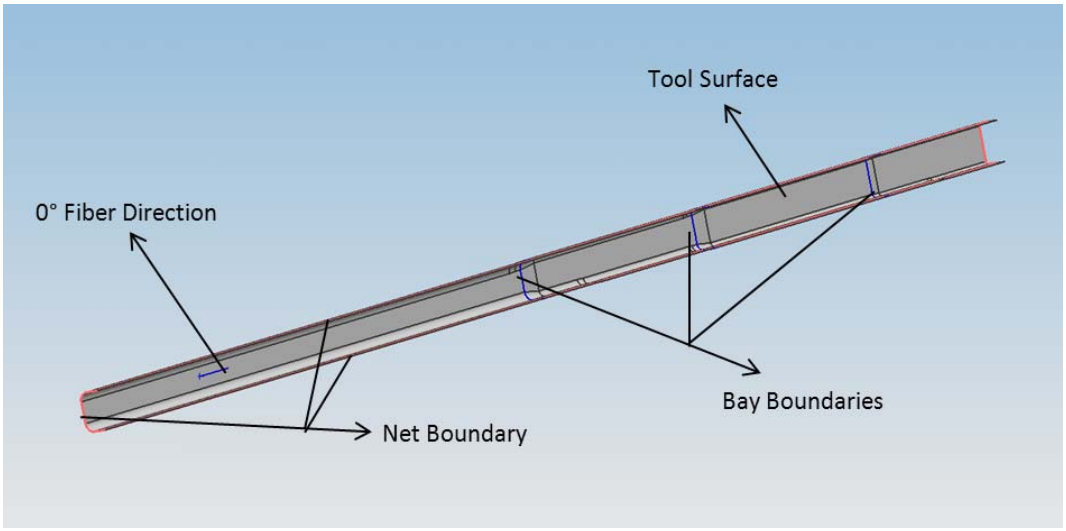

Figure 6.56 The Set-up Model of Rear Spar

A laminate was created called Rear Spar in the laminate part. The tool surface was determined from the laminate section shown in the Figure 6.57. The tool surface was determined to be the female, so the arrow direction was through the torque box. Figure 6.58 shows the net boundary information given in the laminate part.

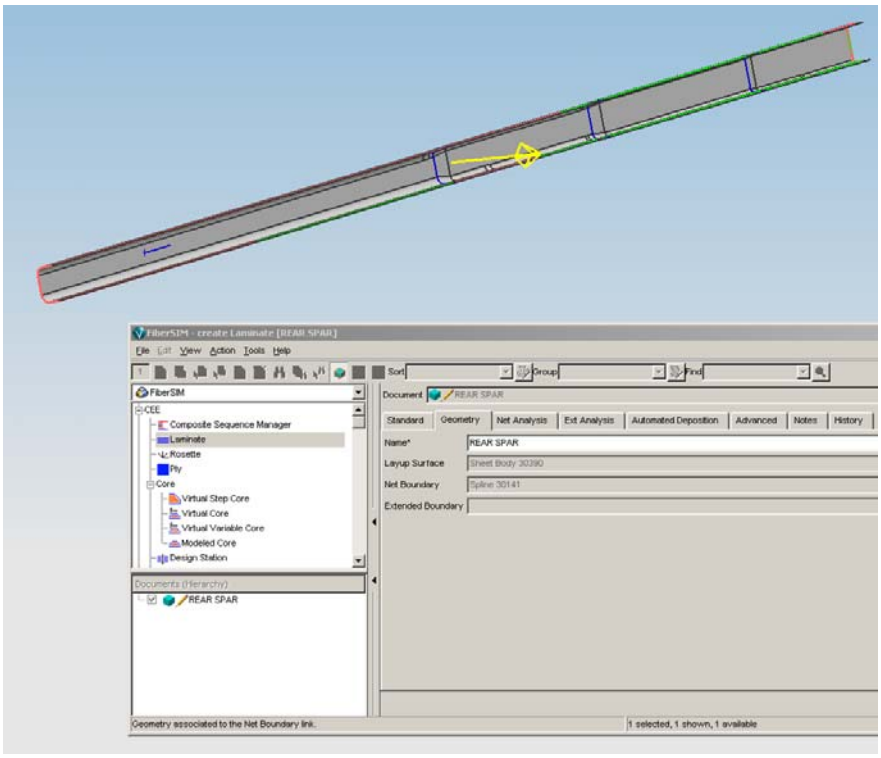

Figure 6.57 Determining the Tool Surface for Spar Production

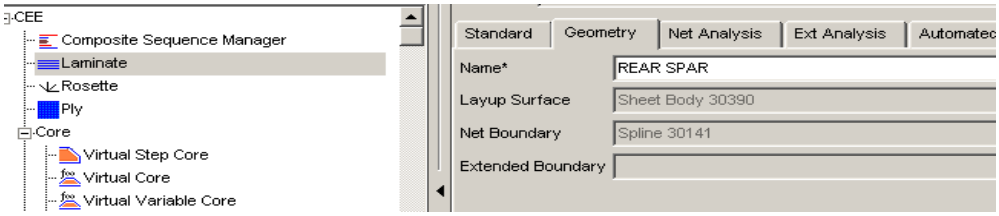

Figure 6.58 Creation of the Spar the Laminate "Rear Spar"

The necessary rosette was created from Rosette part by defining the origin and the direction. The rosette, which gives 0°, 45°, 90° and -45° directions of the plies, is shown in Figure 6.59.

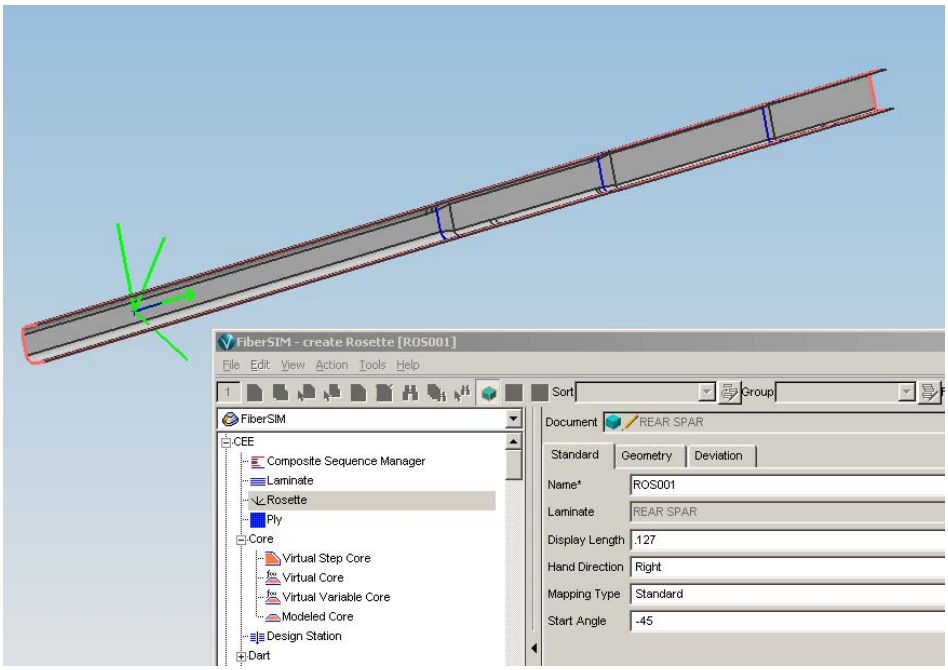

Figure 6.59 Creating Rosette in Spar

The spar consisted of 4 bays, so the Zone-Based Design was employed. The bays would be defined in the Zone part after the sequence of each bay was determined in the laminate specification part. This procedure is shown in the Figure 6.60 to Figure 6.63.

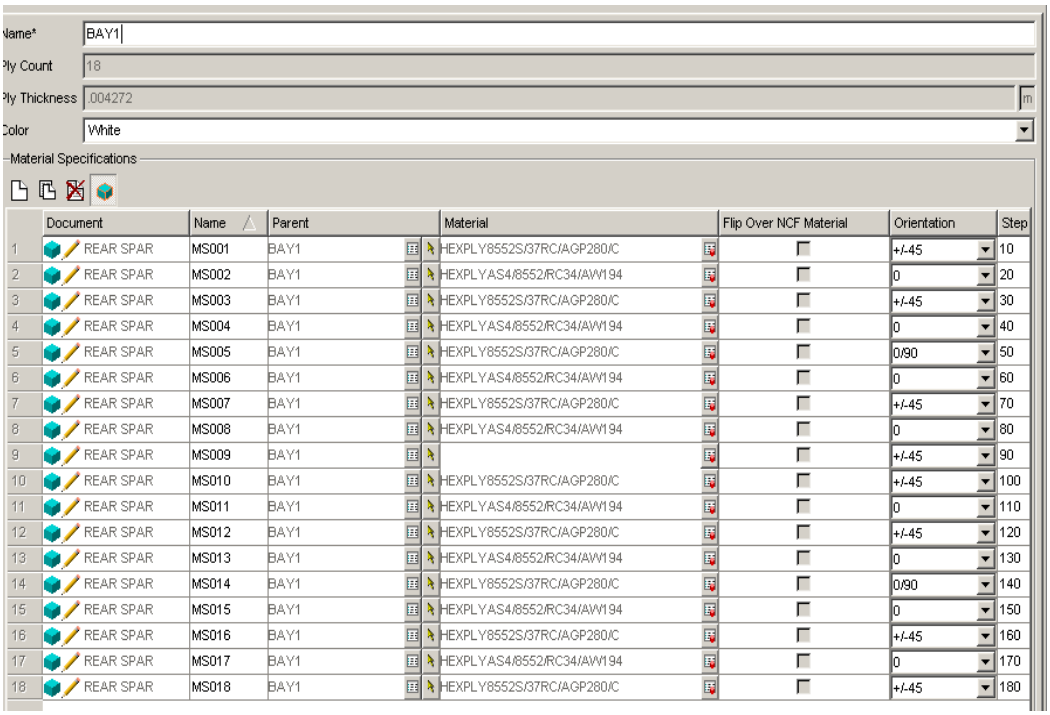

Name* BAY1
Ply Count 18
Ply Thickness .004272 m
Color White

Material Specifications

	Document	Name	Parent	Material	Flip Over NCF Material	Orientation	Step
1	REAR SPAR	MS001	BAY1	HEXPLY8552S/37RC/AGP280/C		+/-45	10
2	REAR SPAR	MS002	BAY1	HEXPLYAS4/8552/RC34/AW194		0	20
3	REAR SPAR	MS003	BAY1	HEXPLY8552S/37RC/AGP280/C		+/-45	30
4	REAR SPAR	MS004	BAY1	HEXPLYAS4/8552/RC34/AW194		0	40
5	REAR SPAR	MS005	BAY1	HEXPLY8552S/37RC/AGP280/C		0/90	50
6	REAR SPAR	MS006	BAY1	HEXPLYAS4/8552/RC34/AW194		0	60
7	REAR SPAR	MS007	BAY1	HEXPLY8552S/37RC/AGP280/C		+/-45	70
8	REAR SPAR	MS008	BAY1	HEXPLYAS4/8552/RC34/AW194		0	80
9	REAR SPAR	MS009	BAY1			+/-45	90
10	REAR SPAR	MS010	BAY1	HEXPLY8552S/37RC/AGP280/C		+/-45	100
11	REAR SPAR	MS011	BAY1	HEXPLYAS4/8552/RC34/AW194		0	110
12	REAR SPAR	MS012	BAY1	HEXPLY8552S/37RC/AGP280/C		+/-45	120
13	REAR SPAR	MS013	BAY1	HEXPLYAS4/8552/RC34/AW194		0	130
14	REAR SPAR	MS014	BAY1	HEXPLY8552S/37RC/AGP280/C		0/90	140
15	REAR SPAR	MS015	BAY1	HEXPLYAS4/8552/RC34/AW194		0	150
16	REAR SPAR	MS016	BAY1	HEXPLY8552S/37RC/AGP280/C		+/-45	160
17	REAR SPAR	MS017	BAY1	HEXPLYAS4/8552/RC34/AW194		0	170
18	REAR SPAR	MS018	BAY1	HEXPLY8552S/37RC/AGP280/C		+/-45	180

Figure 6.60 Laminate Specification of Bay 1

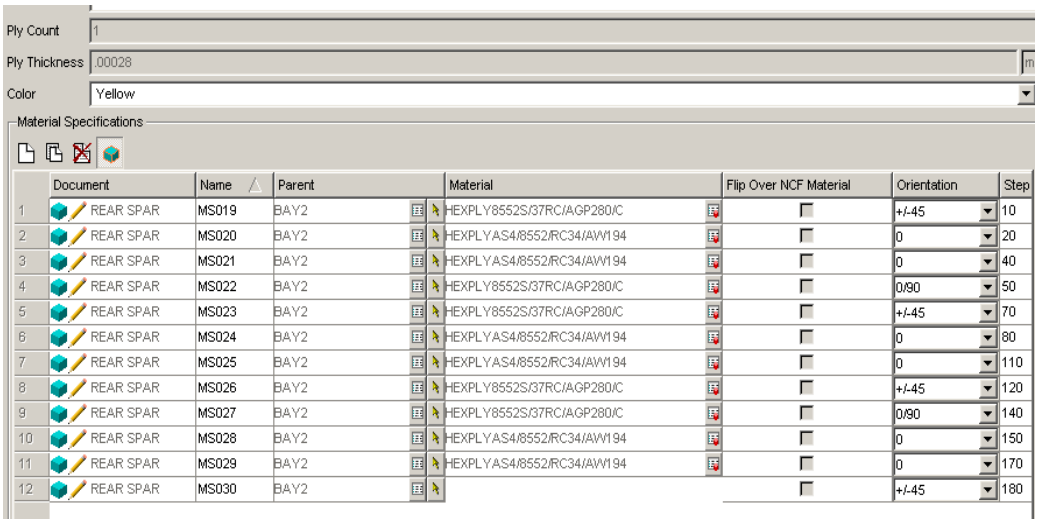

Ply Count 1
Ply Thickness .00028 m
Color Yellow

Material Specifications

	Document	Name	Parent	Material	Flip Over NCF Material	Orientation	Step
1	REAR SPAR	MS019	BAY2	HEXPLY8552S/37RC/AGP280/C		+/-45	10
2	REAR SPAR	MS020	BAY2	HEXPLYAS4/8552/RC34/AW194		0	20
3	REAR SPAR	MS021	BAY2	HEXPLYAS4/8552/RC34/AW194		0	40
4	REAR SPAR	MS022	BAY2	HEXPLY8552S/37RC/AGP280/C		0/90	50
5	REAR SPAR	MS023	BAY2	HEXPLY8552S/37RC/AGP280/C		+/-45	70
6	REAR SPAR	MS024	BAY2	HEXPLYAS4/8552/RC34/AW194		0	80
7	REAR SPAR	MS025	BAY2	HEXPLYAS4/8552/RC34/AW194		0	110
8	REAR SPAR	MS026	BAY2	HEXPLY8552S/37RC/AGP280/C		+/-45	120
9	REAR SPAR	MS027	BAY2	HEXPLY8552S/37RC/AGP280/C		0/90	140
10	REAR SPAR	MS028	BAY2	HEXPLYAS4/8552/RC34/AW194		0	150
11	REAR SPAR	MS029	BAY2	HEXPLYAS4/8552/RC34/AW194		0	170
12	REAR SPAR	MS030	BAY2			+/-45	180

Figure 6.61 Laminate Specification of Bay 2

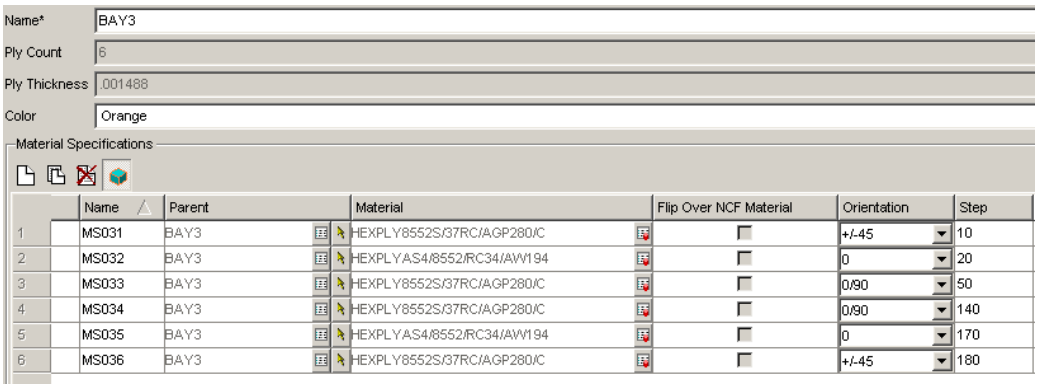

Figure 6.62 Laminate Specification of Bay 3

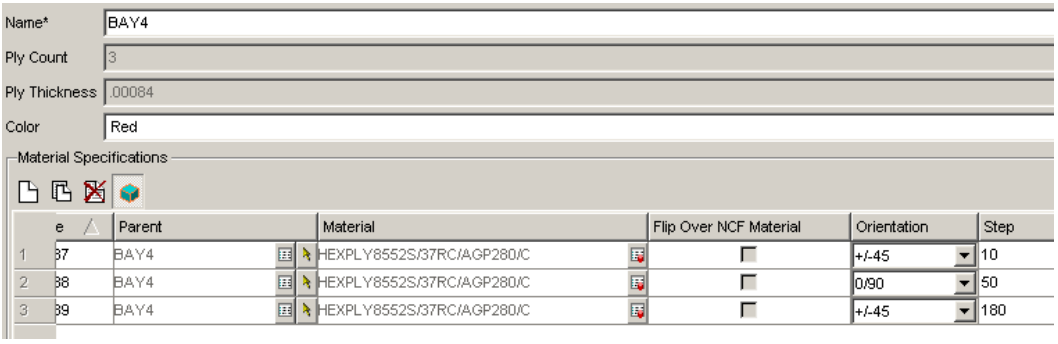

Figure 6.63 Laminate Specification of Bay 4

In the Laminate Specification, each ply was determined with material information, orientation and ordering information with step number.

Table 6.2 gives laminate information for Bay 1 - Bay 4. Figure 6.64 shows final situation of the laminate specification part.

Table 6.2 Laminate Sequence of Rear Spar

STEP NO	PLY NAME	BAY 1	BAY 2	BAY 3	BAY 4
10	P 1	45˚	45˚	45˚	45˚
20	P 2	0˚	0˚	0˚	
30	P 3	45˚			
40	P 4	0˚	0˚		
50	P 5	0˚	0˚	0˚	0˚
60	P 6	0˚			
70	P 7	45˚	45˚		
80	P 8	0˚	0˚		
90	P 9	45˚			
100	P 10	45˚			
110	P 11	0˚	0˚		
120	P 12	45˚	45˚		
130	P 13	0˚			
140	P 14	0˚	0˚	0˚	
150	P 15	0˚	0˚		
160	P 16	45˚			
170	P 17	0˚	0˚	0˚	
180	P 18	45˚	45˚	45˚	45˚

45˚ Woven Fabric
0˚ UD Fabric
0˚ Woven Fabric

Document	Name	Ply Count	Ply Thickness (m)	Color
REAR S...	BAY1	18	.004272	White
REAR S...	BAY2	12	.002784	Yellow
REAR S...	BAY3	6	.001488	Orange
REAR S...	BAY4	3	.000744	Red

Figure 6.64 The List of Laminate Specification of 4 Bays

After determining the laminate specification part, the bays were determined by using the Zone part. In the Standard tab, laminate information, rosette information, origin of the zone information and boundary information were given. Figure 6.65 shows the creation of Bay 3 as an example.

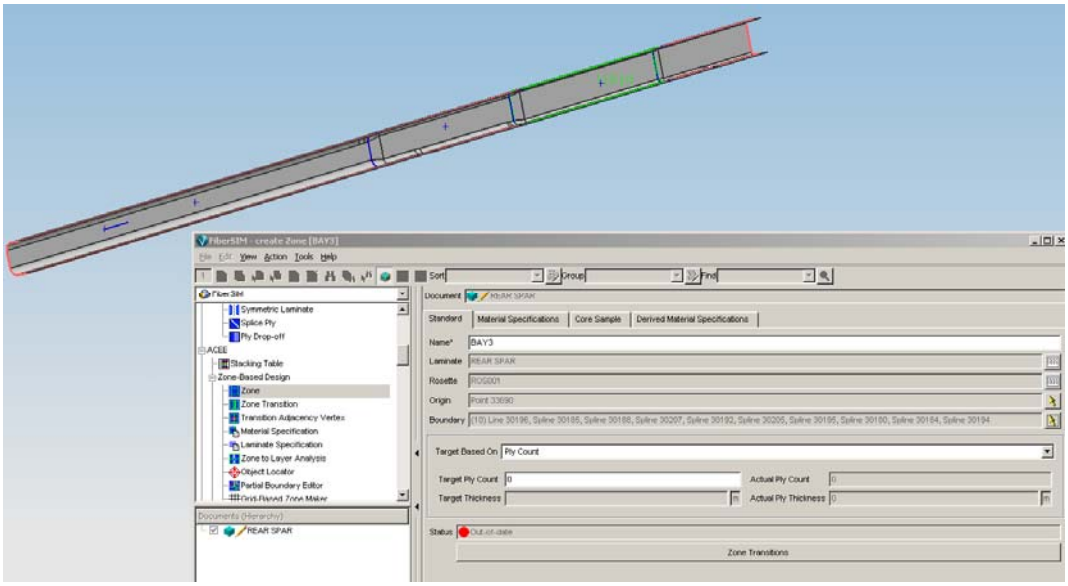

Figure 6.65 Creation of Bay 3 of the Rear Spar

When all the bays were created, the list of the bays is in the form viewed in the Figure 6.66. The Zone to Layer Analysis was performed in order to obtain the plies after Bays are created in the Zone part.

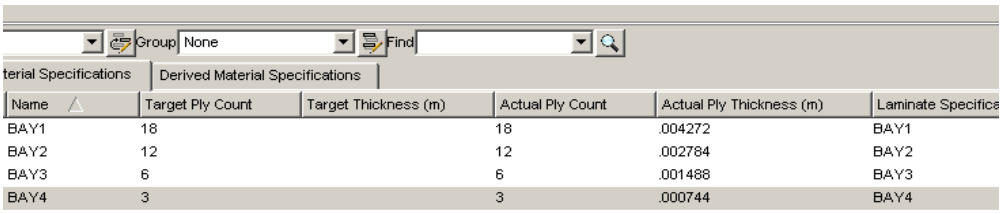

Figure 6.66 List of 4 Bays in Zone Part

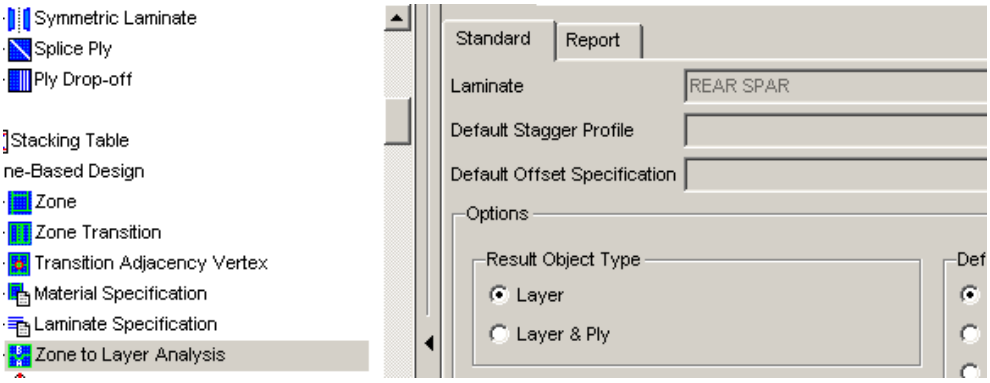

Figure 6.67 Zone to Layer Analysis Applied to the Rear Spar

In the Zone to Layer Analysis, Default Stagger Profile should be defined. There were 6 ply decreases from Bay 1 to Bay 2, Bay 2 to Bay 3 and 3 ply decreases from Bay 3 to Bay 4. When the number of decreased ply in the drop-off was more than two, the drop-off shape was important. The cross section shape of the drop-off was desired to become close to the diamond shape. The drop-off shapes of the spars were chosen as half-diamond shape. Figure 6.68 to Figure 6.70 show Stagger Profiles of the drop-off between bays. In the FiberSIM, the user must input the data in Custom section of the Stagger Profile. The drop-off sequence of the plies is determined via integers in FiberSIM. For example Figure 6.68 expresses that at first 10^{th} ply called P10 should drop, 9^{th} ply called P9 second, P13 third, then P6, then P16 and finally P3 should drop in order to obtain a half

diamond shape. After the determination of drop-off sequence of the plies, integers were given at the end of each ply as seen in figure. The table in Figure 6.68, which determines the pattern of drop-off, was obtained. The pattern from Bay 1 to Bay 2, Bay 2 to Bay 3 is 5,3,1,0,2,4 and the pattern from Bay 3 to Bay 4 is 2,0,1 [7].

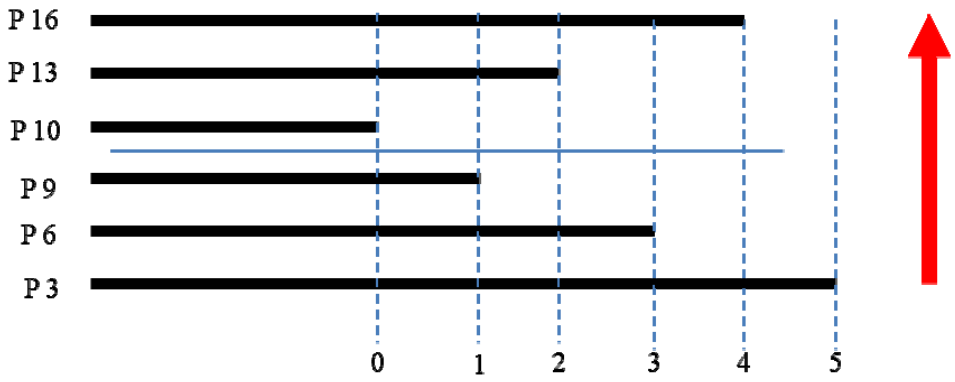

P 3	P 6	P 9	P 10	P 13	P 16
5	3	1	0	2	4

Figure 6.68 Stagger Profile of Drop-off from Bay 1 to Bay 2

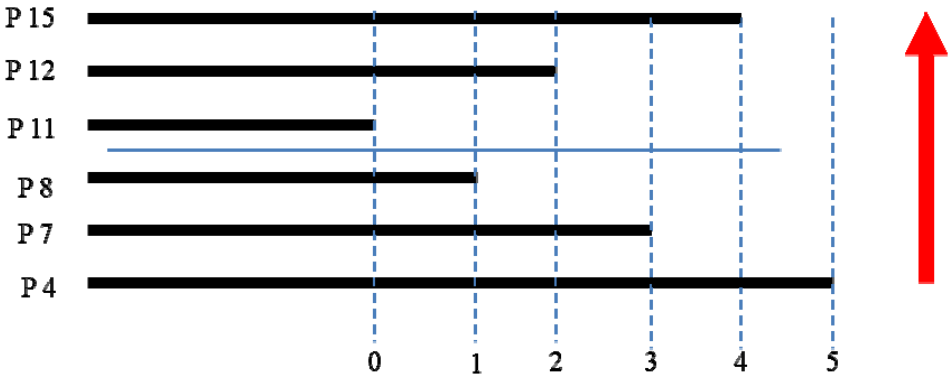

P 4	P 7	P 8	P 11	P 12	P 15
5	3	1	0	2	4

Figure 6.69 Stagger Profile of Drop-off from Bay 2 to Bay 3

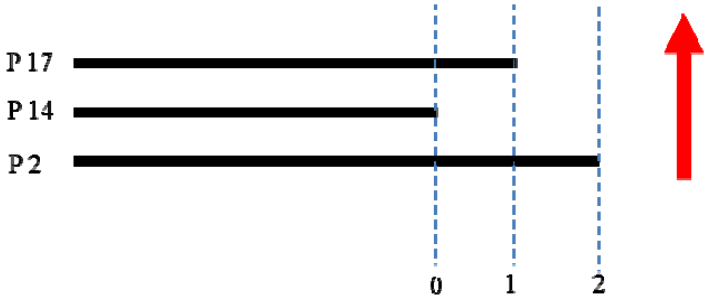

P 2	P 14	P 17
2	0	1

Figure 6.70 Stagger Profile of Drop-off from Bay 3 to Bay 4

Figure 6.71 shows how to input the Custom Stagger Profile in FiberSIM. The default off-set distance was also defined and is shown in Figure 6.72.

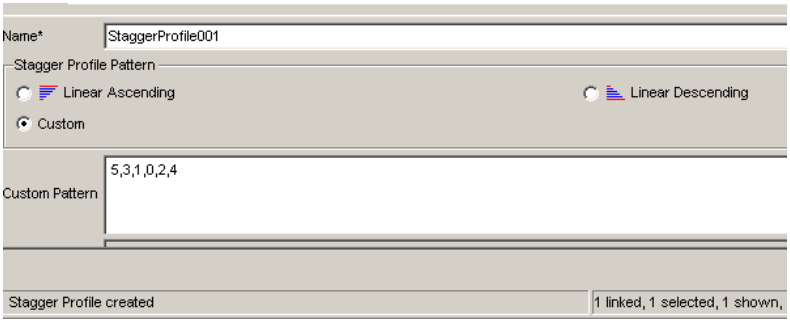

Figure 6.71 Stagger Profile in FiberSIM

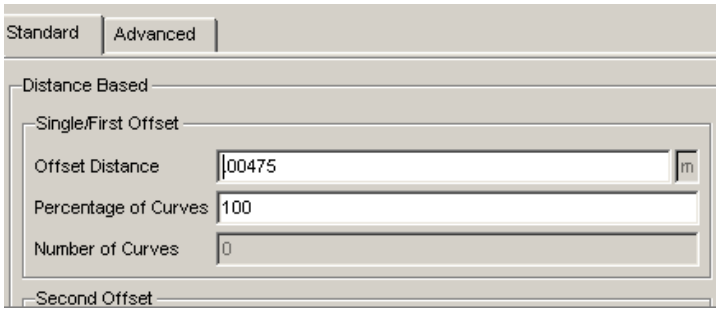

Figure 6.72 Offset Specification of Rear Spar Plies

After the Stagger Profiles and the Offsets were determined, the rear spar model was ready for the producibility analysis. The success message of the steps already completed is shown in Figure 6.73.

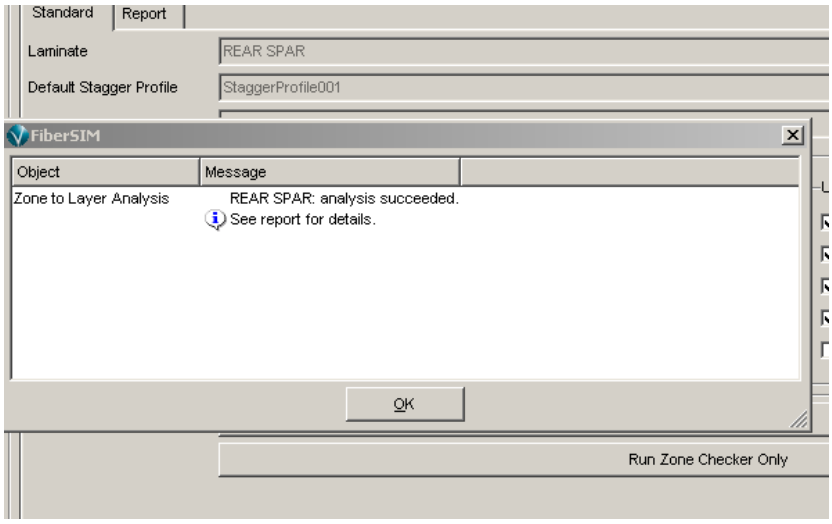

Figure 6.73 The Succeeded Zone to Layer Analysis

Figure 6.74 shows the drop-offs, which were created in the Zone Transition after the analysis. Three drop-offs can be seen as ZT001, ZT002 and ZT003 in Figure 6.75.

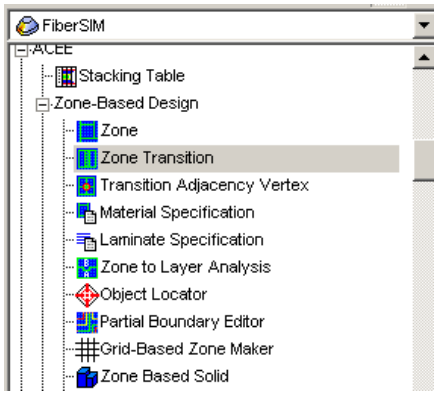

Figure 6.74 Zone Transition in Zone-Based Design

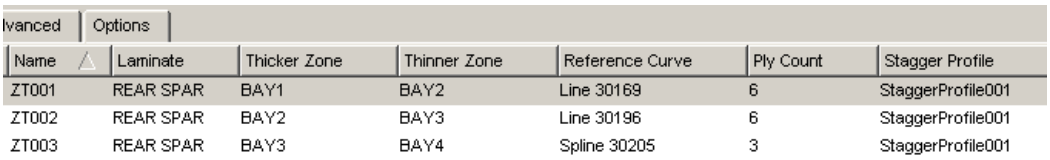

Figure 6.75 The List of Zone Transitions in FiberSIM

After the analysis, the Stagger Profile in ZT003, shown in Figure 6.76, should be modified. The pattern should be changed to 2,0,1 as determined in Figure 6.70. The pattern selection in FiberSIM is shown in Figure 6.77.

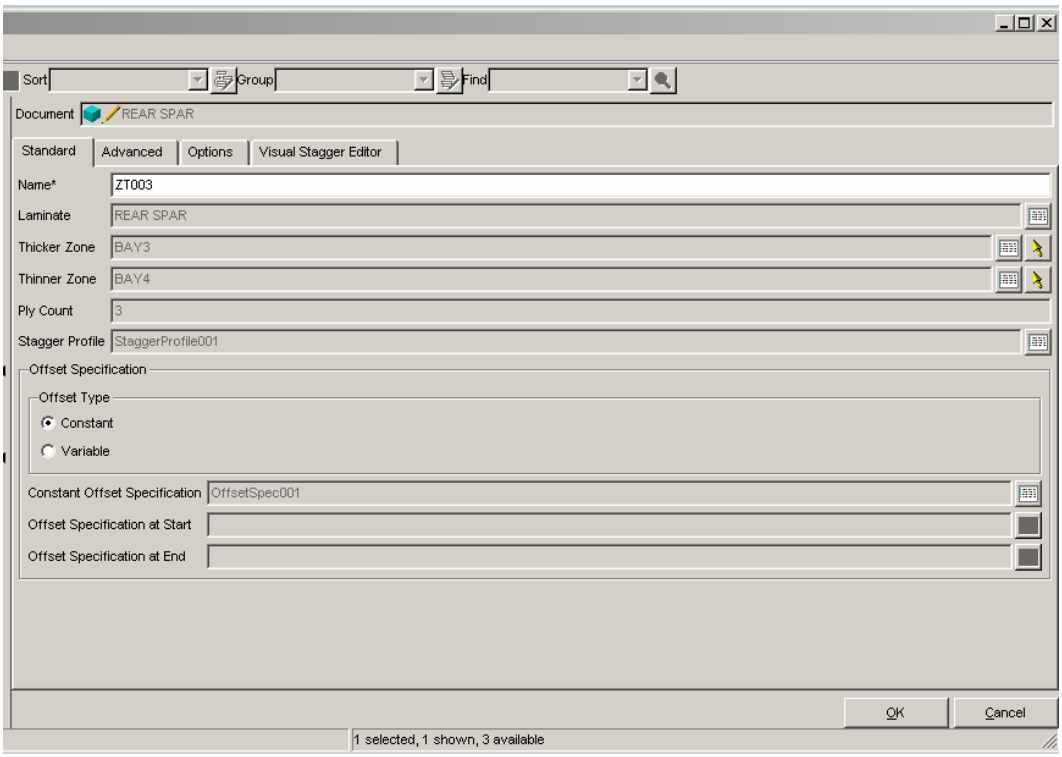

Figure 6.76 Modifying ZT003

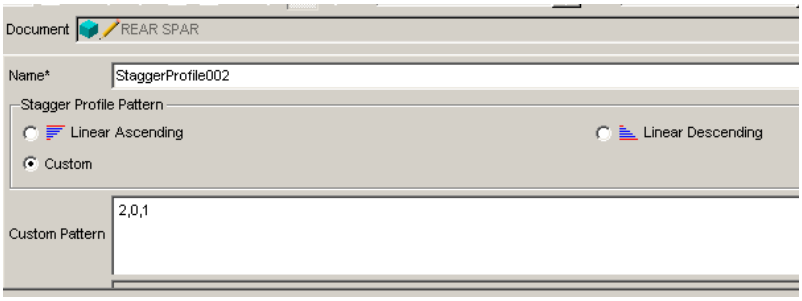

Figure 6.77 Determination of Stagger Profile in ZT003

All the layers of the Rear Spar, obtained from the Zone to Layer Analysis, are shown in Figure 6.78. The plies were then created from the layers. The ply list for the rear spar is given in Figure 6.79.

vanced | Transition Boundary | Result Boundary Features | Notes

Part S	Name	Sequence	Step	Specified Orientation	Zones
	LYR001	A	10	+/-45	(4) BAY1, BAY2, BAY3, BAY4
	LYR002	A	20	0	(3) BAY1, BAY2, BAY3
	LYR003	A	30	+/-45	BAY1
	LYR004	A	40	0	(2) BAY1, BAY2
	LYR023	A	50	0/90	(4) BAY1, BAY2, BAY3, BAY4
	LYR006	A	60	0	BAY1
	LYR007	A	70	+/-45	(2) BAY1, BAY2
	LYR008	A	80	0	(2) BAY1, BAY2
	LYR009	A	90	+/-45	BAY1
	LYR010	A	100	+/-45	BAY1
	LYR011	A	110	0	(2) BAY1, BAY2
	LYR012	A	120	+/-45	(2) BAY1, BAY2
	LYR013	A	130	0	BAY1
	LYR021	A	140	0/90	(3) BAY1, BAY2, BAY3
	LYR015	A	150	0	(2) BAY1, BAY2
	LYR016	A	160	+/-45	BAY1
	LYR017	A	170	0	(3) BAY1, BAY2, BAY3
	LYR018	A	180	+/-45	(4) BAY1, BAY2, BAY3, BAY4

Figure 6.78 Layers of the Rear Spar

Name	Parent	Sequence	Step	Specified Orientation	Material
P001	LYR001	A	10	+/-45	HEXPLY8552S/37RC/AGP280/C
P002	LYR002	A	20	0	HEXPLYAS4/8552/RC34/AW194
P003	LYR003	A	30	+/-45	HEXPLY8552S/37RC/AGP280/C
P004	LYR004	A	40	0	HEXPLYAS4/8552/RC34/AW194
P005	LYR023	A	50	0/90	HEXPLY8552S/37RC/AGP280/C
P006	LYR006	A	60	0	HEXPLYAS4/8552/RC34/AW194
P007	LYR007	A	70	+/-45	HEXPLY8552S/37RC/AGP280/C
P008	LYR008	A	80	0	HEXPLYAS4/8552/RC34/AW194
P009	LYR009	A	90	+/-45	HEXPLY8552S/37RC/AGP280/C
P010	LYR010	A	100	+/-45	HEXPLY8552S/37RC/AGP280/C
P011	LYR011	A	110	0	HEXPLYAS4/8552/RC34/AW194
P012	LYR012	A	120	+/-45	HEXPLY8552S/37RC/AGP280/C
P013	LYR013	A	130	0	HEXPLYAS4/8552/RC34/AW194
P014	LYR021	A	140	0/90	HEXPLY8552S/37RC/AGP280/C
P015	LYR015	A	150	0	HEXPLYAS4/8552/RC34/AW194
P016	LYR016	A	160	+/-45	HEXPLY8552S/37RC/AGP280/C
P017	LYR017	A	170	0	HEXPLYAS4/8552/RC34/AW194
P018	LYR018	A	180	+/-45	HEXPLY8552S/37RC/AGP280/C

Figure 6.79 Plies of the Rear Spar

The producibility analysis of each ply was then performed. The results of producibility analysis of 9 ply are given in Figure 6.80 to Figure 6.88.

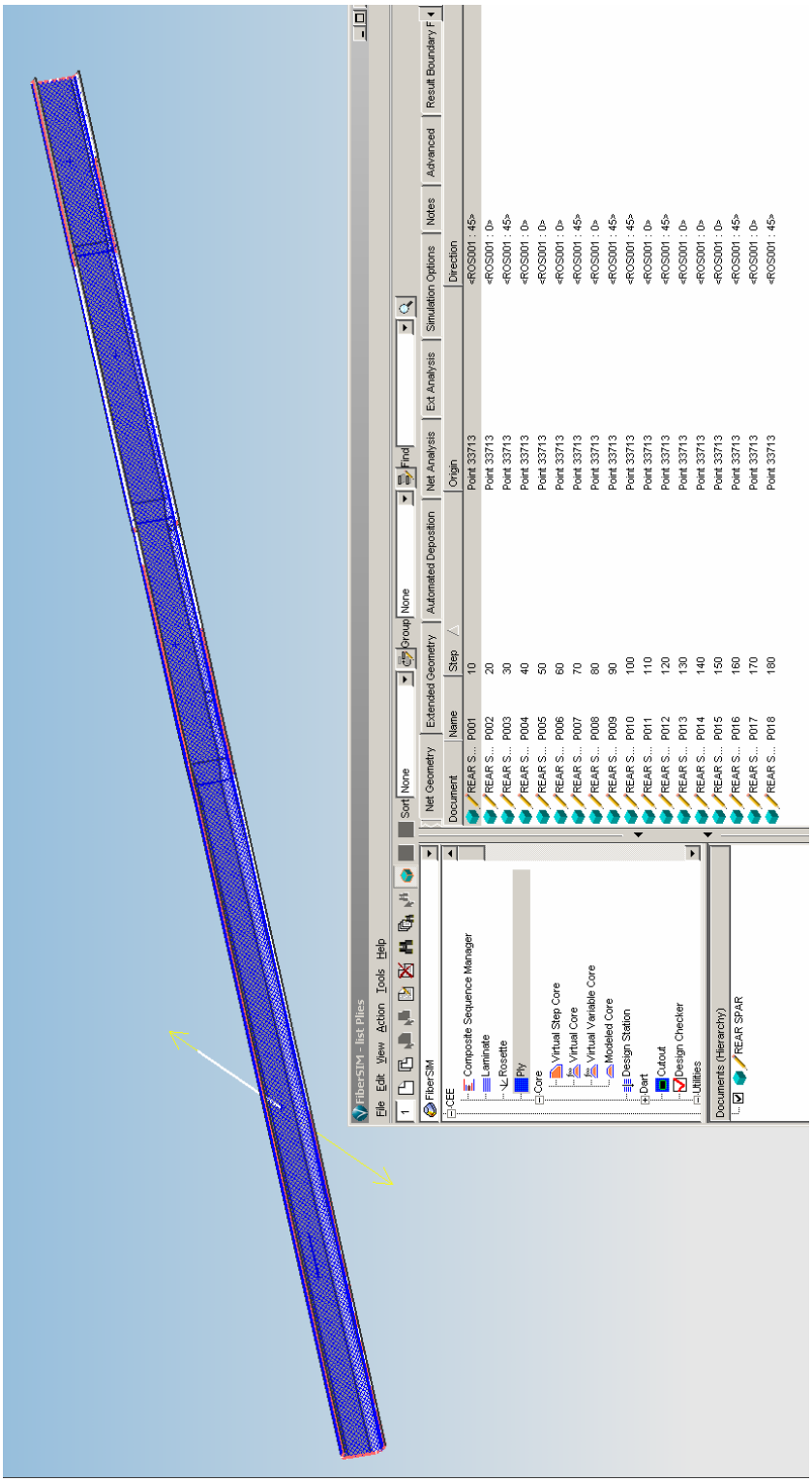

Figure 6.80 Producibility Analysis Results of Ply 1

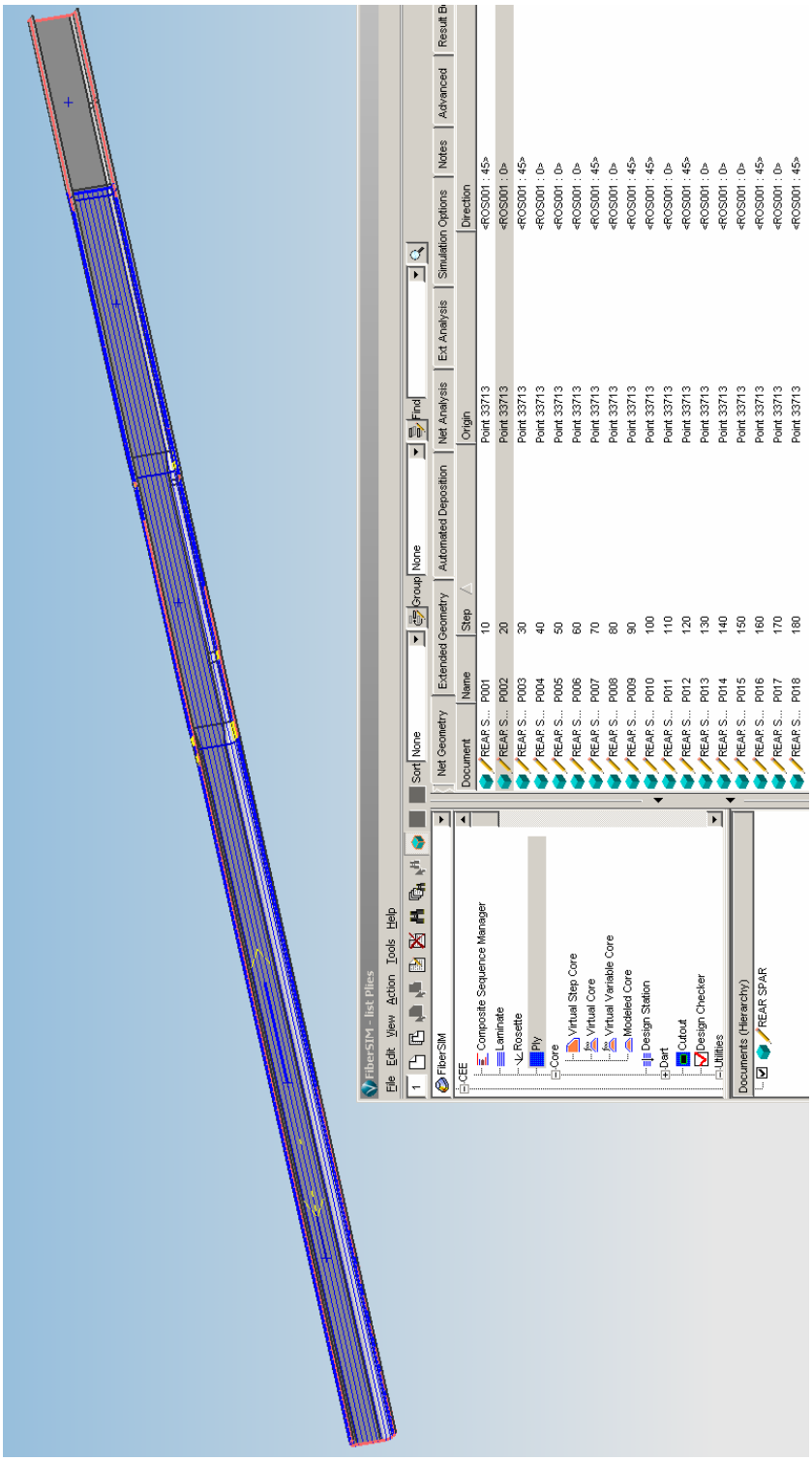

Figure 6.81 Producibility Analysis Results of Ply 2

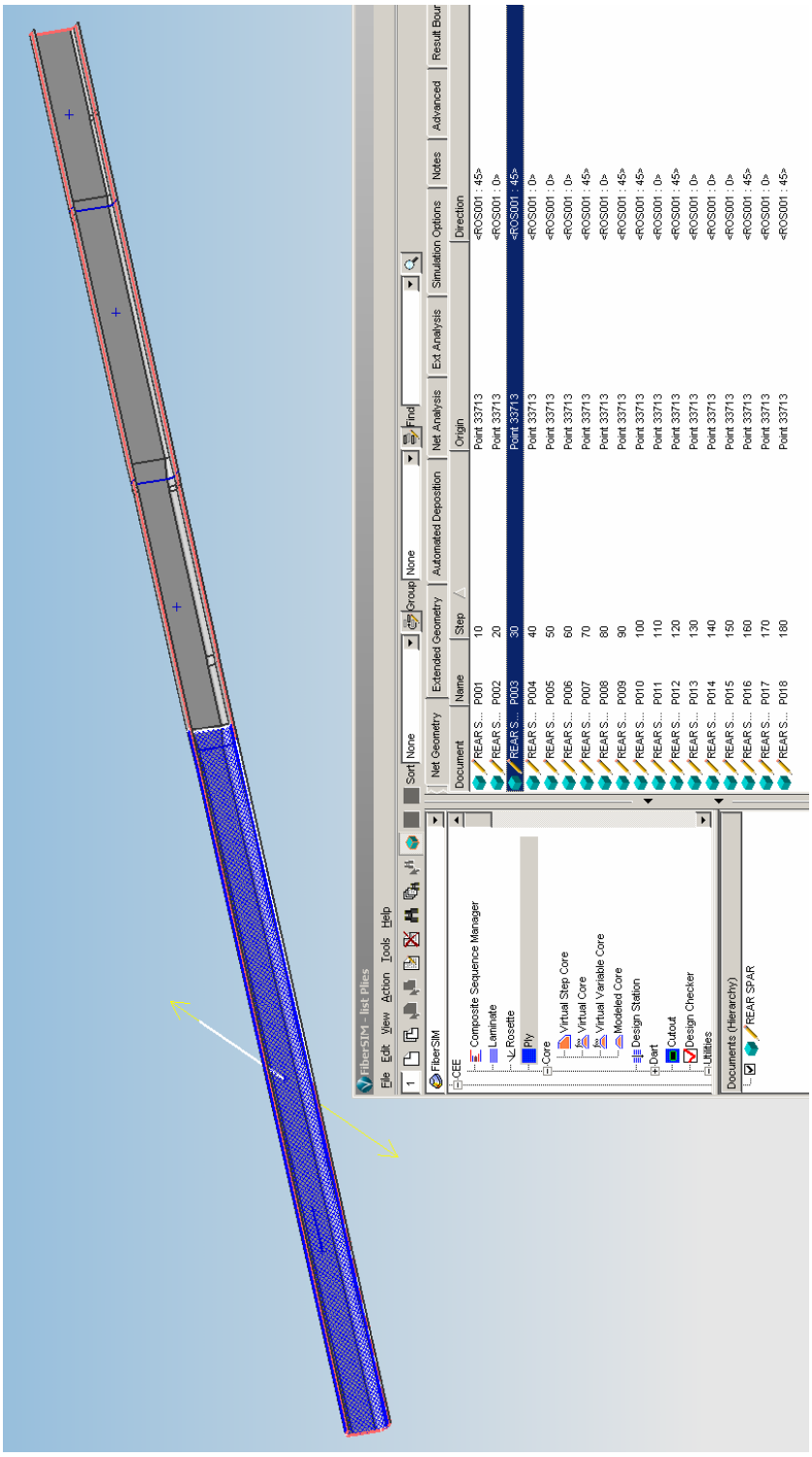

Figure 6.82 Producibility Analysis Results of Ply 3

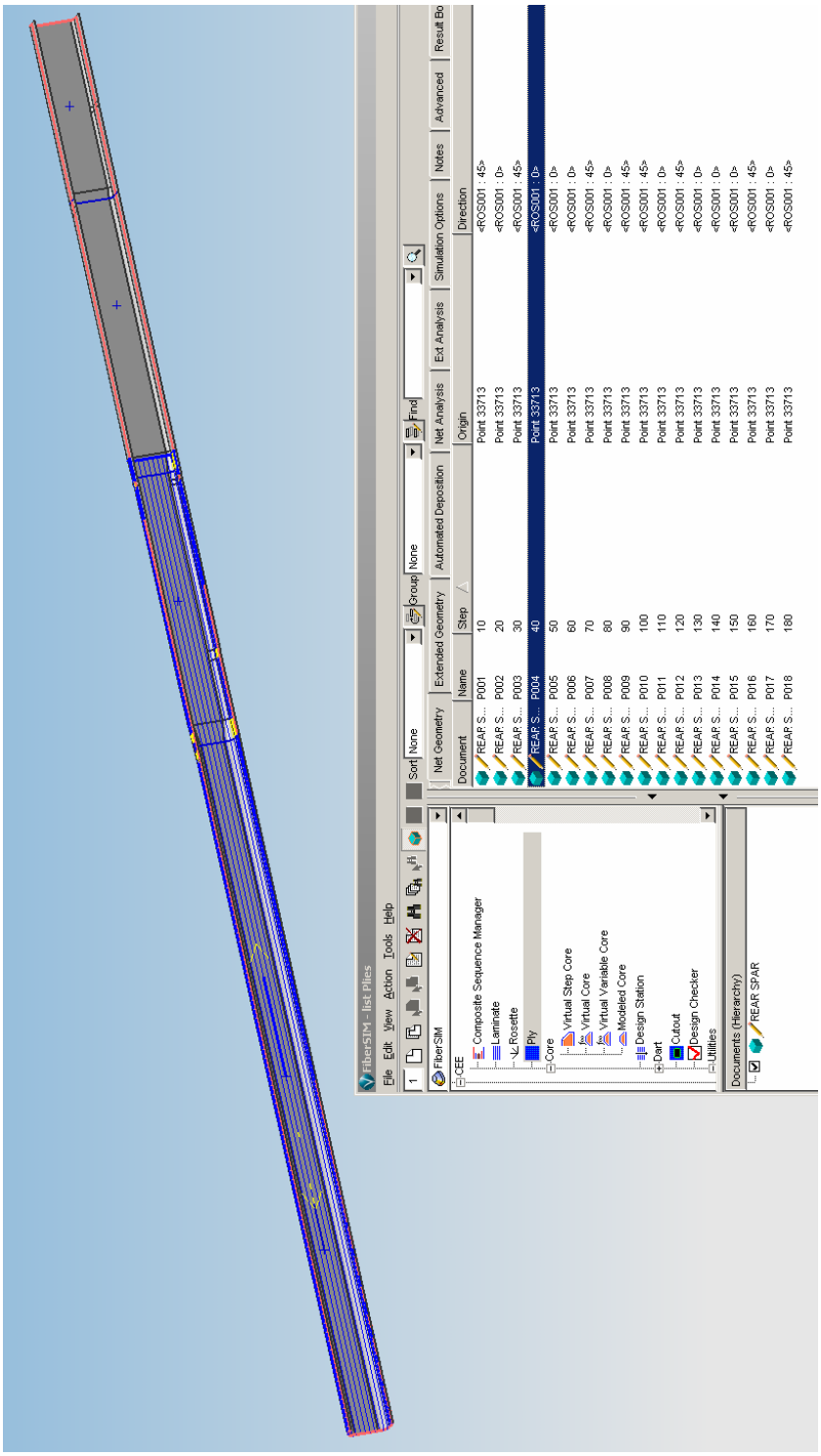

Figure 6.83 Producibility Analysis Results of Ply 4

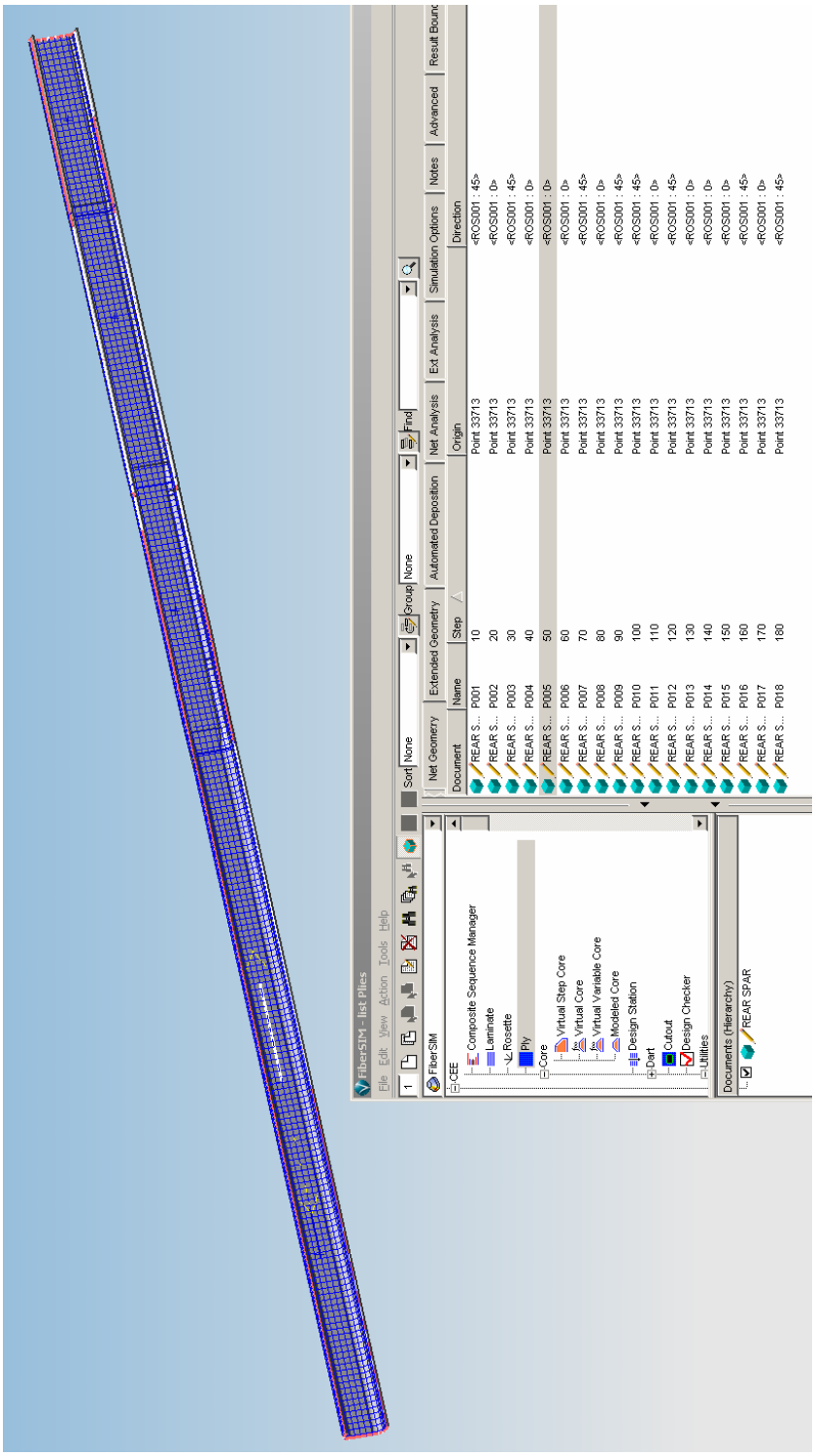

Figure 6.84 Producibility Analysis Results of Ply 5

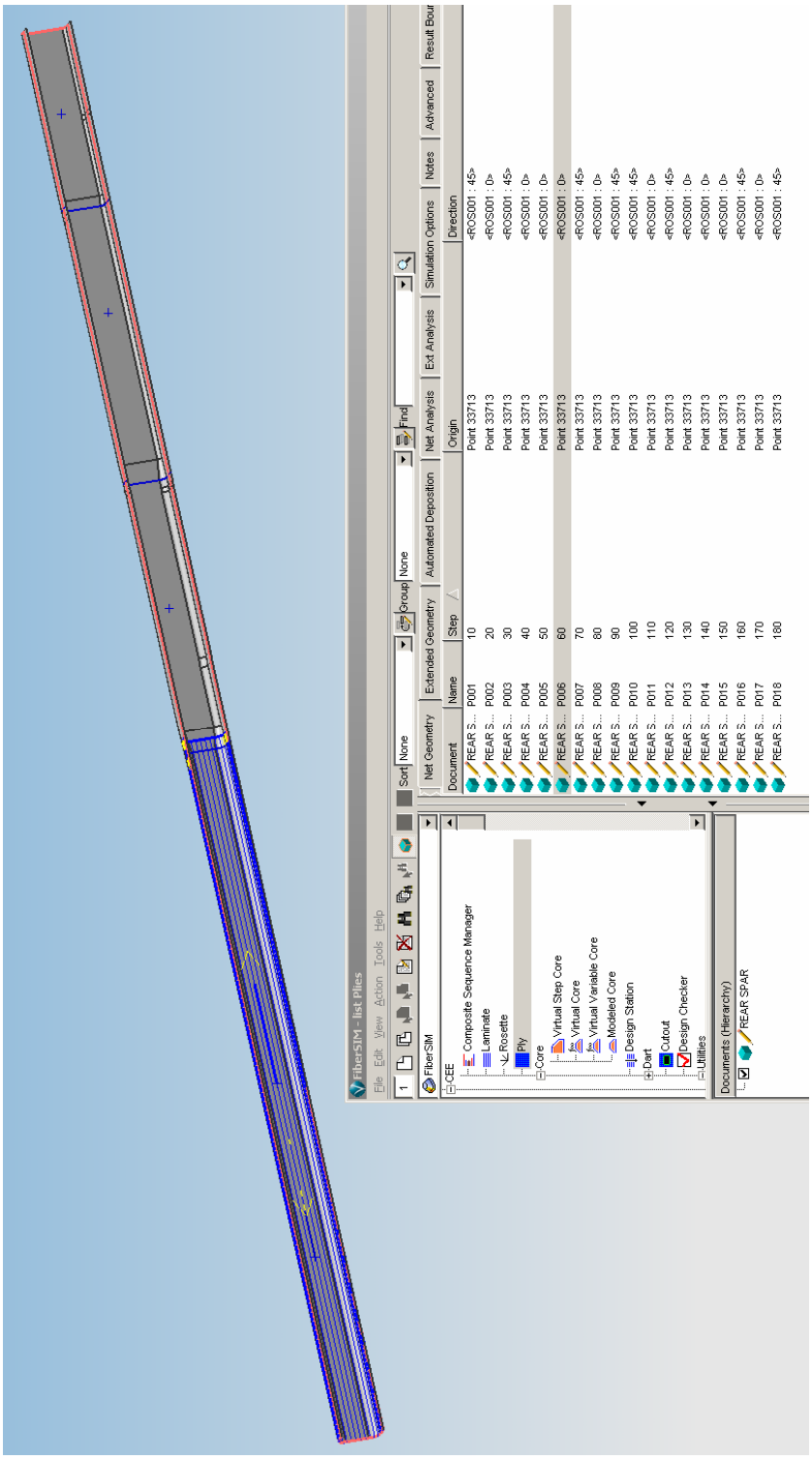

Figure 6.85 Producibility Analysis Results of Ply 6

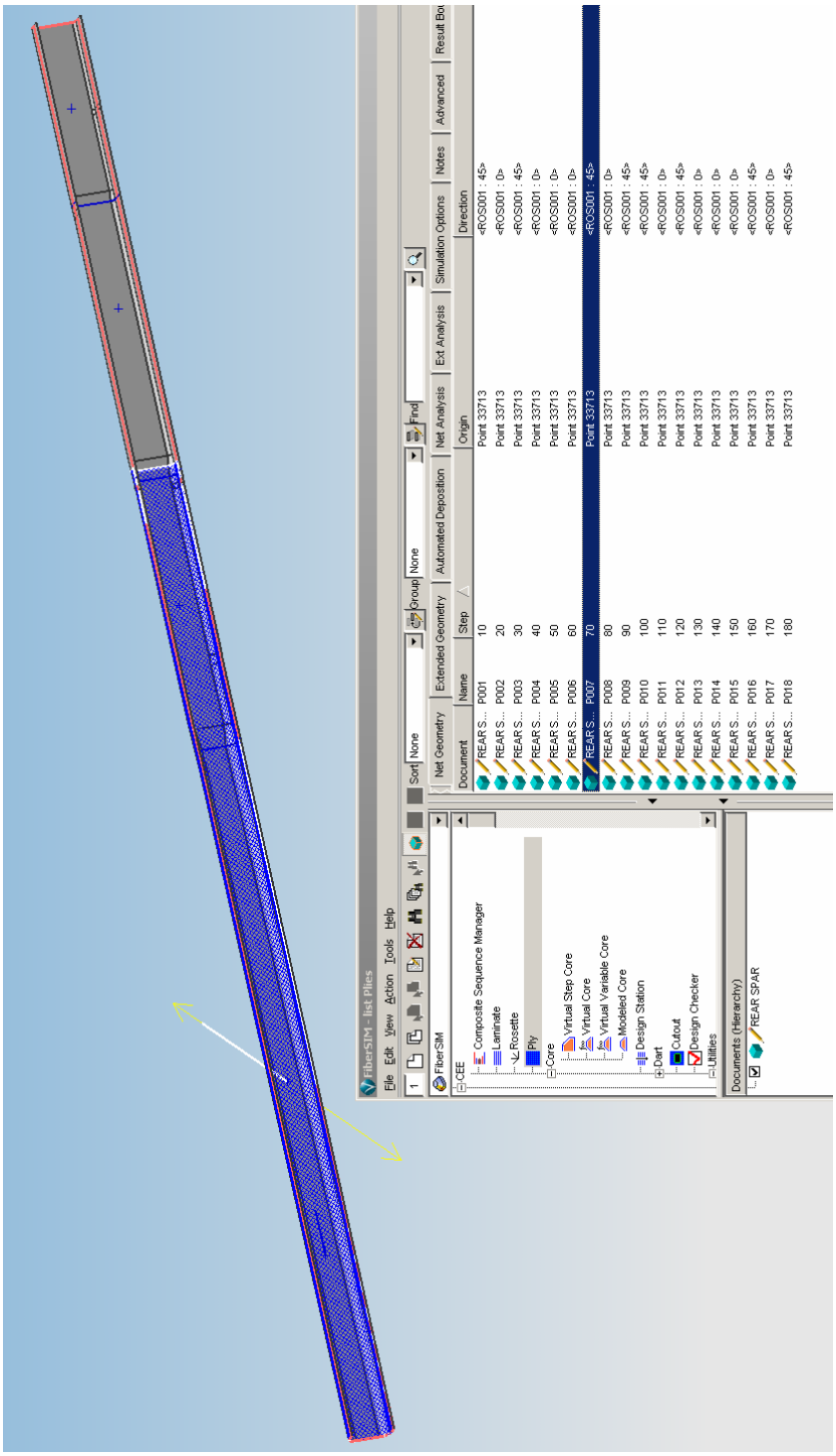

Figure 6.86 Producibility Analysis Results of Ply 7

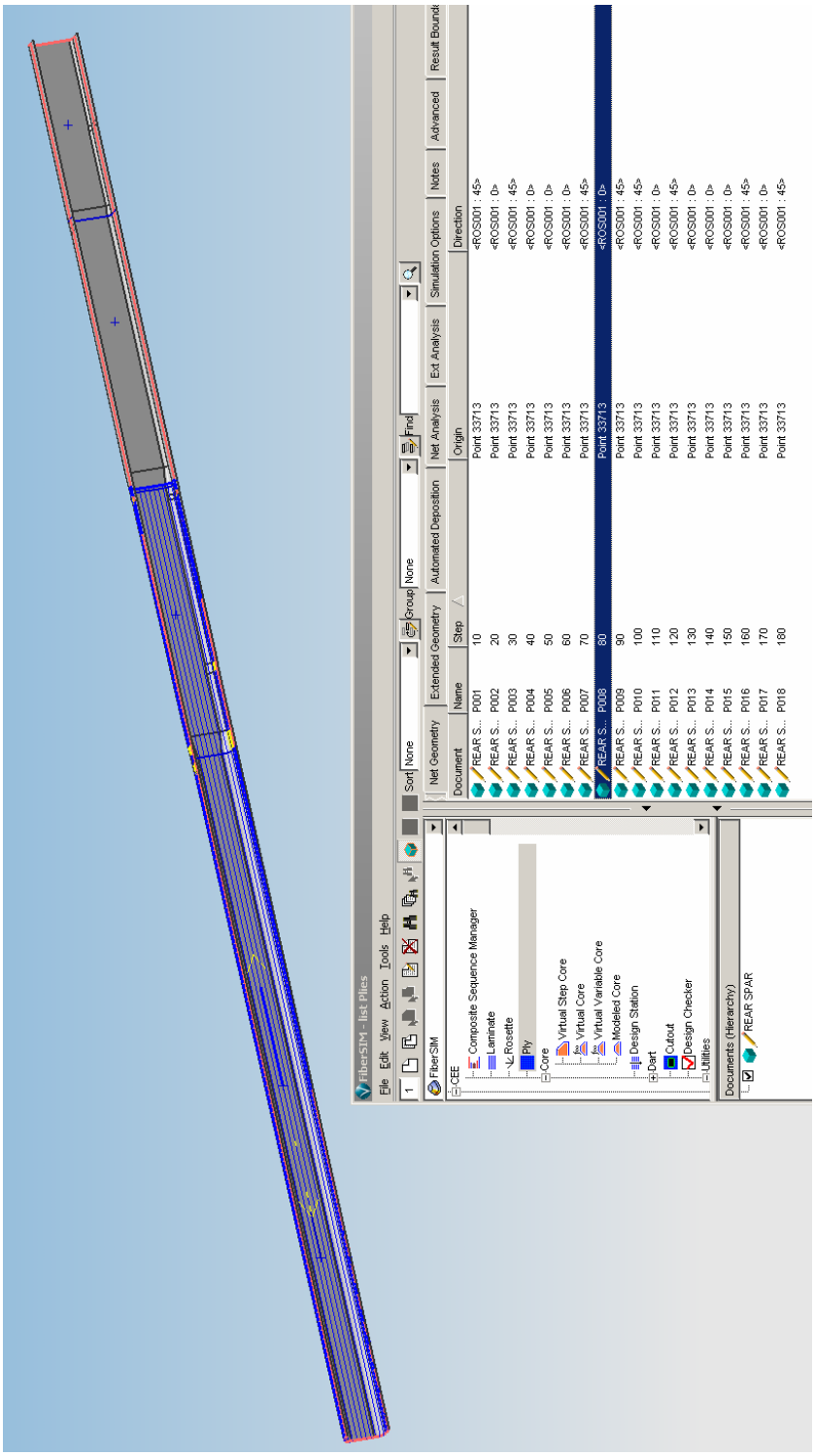

Figure 6.87 Producibility Analysis Results of Ply 8

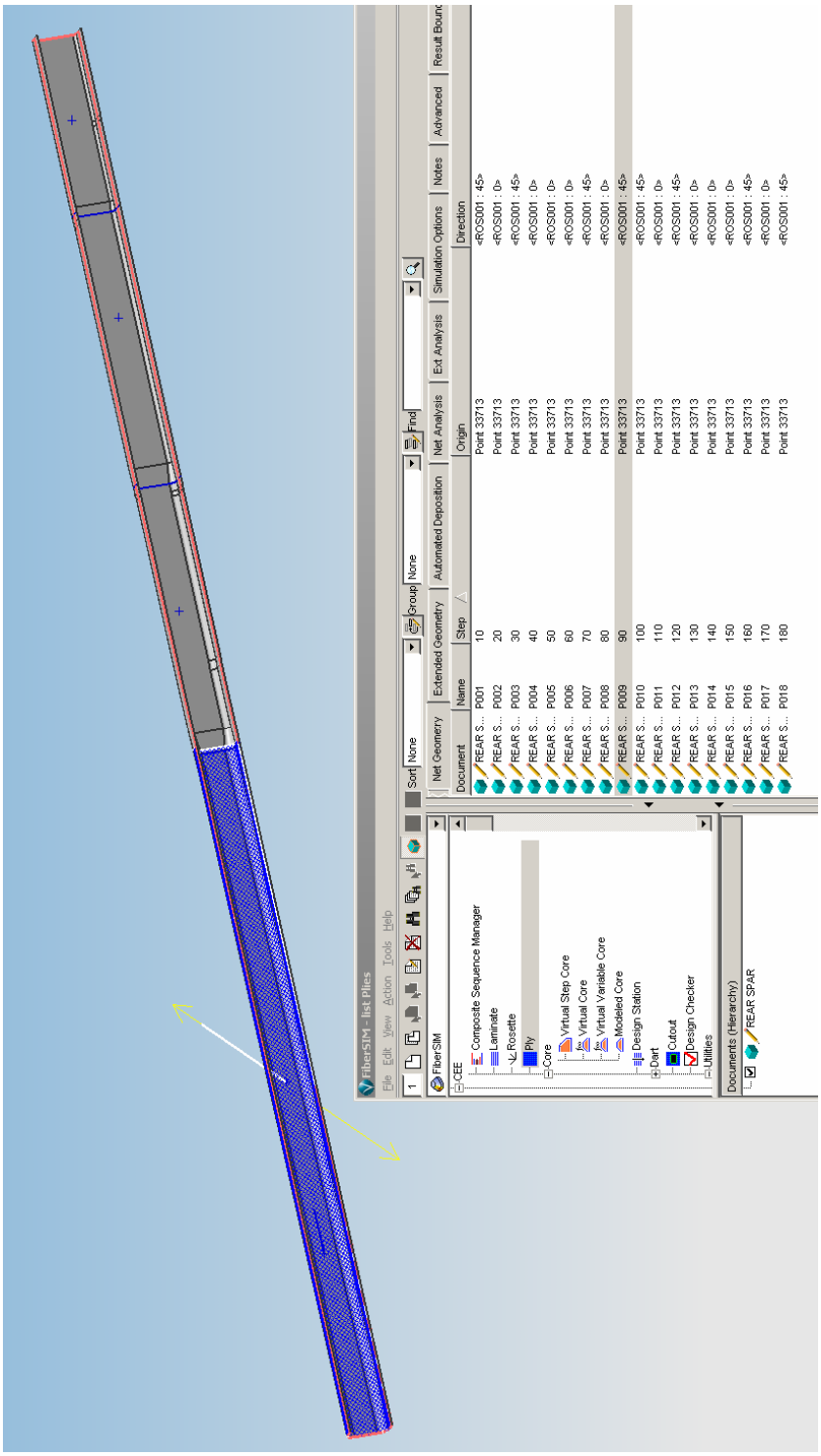

Figure 6.88 Producibility Analysis Results of Ply 9

After the creation of all the plies, the flat patterns of the 18 plies were created and they are shown in Figure 6.89. The flat pattern data were to be transferred to automatic cutting machine as previously explained.

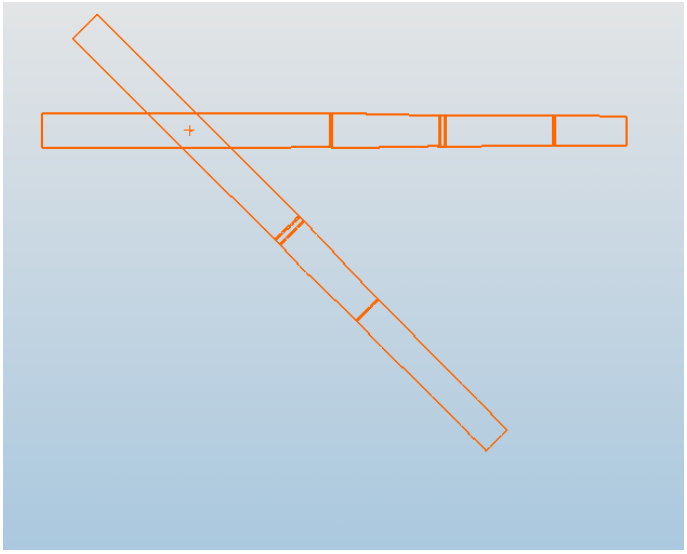

Figure 6.89 The Flat Pattern of 18 Plies of Rear Spar

From Boundary Simplication part, the boundaries of 14 plies were created and are highlighted in Figure 6.90.

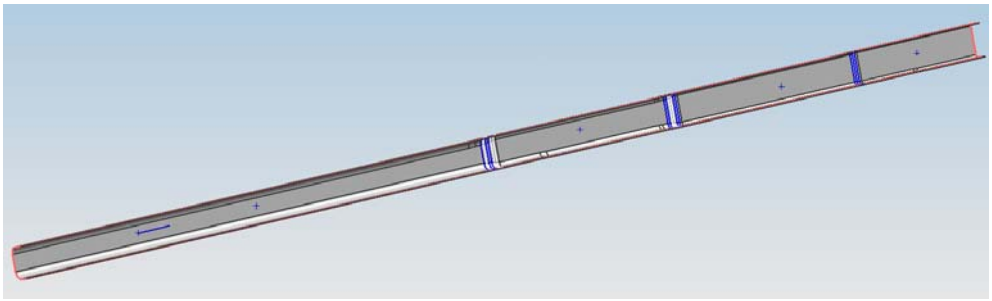

Figure 6.90 Boundary Simplification Result

The cross section of the laminate was then obtained by using 3D Cross Section in the Documentation part. The results are shown in Figure 6.91 to Figure 6.95.

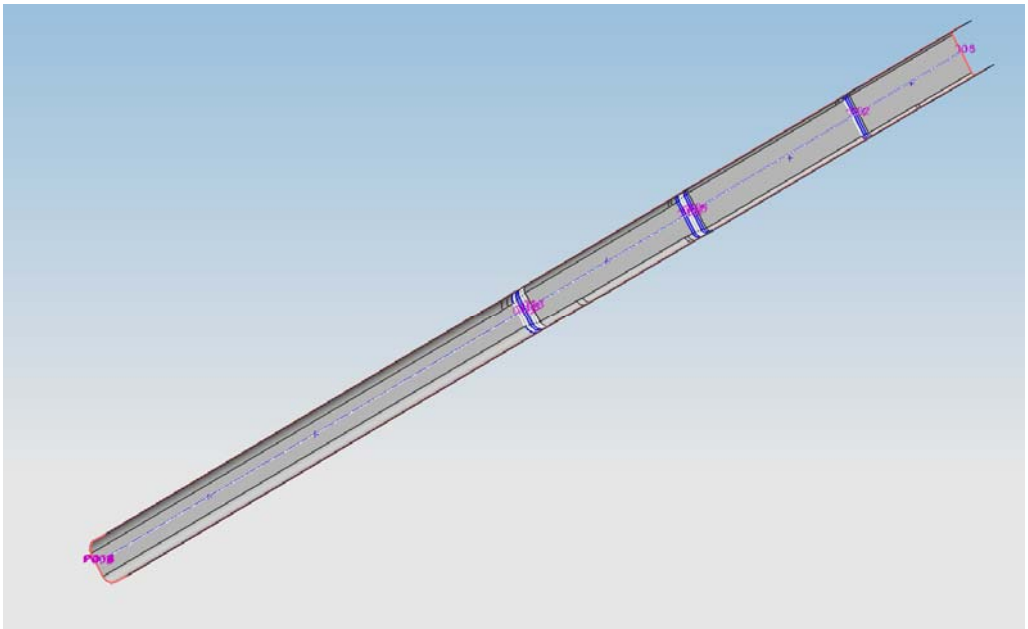

Figure 6.91 The General View of 3D Cross Section Result

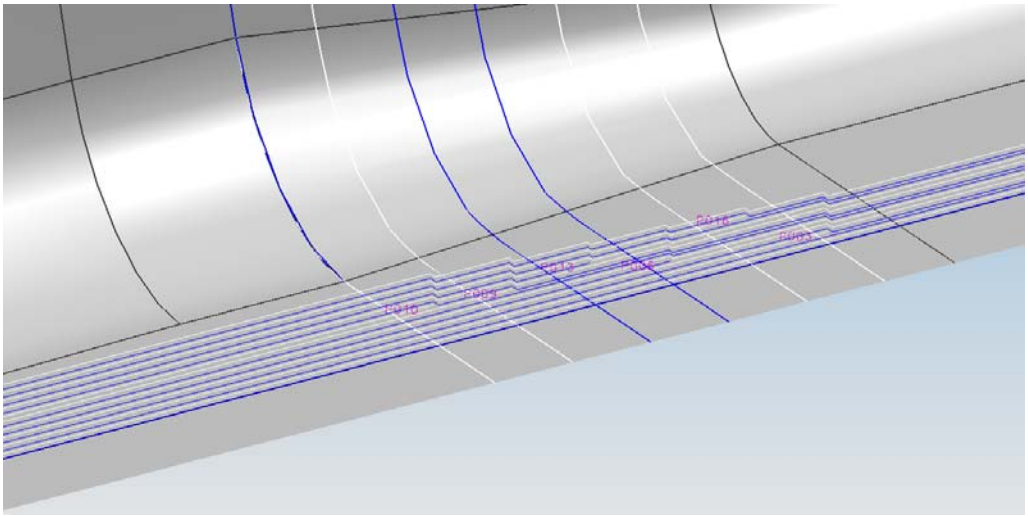

Figure 6.92 The Drop-off Result From Bay 1 to Bay 2

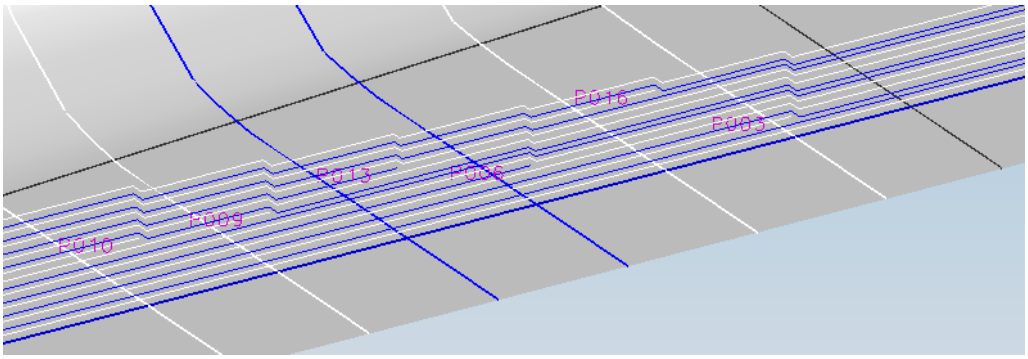

Figure 6.93 The Drop-off Result From Bay 1 to Bay 2

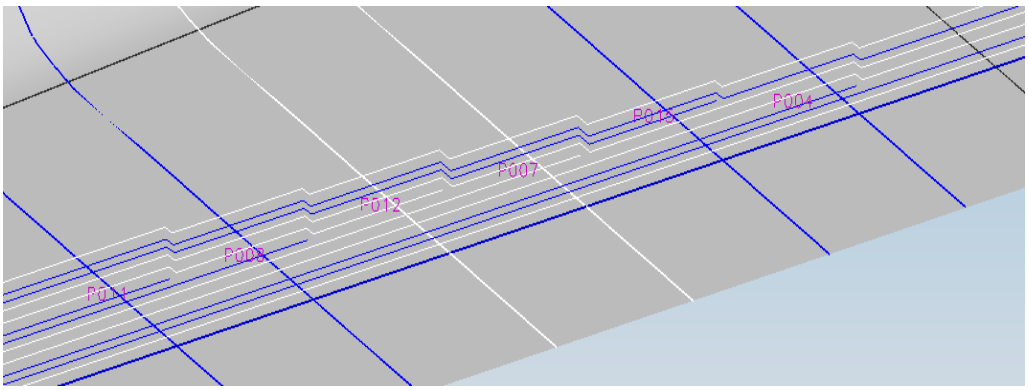

Figure 6.94 The Drop-off Result From Bay 2 to Bay 3

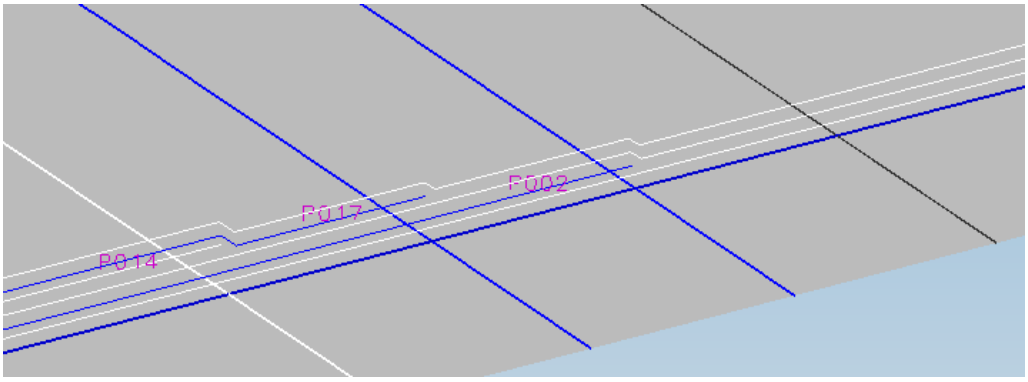

Figure 6.95 The Drop-off Result From Bay 3 to Bay 4

6.2.3 Rib Producibility Analysis

The producibility analyses of ribs were simpler as compared to other. The model was obtained by preparing the tool surface, net boundary curve and 0° fiber direction curve as shown in Figure 6.96. Figure 6.97 shows the creation of the relevant rosette with origin and fiber direction.

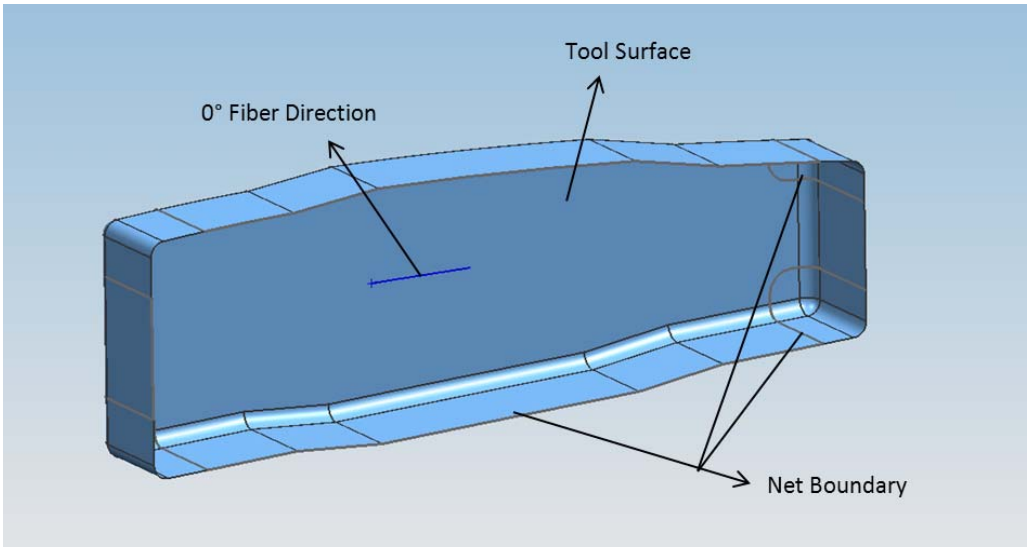

Figure 6.96 Model of Rib for FiberSIM

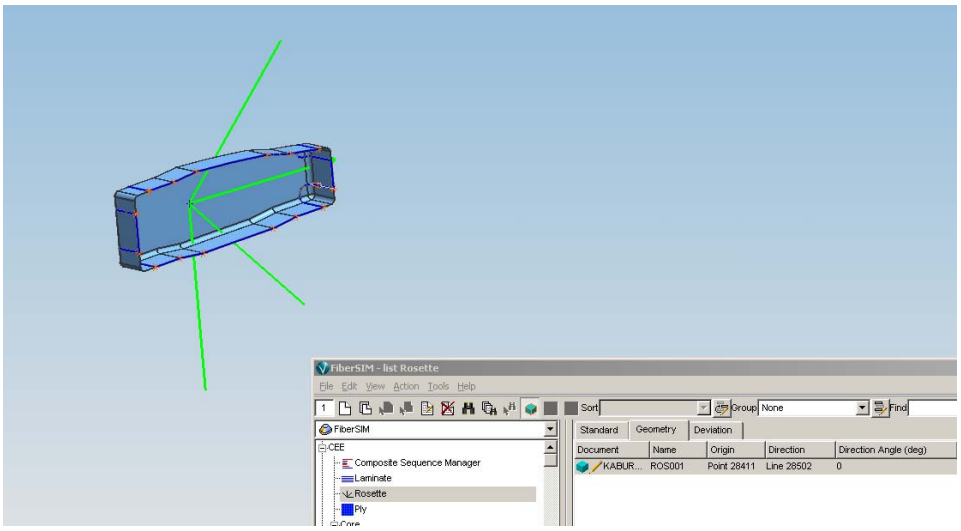

Figure 6.97 The Rosette of the Rib

Then three plies for ribs were created. The sequences and material information for the ribs were given in Figure 6.98. After the plies were created, the producibility analysis was conducted. Figure 6.99 and Figure 6.100 show the results of the producibility anlaysis of Ply 1 having 45° direction and Ply 2 having 0° direction.

Name	Parent	Sequence	Step	Specified Orientation	Material
P001	RIB	A	10	+/-45	HEXPLY8552S/37RC/AGP280/C
P002	RIB	A	20	0/90	HEXPLY8552S/37RC/AGP280/C
P003	RIB	A	30	+/-45	HEXPLY8552S/37RC/AGP280/C

Figure 6.98 Plies of the Rib

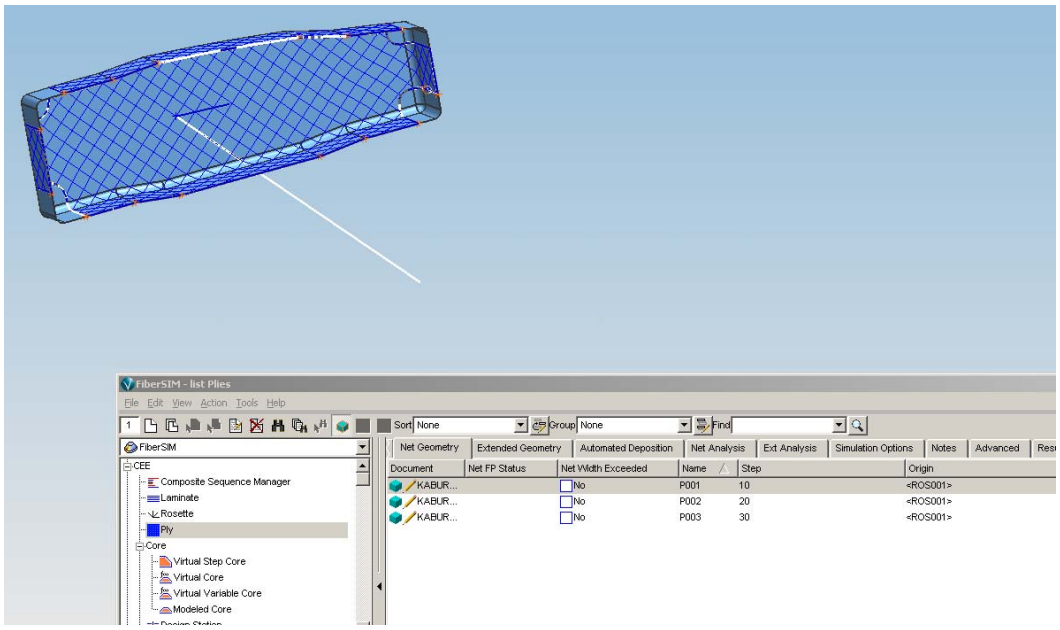

Figure 6.99 Producibility Analysis Results of Ply 1

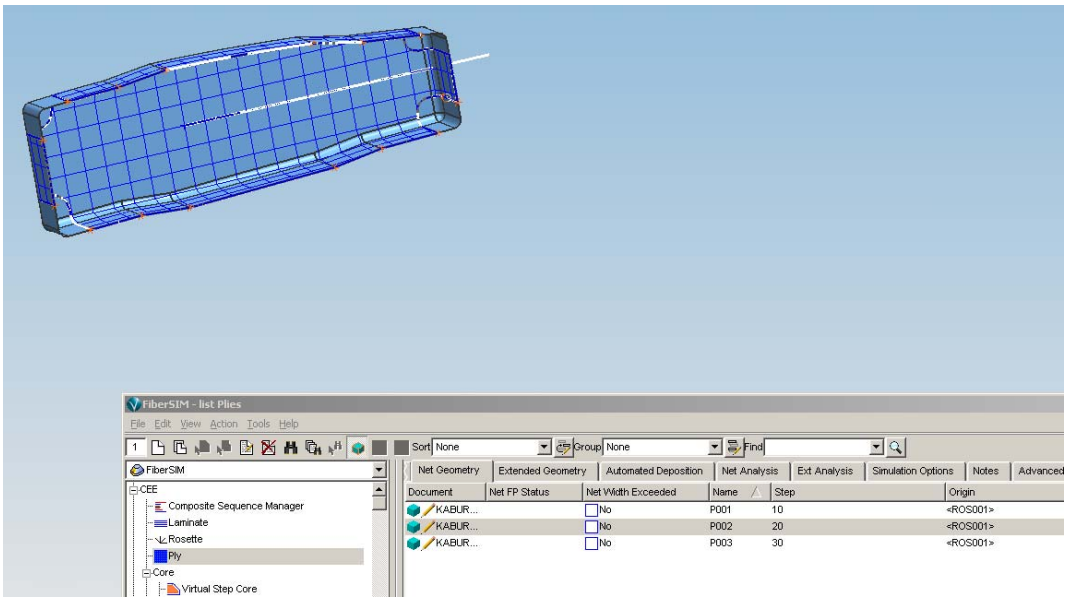

Figure 6.100 Producibility Analysis Results of Ply 2

Flat pattern result obtained is given in Figure 6.101. Cross section of the laminate was obtained using 3D Cross Section in the Documentation part. 3D Cross Sections of the ribs are shown in Figure 6.102 and Figure 6.103.

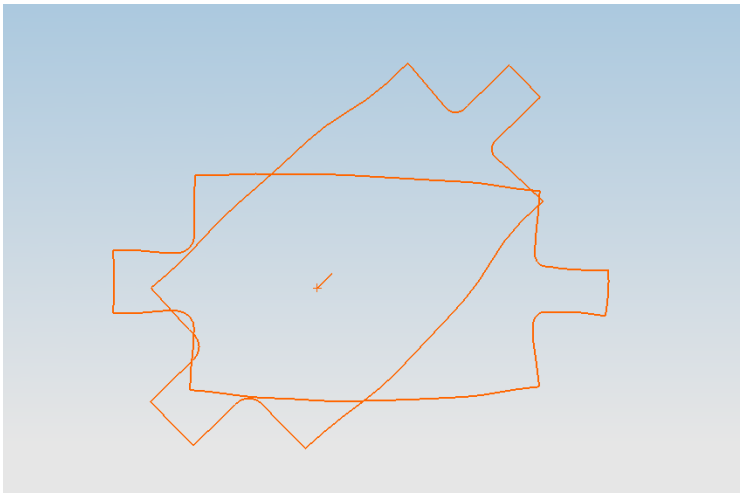

Figure 6.101 Flat Pattern Result for Ribs

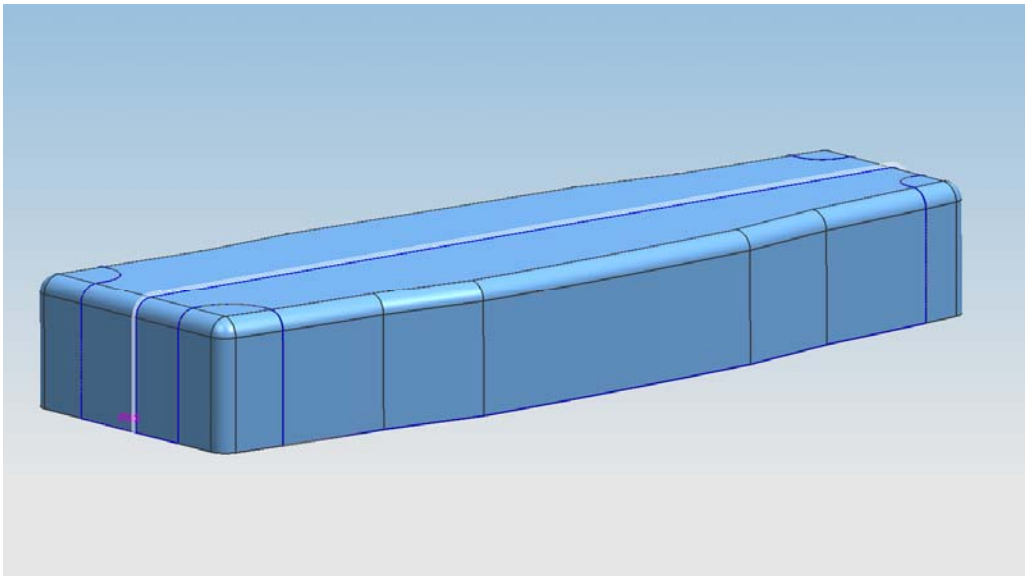

Figure 6.102 The General View of 3D Cross Section Result

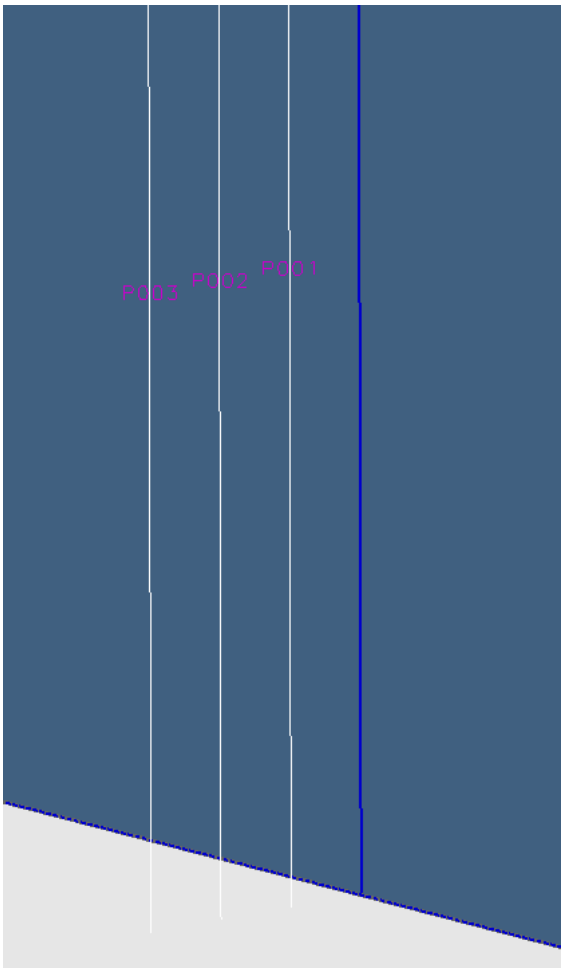

Figure 6.103 3D Cross Section Result of the Rib, Zoomed to a Section

6.3 Conclusion

In this chapter, the producibility analysis of skin, spar and the ribs were performed using by FiberSIM package program. In the analysis, the ply lay-up was simulated and producibility of each bay or zone was checked. It was seen that some of the layers for the upper skin could not be laid up on the tool as a full ply. Thus, plies were spliced at appropriate locations in order to cover the surface. The lay-ups for the spar and rib lay-ups were also verified, and it was determined that no changes were needed in the design.

3D Cross Section Results for each part was also checked and drop-off patterns were controlled. Finally the flat patterns for every part were obtained and these flat patterns were meant to send to manufacturing. That ensured that the producible parts were sent to manufacture and automated manufacturing methods could then efficiently be used.

CHAPTER 7

DISCUSSION & CONCLUSION

7.1 General Conclusion

The aim of this thesis was to determine the optimum design for an unmanned aerial vehicle (UAV) wing. Three different wings having the same aerodynamic geometry and structural configuration under the same flight conditions but made of different materials, were examined and compared.

Three wing designs, which were the prepreg wing model, wet lay-up wing model and aluminum wing model, were modeled by using Unigraphics NX according to assumed sizing. After the modeling, the total mass of each wing was calculated. The mass result showed that aluminum wing model was the heaviest. Therefore, it was eliminated and no further structural analysis was conducted for the aluminum wing model.

The finite element models of the wet lay-up wing model and prepreg wing model were prepared by using MSC Patran package program. Afterwards, the aerodynamic loads were applied on the finite element models and the structural analyses were conducted by using MSC Nastran package program. The structural analysis for the wet lay-up wing model and prepreg wing model were performed for cruise and gust conditions. The displacement values were examined and the stress checks were done by using maximum stress failure criteria. During the verifications it was determined that the initially sized wet lay-up wing model failed; hence the modifications were done in order to strengthen the wing. However, that caused a heavier design and the wet lay-up wing model was eliminated because of its excess weight. The displacement result and the stress

check of prepreg wing model showed that the wing was more stiff and heavier than it should be. The modifications on sizing of the prepreg wing model were also done for the removal of the excess plies and an optimum design was selected considering the displacement result and total mass.

Finally, the producibility analysis of prepreg wing model was also done by using FiberSIM package program. The ply lay-up simulation of each part was done and the ply lay-ups were verified to achieve a correct design of a composite part to be manufactured at first time.

7.2 Future Work Recommendations

The dynamics characteristics of the wing models can be considered in the material selection and composite layer configuration.

Aeroelastic analysis can be performed to classify flutter and divergence performance of different wing models.

Detailed gust modeling for discrete and continuous gusts can be employed in order to accurately represent gust loading. Additionally the transient analyses should also be conducted for the exact determination of changing aerodynamic properties and to highlight their resultant effects.

REFERENCES

[1] Ünlüsoy, L., Structural Design and Analysis of a Mission Adaptive, Unmanned Aerial Vehicle Wing, M.S. Thesis, Middle East Technical University, February 2010.

[2] İnsuyu, E. T., Aero-Structural Design and Analysis of an Unmanned Aerial Vehicle and its Mission Adaptive Wing, M.S. Thesis, Middle East Technical University, February 2010.

[3] Sakarya, E., Structural Design and Evaluation of an Adaptive Camber Wing, M.S. Thesis, Middle East Technical University, February 2010.

[4] Niu, M., C. Y., Composite Airframe Structures, Hong Kong Conmilit Press Ltd., 2005.

[5] Mazumdar, S. K., Composites Manufacturing Materials, Product and Process Engineering, CRC Press LLC, 2002.

[6] FiberSIM User Manual, VISTAGY, 2007.

[7] Jones, R. M., Mechanics of Composite Materials, Brunner-Routledge, 1998.

[8] MSC.Patran, Reference Manual, MSC.Software, 2007.

[9] MSC MD NASTRAN, Quick Reference Guide, MSC.Software, 2006.

[10] HexPly 8552 Epoxy Matrix (180°C/356°F curing matrix) Product Data Sheet, Hexcel, October 2008.

[11] Rohacell A Polymethacrylimide Foam, Aircraft Grade Product Information Data Sheet, Evonik Industries.

[12] Paul, P. C., Saff C. R., Sanger K. B., Mahler M. A., Kan H. P., Kautz E. F., Out of Plane Analysis for Composite Structures, NASA Document ID: 19920023283, 1990.

[13] Klomp-de Boer, R., Development of a Cost Effective Composite Wingbox for Small Aircraft, NLR, Report No: NLR-TP-2010-047, 2010.

[14] Romano, F., Fiori, J. and Mercurio, U., Structural Design and Test Capability of a CFRP Aileron, Elsevier Ltd., 2008.

[15] Guillermin, O., Advanced Composite Engineering using MSC.Patran and FiberSIM, Composite Design Technologies, Waltham, MA 02451, USA.